Universidade do Minho
Escola de Engenharia

Sara Tribuzi de Melo Nunes de Morais

Development of a Biomechanical Spine Model for Dynamic Analysis

Dissertação de Mestrado
Ciclo de Estudos Integrados Conducentes ao
Grau de Mestre em Engenharia Biomédica

Trabalho realizado sob a orientação de
Professor Doutor João Paulo Flores Fernandes
Universidade do Minho

Outubro de 2011

DECLARAÇÃO

Nome: Sara Tribuzi de Melo Nunes de Morais

Endereço eletrónico: a49993@alunos.uminho.pt Telefone: +351 927 668 087

Número do Bilhete de Identidade: 13350994

Título dissertação:

Development of a Biomechanical Spine Model for Dynamic Analysis

Ano de conclusão: 2011

Orientador:

Professor Doutor João Paulo Flores Fernandes

Designação do Mestrado:

Ciclo de Estudos Integrados Conducentes ao Grau de Mestre em Engenharia Biomédica

Área de Especialização: Biomateriais, Reabilitação e Biomecânica

Escola: de Engenharia

Departamento: de Engenharia Mecânica

DE ACORDO COM A LEGISLAÇÃO EM VIGOR, NÃO É PERMITIDA A REPRODUÇÃO DE QUALQUER PARTE DESTA TESE/TRABALHO.

Guimarães, _____/_____/_____

Assinatura: _____

Acknowledgments

To my supervisor, João Paulo Flores Fernandes, for the guidance throughout this last project of my Integrated Master degree.

To the project NP Mimetic - Biomimetic Nano-Fiber Based Nucleus Pulposus Regeneration for the Treatment of Degenerative Disc Disease, funded by the European Commission under FP7 (grant NMP3-SL-2010-246351), for providing my MSc student grant.

To my co-workers at Centre for Mechanical and Materials Technologies (CT2M), University of Minho, for the excellent work environment and team spirit provided, and especially to Margarida Machado, for always having a helpful advice for my doubts.

To my friends who, no matter how near or far, encouraged me to pursuit this goal.

And last and most importantly, to my family for supporting me in every way through these last five years of education and personal development.

Abstract

Development of a Biomechanical Spine Model for Dynamic Analysis

The vertebral column is a complex structure that has a variety of functions in human body stability. This stability can be affected by a myriad of pathologies, from which the degenerative disc diseases group is one of the most relevant, since it is related to low back pain, a symptom that affects the majority of the population at some point of their lives.

This six-month master degree dissertation aims at developing an useful computational tool for the dynamic analysis of the lumbar spine in response to traumatic and degenerative events.

To accomplish this goal, a two-dimensional lumbar spine model (from vertebra L1 to S1) was developed, composed by a set of rigid bodies, constrained by nonlinear viscoelastic elements as ligaments, linear viscoelastic bushing elements as intervertebral discs and contacts between facet joints and spinous processes, following the hertzian contact theory augmented with a dissipative term.

The developed methodologies were individually analyzed in order to validate their implementation in the context of multibody dynamics.

The application of the produced model to different test scenarios was considered, namely the test of the physiologic limits of the relative motion of the vertebrae, the influence of the existence of pathologies and the effect of the application of an external load.

The computational methodologies developed in this work unfold under the objectives of the European Commission's Seventh Framework Programme project *NPmimetic* (Project ID: 246351), in the research area NMP-2009-2.3-1 - Biomimetic gels and polymers for tissue repair.

Resumo

Desenvolvimento de um Modelo Biomecânico da Coluna para Análise Dinâmica

A coluna vertebral é uma estrutura complexa que possui diversas funções no que respeita à estabilidade do corpo humano. Esta estabilidade pode ser afetada por uma miríade de patologias, das quais o grupo das doenças degenerativas do disco intervertebral é um dos relevantes, uma vez que está relacionado com a dor lombar, um sintoma que afeta a grande maioria da população numa determinada fase da sua vida.

Esta dissertação de mestrado desenvolvida em seis meses tem como objetivo desenvolver uma ferramenta computacional útil para a análise dinâmica da coluna lombar em resposta a eventos de ordem traumática e degenerativa.

De modo a alcançar este objetivo, foi desenvolvido um modelo bidimensional da coluna lumbosacral (da vértebra L1 até à S1) constituído por corpos rígidos, constrangidos por elementos viscoelásticos não-lineares como ligamentos, juntas viscoelásticas lineares como discos intervertebrais e contactos entre facetas articulares e apófises espinhosas, seguindo a teoria de contacto de Hertz acrescida de um termo dissipativo.

As metodologias desenvolvidas foram analisadas individualmente de modo a validar a sua implementação no contexto da dinâmica de sistemas multicorpo.

Foi considerada a aplicação do modelo produzido a diferentes cenários, tais como o teste dos limites fisiológicos do movimento relativo das vértebras, a influência da existência de patologia e o efeito da aplicação de uma carga externa.

As metodologias computacionais desenvolvidas neste trabalho vão de encontro aos objetivos do projeto *NPmimetic* (ID do projeto: 246351) do Seventh Framework Programme (FP7) da Comissão Europeia, na área de investigação NMP-2009-2.3-1 - Géis e polímeros biomiméticos para reconstrução de tecidos.

Contents

Acknowledgments iii
Abstract v
Resumo vii
Contents ix
List of Abbreviations and Acronyms xi
List of Figures xiii
List of Tables xvii
Chapter 1 Introduction 1
1.1. Motivation and Scope 1
1.2. Literature Review 2
1.3. Objectives of this Work 11
1.4. Structure of the Thesis 11
1.5. Contribution of this Work 12
Chapter 2 Characterization of the Spine 13
2.1. Anatomy 13
2.1.1. The Vertebrae 16
2.1.2. The Intervertebral Disc 17
2.1.3. The Lumbar Ligaments 18
2.2. Spinal Disorders 21
2.3. Solutions for Degenerative Disc Disease 26
2.4. Summary and Discussion 28
Chapter 3 Multibody Systems Formulation 29
3.1. Multibody System Concept 29
3.2. Cartesian Coordinates 30
3.3. Equations of Motion for Constrained Systems 32
3.4. Solution of the Equations of Motion 33
3.4.1. Simulation Software 35
3.5. Summary and Discussion 36
Chapter 4 Biomechanical Multibody Spine Model 37
4.1. Description of the Model 37
4.1.1. The Vertebrae 37

4.1.2. The Intervertebral Discs 39
4.1.3. The Ligaments 41
4.2. Kinematics of the Contact 47
4.2.1. Articular Facets 51
4.2.2. Spinous Process 52
4.3. Contact Force Model 52
4.4. Summary and Discussion 54
Chapter 5 Results and Discussion 55
5.1. Validation of the Developed Methodologies 55
5.1.1. Ligaments 55
5.1.2. Bushing Elements 57
5.1.3. Contact 62
5.2. Application to a Functional Spinal Unit 66
Chapter 6 Conclusions and Future Work 69
6.1. Conclusions 69
6.2. Future Work 70
References 71
Appendix A – Input File for MUBODYNA 75

List of Abbreviations and Acronyms

2D	Two-dimensional
3D	Three-dimensional
AF	Annulus Fibrosus
ALL	Anterior Longitudinal Ligament
BE	Bushing Elements
CL	Capsular Ligament
CT	Computer Tomography
DDD	Degenerative Disc Disease
DIM	Direct Integration Method
DOF	Degree-of-freedom
EP	Endplate
EPI	Endplate Inclination
F	Flores *et al.* contact force model
FE	Finite Elements
FSU	Functional Spinal Unit
IDET	Intradiscal Electrothermal Therapy
ISL	Interspinous Ligament
IVD	Intervertebral Disc
HIC	Head Injury Criteria
LBP	Low Back Pain
L & N	Lankarani and Nikravesh contact force model
LF	Ligamentum Flavum
MBS	Multibody System
NP	Nucleus Pulposus
PLL	Posterior Longitudinal Ligament
SSL	Supraspinous Ligament
UHMWPE	Ultra High Molecular Weight Polyethylene

List of Figures

Figure 1.1 – Lateral view of de Jager's model: base of the skull and vertebrae, showing the body local coordinate systems {Adapted from (de Jager, 2000)}. 4

Figure 1.2 – Spine/neck and head model developed for analysis of spinal loading {Adapted from (Waters *et al.*, 2003)}..... 5

Figure 1.3 – Esat multibody model of the lumbar spine {Adapted from (Esat, 2006)}. 5

Figure 1.4 – Configuration of the model during the lateral impact simulation (from t=0 s to t=0.18 s). The upper row represents the sagittal view and the lower row a frontal view {Adapted from (Ferreira, 2008)}..... 6

Figure 1.5 - Multibody model of the lumbar spine developed in Simulink™, under a loading situation {Adapted from (Fairman *et al.*, 2009)}. 7

Figure 1.6 – MBS model of the lumbar spine (L2 - sacrum) obtained by Juchem {Adapted from (Bauer and Gruber, 2009)}..... 8

Figure 1.7 – Hybrid model developed by Monteiro: (a) co-simulation model; and (b) fixation plate model with titanium fixation screws {Adapted from (Monteiro, 2009)}. 9

Figure 1.8 – Detailed musculoskeletal model of the lumbar spine developed by Christophy, comprising 238 muscle fascicles, 13 rigid bodies, and 5 intervertebral joints: (a) neutral posture and (b) 50° flexion {Adapted from (Christophy, 2010)}. 10

Figure 1.9 – Lumbar spine model (L1-sacrum) obtained with MSC.ADAMS® software {Adapted from (Abouhossein *et al.*, 2011)}. 11

Figure 2.1 - Views of the vertebral column, showing the different regions: (a) frontal view; (b) lateral view {Adapted from (Gray, 1918)}. 14

Figure 2.2 – Mobility of the vertebral column: the extent of mobility from zero position (0°) is given in degrees {Adapted from (Faller *et al.*, 2004)}..... 15

Figure 2.3 – Parts of a typical lumbar vertebra: (a) top view; (b) lateral view {Adapted from (Bogduk, 2005)}..... 16

Figure 2.4 – The sacrum: (a) frontal, (b) sagittal and (c) transverse view. Anterior sacral foramina (asf), remnants of the intervertebral disc (ivd), lamina (la), lateral mass (lm), superior articular process (sap), sacral canal (sc), sacral hiatus (sh), spinous process of S1 (sp) and vertebral bodies (vb) {Adapted from (Bogduk, 2005)}. 17

Figure 2.5 - The intervertebral disc: (a) sagittal section and (b) transverse section {Adapted from (Bogduk, 2005)}..... 18

Figure 2.6 – Hierarchical organization of the ligaments: names and diameters of the subelements {Adapted from (Herman, 2007)}. 19
Figure 2.7 – Ligaments in the lumbar spine: division in intra- and intersegmental. 19
Figure 2.8 - Medial sagittal section of two lumbar vertebrae and their ligaments {Adapted from (Gray, 1918)}. 20
Figure 2.9 – Spinal disorders: a division in specific and nonspecific disorders. 21
Figure 2.10 – Macroscopic disc changes due to DDD, according to Thompson's classification: (a) grade I; (b) grade II; (c) grade III; (d) grade IV; (e) grade V {Adapted from (Boos and Aebi, 2008)}. 22
Figure 2.11 – Load sharing and intervertebral disc degeneration: (a) normal disc; (b) degenerated disc {Adapted from (Pollintine *et al.*, 2004)}. 24
Figure 2.12 – The three column spine: (a) anterior, (b) middle, and (c) posterior column {Adapted from (Denis, 1983)}. 24
Figure 2.13 – Major spinal injury types {Adapted from (Denis, 1983)}. 25
Figure 2.14 – Operative techniques for the treatment of lumbar DDD. 26
Figure 2.15 – Lumbar disc replacement prosthesis: (a) Baguera ® L, from Spine Art; (b) LP-ESP ®, from FH Orthopedics; (c) Prodisc-L ®, from Synthes; (d) activ® L, from B|Braun. 28
Figure 3.1 – Generic representation of a multibody system. 29
Figure 3.2 – Multibody systems and the possible analyses of biomechanical systems. 30
Figure 3.3 – Locating point *P* relative to the body-fixed and global coordinate systems {Adapted from (Nikravesh, 1988)}. 31
Figure 3.4 – Flowchart of computational procedure for dynamic analysis of multibody systems – Direct Integration Method {Adapted from (Flores and Seabra, 2010). 34
Figure 4.1 - Posterior vertebral body height (VBHp), and upper (EPDu) and lower (EPDl) endplate depth in a vertebra. 38
Figure 4.2 – Upper (ψ_U) and lower (ψ_L) endplate inclination for a vertebral body considered in the model. 38
Figure 4.3 - Geometric definition of the bushing element and representation of the initial translational offset. 40
Figure 4.4 – Mechanical behavior of the ligament: load-strain curve Adapted from (Wismans, 1980). 42

Figure 4.5 – Ligament hysteresis: loading and unloading. The shaded area represents the energy loss due to the hysteretic behavior (Yahia *et al.*, 1991). 43
Figure 4.6 – Location of the supraspinous (SSL) ligament. 47
Figure 4.7 – Schematic representation of the contact between a sphere and a plane. 48
Figure 4.8 – Schematic representation of the relative contact velocity. 50
Figure 5.1 – Schematic representation of a ligament. 55
Figure 5.2 – Ligament behavior: (a) ligament length versus time; (b) ligament velocity versus time; (c) strain versus time; (d) strain rate versus time; (e) elastic force versus strain; (f) total force versus strain. 56
Figure 5.3 – Schematic representation of a bushing element actuating on the y-direction. 57
Figure 5.4 – Behavior of the bushing element (*y*-direction, v_i^0=0 m/s): (a) bushing length; (b) bushing velocity; (c) elastic force; (d) damping force; (e) total vertical force. 58
Figure 5.5 - Behavior of the bushing element (y-direction, v_i^0=10 m/s): (a) bushing length; (b) bushing velocity; (c) elastic force; (d) damping force; (e) total vertical force. 59
Figure 5.6 – Schematic representation of a bushing element acting on the *x*-direction. 60
Figure 5.7 - Behavior of the bushing element (*x*-direction, v_i^0=0 m/s): (a) bushing length; (b) bushing velocity; (c) elastic force; (d) damping force; (e) total horizontal force. 61
Figure 5.8 – Behavior of the bushing element (ϕ-direction): (a) orientation of body *i*; (b) angular variation; (c) relative angular velocity; (d) elastic moment; (e) damping moment; (f) total bushing moment. 61
Figure 5.9 – Bouncing ball example. 63
Figure 5.10 – Kinematic simulation results of a ball falling on the ground: (a) ball position; (b) ball velocity. 63
Figure 5.11 – Influence of the contact model on the bouncing ball behavior (c_r=0.9): (a) deformation; (b) velocity of deformation; (c) contact force; (d) contact force-deformation relation. 64
Figure 5.12 – Influence of the contact model on the bouncing ball behavior (c_r=0.616): (a) deformation versus time; (b) velocity of deformation versus time; (c) contact force versus time; (d) contact force-deformation relation. 65
Figure 5.13 – Multibody model of two consecutive vertebrae and their fundamental elements (bodies, ligaments, bushing elements and potential contact areas) {Adapted from (Tribuzi *et al.*, 2012)}. 66

Figure 5.14 - Developed lumbar spine multibody model (from L1 to S1). 67

List of Tables

Table 1.1 - Landmarks in the history of spinal biomechanics {Adapted from (Sanan and Rengachary, 1996)}.....2

Table 2.1 – Spinal regions and vertebrae numbering and main functions. 13

Table 2.2 – Limits and representative values of ranges of rotation of the lumbar spine {Adapted from (White and Panjabi, 1990)}. 15

Table 2.3 – Lumbar ligaments: acronyms, anatomical areas connected and functions. 20

Table 4.1 – Initial coordinates of the center of mass, local frame orientation, mass and moment of inertia of the rigid bodies considered in the presented model {Adapted from (Monteiro, 2009)}.....37

Table 4.2 – Posterior vertebral body height (VBHp), and upper (EPDu) and lower (EPDl) endplate depth of each considered vertebral body {Adapted from (Panjabi *et al.*, 1992)}.....38

Table 4.3 – Upper (ψ_U) and lower (ψ_L) endplate inclination for each vertebral body considered in the model (Adapted from (Panjabi *et al.*, 1992)). 39

Table 4.4 – Local coordinates of the points defining the bushing element (BE) and initial translational and angular offset between those points: S - slave body; M - master body {Adapted from (Monteiro, 2009)}. 39

Table 4.5 - Material properties of the bushing elements (BE) for several load directions {Adapted from (Monteiro, 2009)}.....41

Table 4.6 – Properties of the lumbar ligaments: stiffness coefficient, and transition and maximum strains {Adapted from (Pintar *et al.*, 1992)}.....44

Table 4.7 – Local coordinates used in the definition of the capsular ligaments (CL) in the lumbar spine {Adapted from (Monteiro, 2009)}. 44

Table 4.8 – Local coordinates used in the definition of the interspinous ligaments (ISL) in the lumbar spine {Adapted from (Monteiro, 2009)}. 44

Table 4.9 – Local coordinates used in the definition of the ligamentum flavum (LF) in the lumbar spine {Adapted from (Monteiro, 2009)}. 45

Table 4.10 – Local coordinates used in the definition of the anterior longitudinal ligaments (ALL) in the lumbar spine {Adapted from (Monteiro, 2009)}.....45

Table 4.11 – Local coordinates used in the definition of the posterior longitudinal ligaments (PLL) in the lumbar spine {Adapted from (Monteiro, 2009)}. 46

Table 4.12 – Local coordinates used in the definition of the supraspinous ligaments (SSL) in the lumbar spine {Adapted from (Monteiro, 2009)}. 46

Table 4.13 – Geometrical properties of the sphere-plane contacts: plane and sphere reference point and its corresponding limits for the articular facets {Adapted from (Monteiro, 2009)}..... 51

Table 4.14 – Geometrical properties of the sphere-plane contacts: plane and sphere reference points and its corresponding limits for the spinous process contacts {Adapted from (Monteiro, 2009)}..... 52

Chapter 1

Introduction

"Low back pain, the most common spinal disorder, affects over 80% of persons at some point in their life, and from 4 to33% of a population at any one time."

in *World Health Organization*, 2011

1.1. Motivation and Scope

The World Health Organization reports chronic diseases as the most common cause of mortality, with 63% of deaths worldwide. In 2008, 36 million people died from pathologies of this group, such as heart disease, stroke, cancer, chronic respiratory diseases or diabetes, among other, and from those, 9 million of the victims were younger than 60 years and 90% of those deaths occurred in low and middle-income countries (WorldHealthOrganization, 2011).

Such a broad group of pathologies embraces several types of disorders. For instance, the chronic rheumatic conditions is a subgroup of chronic diseases that comprises more than 150 diseases and syndromes that affect the musculoskeletal system and are generally progressive and associated with pain. The Portuguese Health Ministry reports rheumatic diseases as the most frequent group of illnesses in developed countries, having a vast socio-economic impact, since they originate functional disability and incapacity for work (MinistériodaSaúde, 2011).

From the chronic rheumatic conditions group, the pathologies with greatest impact on society are rheumatoid arthritis, osteoarthritis, osteoporosis and spinal disorders. This set of diseases can be even more narrowed as spinal disorders are a common source of incapacity, especially when related to rachialgia, or pain in the vertebral column. The most common type of rachialgia is low back pain (LBP), and this is a symptom rather than a disorder, since approximately 80% of the cases have no known cause.

Approximately 80% of the population has LBP at some point of their life and 5% has it continuously. The high incidence of this symptom does not mean it is fully understood, as 80-85% of the LBP occurrences do not have a known cause. Thereby, this is the most common cause of disability among people younger than 45 years.

From the known causes of LBP, the lumbar disc disease has been identified as the most common cause (Kraemer, 2008). This evidence is the motivation for this work, whose purpose is to develop a multibody lumbar spine model useful for simulation of this spinal region in several conditions such as the test of the physiologic limits.

1.2. Literature Review

Spinal biomechanics is a branch of Biomechanics, which is broadly described as the application of mechanical principles to biological systems, and has its roots back in the ancient Egypt. The first proof ever found about the study of the mechanics of the vertebral column dates back to 2000 BC and reports about spinal injury. A brief description of the most important publications in spinal biomechanics history is organized in Table 1.1.

Table 1.1 - Landmarks in the history of spinal biomechanics {Adapted from (Sanan and Rengachary, 1996)}.

Year	Author	Document	Significance
2600-2200 BC	Imhotep ?	*Edwin Smith surgical papyrus*	First record of spinal injury
3500-1800 BC	Unknown	*Srimad Bhagwat Mahapuranam*	First record of treatment for spinal deformity
460-361 BC	Hippocrates	*Corpus Hippocraticum*	Spinal manipulation practiced
1452-1519	da Vinci	*De Figura Humana*	First attempt to describe spinal stability
1543	Vesalius	*De Humani Corporis Fabrica*	Spinal anatomy accurately described
1646	Hildanus	*Opera quae Extant Omnia*	Routinely reduced cervical dislocations
1675	Descartes	*Tractus de Homine et de Fomatione Foetus*	Proposed mechanistic theory of the human body
1680	Borelli	*De Motu Animalium*	The "Father of Spinal Biomechanics"
1736	Euler	*De Curvas Elasticus*	Described mathematical stability of a column
1892	Wolff	*Das Gesetz der Transformation der Knochen*	Noted that trabeculae align along stress lines
1905	Burrell	*Fracture of the spine*	Seminal observations on spinal cord injury
1913	Wood-Jones	*The ideal lesion produced by judicial hanging*	Described the "hangman's fracture"
1970	Holdsworth	*Fracture, dislocations, and fracture-dislocations of the spine*	Two-column model of spinal stability
1983	Denis	*The three column spine and its significance in the classification of acute thoracolumbar spinal injuries*	Three-column model of spinal stability

Even though he was not the first author to describe spinal biomechanics, Giovanni Borelli is considered the "Father of Spinal Biomechanics", due to his 1680 book *"De Motu Animalium"*, in

which concepts such as the viscoelasticity of intervertebral discs are already described (Sanan and Rengachary, 1996).

Since then, the biomechanical study of the human vertebral column has evolved in several fields, from the clinical point of view in the analysis of vertebral geometries to the mechanical importance of spinal elements, such as muscles or the contact between facet joints.

The wide range of publications in this field becomes a large path in the search for information useful for the development of this work. Due to this circumstance, this literature review focuses on the multibody or hybrid spine models available, whether their focus is the cervical, lumbar or whole spine, having in mind its importance for the scope of this work. Apart from this field, a single reference is made to the work performed by Panjabi *et al.* (1992) in the geometric definition of the spinal components, accentuating the importance of this series of works in the creation of computer models, not only in the present project but also for various authors.

In 1995, Menon developed a two-dimensional model for the human head-neck-torso system using both rigid and rigid-flexible approaches to study the dynamic response and injury mechanisms of this system, by subjecting it to different acceleration/force pulses in order to simulate real crash situations. The multibody model included nine rigid bodies (head, 7 cervical vertebrae and the first thoracic vertebra) connected by revolute joints and resulting in nine degrees--of-freedom (DOF). The effect of muscles, intervertebral discs (IVD), cartilage, ligaments, cerebrospinal fluids and other tissues was included through non-linear rotational springs and dampers. The performed simulation analyzed the head's resultant linear and angular accelerations, velocity and position for acceleration values of 6 and 15 G applied to the T1 vertebra. The model has proved to be suitable for the correct evaluation of the Head Injury Criterion (HIC) (Menon, 1995).

De Jager (2000) presented a detailed three-dimensional mathematical model describing the dynamic behavior of the human head and neck in accident situation without head contact. His work has developed in three stages: (i) a global head-neck model was built, with rigid head and vertebrae, connected through 3D nonlinear viscoelastic elements that lumped the characteristics of IVD, ligaments and facet joints; (ii) detailed segments of the cervical spine were proposed, with 3D linear viscoelastic elements for the IVD, nonlinear viscoelastic elements for the ligaments, and frictionless contacts in the facet joints; and finally (iii) Hill-type muscles were included in the model

developed in the previous step (de Jager, 2000). Figure 1.1 shows the schematic representation of the global model with local coordinate systems.

After several tests, calibration with human volunteers, introduction of loads, de Jager concluded that the active muscle behavior was essential to describe the system's response to impact and that his model was computationally efficient, suitable for car safety improvement, and calculation of neck injury criteria, since the loads and deformations of individual tissues are computed through the model.

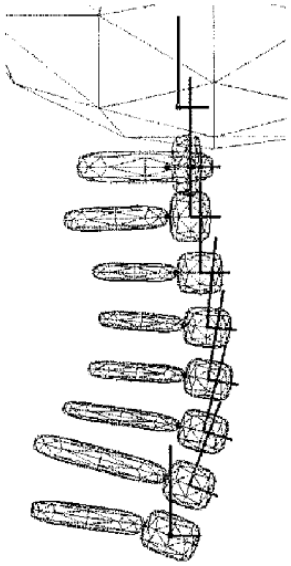

Figure 1.1 – Lateral view of de Jager's model: base of the skull and vertebrae, showing the body local coordinate systems {Adapted from (de Jager, 2000)}.

A detailed geometry is not always a synonym of accuracy on the outputs. Waters and co-workers (2003) presented a multibody model for the assessment of the risk of low back disorders due to occupational exposure to jarring and jolting from operation of heavy mobile equipment. The full 17 rigid bodies model of the whole body initially used was replaced by a simpler approach. Figure 1.2 illustrates the 4-body model representing head/neck and upper, middle and lower torso interconnected by a set of springs and dampers that was used to simulate the gross motion of the spine, becoming a more efficient system and not losing accuracy.

Using seat acceleration data from vehicles as input this model allows for the evaluation of the forces generated at the seat, and the force at the L5/S1 joint for the same input. It is also possible to calculate the cumulative adverse health effects factor for a low and high risk jarring and jolting.

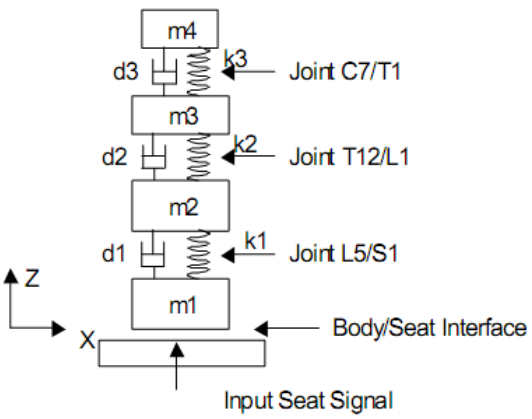

Figure 1.2 – Spine/neck and head model developed for analysis of spinal loading {Adapted from (Waters *et al.*, 2003)}.

The work proposed by Esat (2006) represents a hybrid model of the whole spine, comprising a multibody model used for dynamics analysis of impact situations, and a finite element analysis to study the causes of injury in specific spinal components. The reaction forces associated with lumbar motion segments, for instance, are used to analyze the gross kinetics and kinematics of the spine, and also as the boundary conditions for the finite element model of the selected spinal components.

This multibody model used geometric data from computer tomography (CT) imaging, improving the definition of surfaces and therefore providing more realistic data to the contacts. The vertebrae were modeled as rigid bodies, interconnected by linear viscoelastic IVD elements, nonlinear viscoelastic ligaments and contractile muscle elements with passive and active behavior. The influence of the contact forces was not included. The validation of this model was performed by subjecting the model to a 10 Nm flexion moment at the L1 level, and comparing the flexion moment results and intradiscal pressure obtained with other validated models. The model showed good agreement with literature data in both situations.

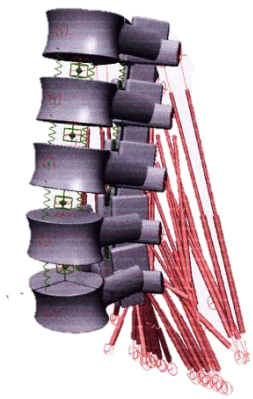

Figure 1.3 – Esat multibody model of the lumbar spine {Adapted from (Esat, 2006)}.

Ferreira (2008) established a three-dimensional cervical multibody spine model with 9 rigid bodies (head, 7 cervical vertebrae and the first thoracic), connected by six bushing elements with 6 DOF each (for the IVD) and constrained by nonlinear viscoelastic elements simulating the ligaments. Contact events between bony elements (between facet joints and spinous processes) were also included as sphere-plane nonlinear contact forces, following the Kelvin-Voigt formulation.

The model was built for simulation of traumatic and degenerative disorders, such as rheumatoid arthritis. Figure 1.4 shows the sagittal (upper row) and frontal view (lower row) of the configuration of the model during an impact simulation. Changing the range of motion and other properties of the elements of the model, according to the effects of the disorder reported in literature, allowed to conclude that the transverse ligament is the most important in maintaining the neck stability, whereas the lateral impact simulation reported element forces and ranges of motion for the different cervical levels.

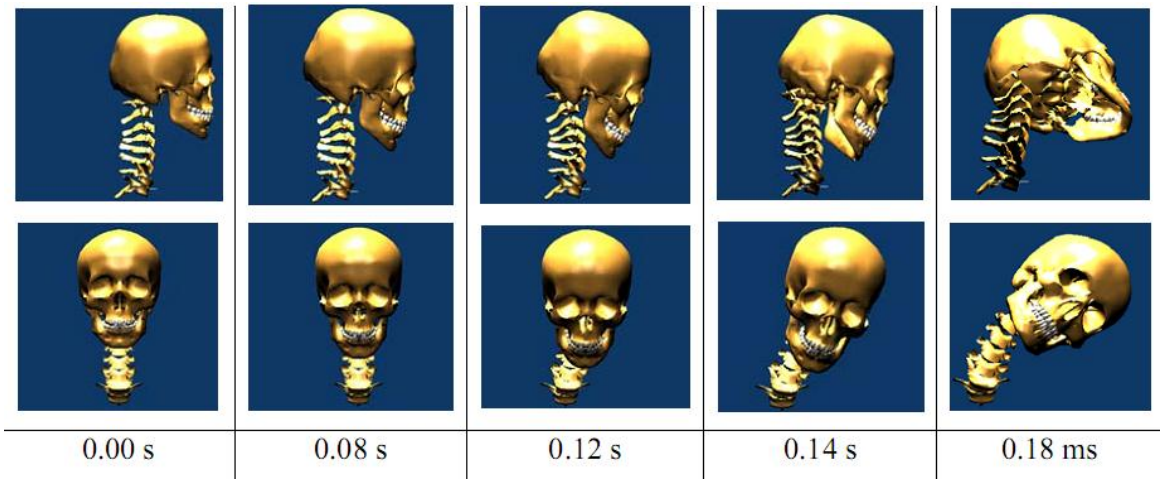

Figure 1.4 – Configuration of the model during the lateral impact simulation (from t=0 s to t=0.18 s). The upper row represents the sagittal view and the lower row a frontal view {Adapted from (Ferreira, 2008)}.

Fairman *et al.* (2009) developed a multibody model of the lumbar spine with the MATLAB® simulation tool Simulink™. Simple geometric shapes were used to model the vertebrae, and the joints between them were modeled as a network of springs and dampers representing not only IVDs but also ligaments. Virtual muscles were added as actuators of the model. Figure 1.5 depicts the model obtained by Fairman and co-workers under a loading situation.

A forward dynamics analysis was performed and the forces in the lumbar joints could not be calculated through this simulation. The model was tested with the input of a sinusoidal path to encourage smoothness of the motion (amplitude of 20 degrees and frequency of 1.67 Hertz),

considering only the L5-S1 joint as a working joint, and results showed that the maximal compression forces at the pelvis reached 1600 N, and over 1000 N when lifting a 10 kg load.

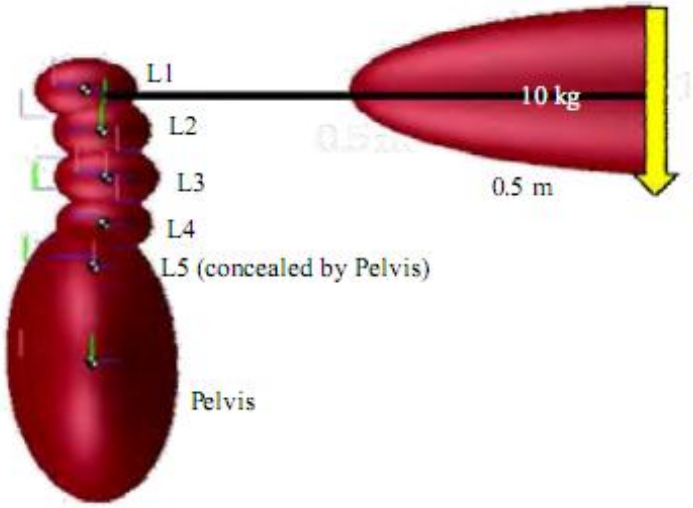

Figure 1.5 - Multibody model of the lumbar spine developed in Simulink™, under a loading situation {Adapted from (Fairman *et al.*, 2009)}.

The work of Juchem (2009) comprised a three-dimensional computer model of the lumbar spine for the determination of mechanical stresses. Five rigid bodies were modeled (L2 to L5 vertebrae and the sacrum), and their geometries were obtained through computer tomography (CT) measurements. The multibody system (MBS) methodology was applied and the IVDs were modeled as elastic elements between the corresponding vertebral bodies. The effect of the ligaments and the contacts between bony parts (facet joints) were also included. Figure 1.6 represents the lumbar spine model obtained, comprising vertebrae L2 to sacrum.

The model was subjected to an external force of 395 N acting on the top of the L2 vertebra to simulate the upper body's weight. The performed simulation allowed the calculation of forces and moments in each IVD as well as the forces in the ligaments, confirming the aptitude of the MBS modeling in the estimation of forces and moments in biological structures. It was referred the further applicability of the model in calculating stresses in intact IVDs resulting from the implantation of devices (Bauer and Gruber, 2009; Juchem, 2009; Juchem and Gruber, 2009).

Figure 1.6 – MBS model of the lumbar spine (L2 - sacrum) obtained by Juchem {Adapted from (Bauer and Gruber, 2009)}.

Recently, a hybrid model was created by Monteiro (2009), using multibody system dynamics and finite element analysis in a cervical and lumbar detailed model, for the analysis of the intersomatic fusion between one or more spine levels. The multibody formulation was used for the rigid vertebrae, ligaments, contacts between facet joints and spinous processes and some intervertebral discs, and the finite element models were applied to some other intervertebral discs and the fixation plate used to implement the intersomatic fusion.

Figure 1.7(a) denotes a two vertebrae co-simulation model and Figure 1.7(b) shows a representation of the finite element mesh of a fixation plate model with titanium fixation screws, both used in the hybrid simulation.

The IVD were modeled as 6 DOF linear viscoelastic bushing elements, the ligaments as nonlinear elastic springs with hysteretic behavior and the Kelvin-Voigt contact force model was applied to the spinal contacts. The muscles were not included in this model.

The validation of the lumbar spine for flexion-extension movements showed moments within the range of the literature consulted by Monteiro. This model was subjected to a 1.5 Nm moment applied to the L1 vertebra during 400 ms while the S1 was kept fixed and a 500 N load was applied to the upper surface of L1 to simulate the torso weight, and allowed to confirm its capacity of predicting accurately axial rotation and extension motion (Monteiro, 2009).

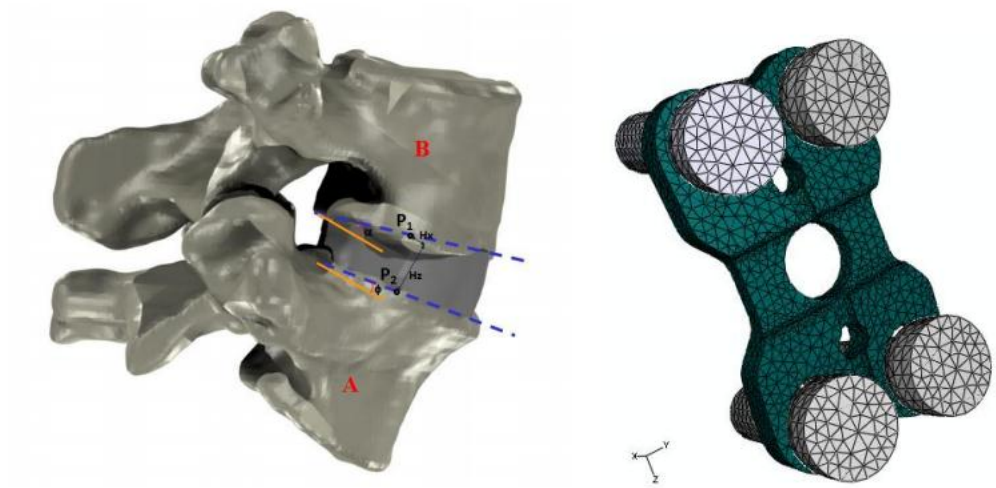

(a) (b)

Figure 1.7 – Hybrid model developed by Monteiro: (a) co-simulation model; and (b) fixation plate model with titanium fixation screws {Adapted from (Monteiro, 2009)}.

Christophy (2010) presented a detailed open-source musculoskeletal model of the human lumbar spine, focusing on the effect of the muscles in the spine motion. Figure 1.8 shows the model obtained using the toolbox OpenSim, that uses the dynamics engine known as SimBody, where it is possible to see two different postures (neutral and 50° flexion) evidencing the muscle fascicles, rigid bodies and intervertebral joints.

The intervertebral joints have 6 DOF and the muscles follow the Hill-type and the Thelen's muscle models. As main results of the performed simulation, the moments developed at the L5/S1 joint by the different groups of muscles in the flexion/extension movement were computed. It was possible to confirm the two primary flexor muscle groups (erector spinae and rectus abdominis) generated larger moments (approximately 60 Nm) than the stabilizer muscles (quadratus laborum, multifidus, and psoas) (approximately 10 Nm). Despite the good results and accuracy of the model, the force produced by ligaments and the contact between facet joints is not modeled. However, this model represents a starting point for the study of low back pain as a consequence of joint degeneration in combination with altered muscle activation patterns (Christophy, 2010).

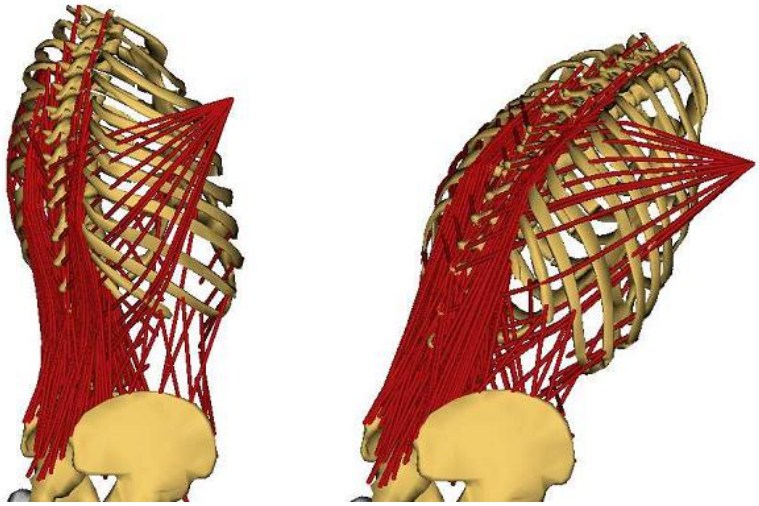

(a) (b)

Figure 1.8 – Detailed musculoskeletal model of the lumbar spine developed by Christophy, comprising 238 muscle fascicles, 13 rigid bodies, and 5 intervertebral joints: (a) neutral posture and (b) 50° flexion {Adapted from (Christophy, 2010)}.

Abouhossein and co-workers (2011) created a three-dimensional multibody lumbar spine model to determine the load sharing between passive elements of the spine. Figure 1.9 shows the model developed with the MSC.ADAMS software®. The model comprises 6 rigid bodies (5 lumbar vertebrae and sacrum), nonlinear flexible elements with 6 degrees-of-freedom for the IVD, tension-only force elements for the ligaments and Kelvin-Voigt contact forces between facet joints, not including muscle force.

The application of three different input moments (-15 Nm extension, 15 Nm flexion and 30 Nm flexion) to the center of the L1 vertebral body allowed to retrieve the load sharing between each IVD, the different ligaments and the facet joints, in the L4/L5 segment, showing a slight difference to the literature, justified by the lack of geometrical information match between model and comparative literature, and by the absence of nonlinear damping coefficients with changes depending on velocity values for each segment (Abouhossein *et al.*, 2011).

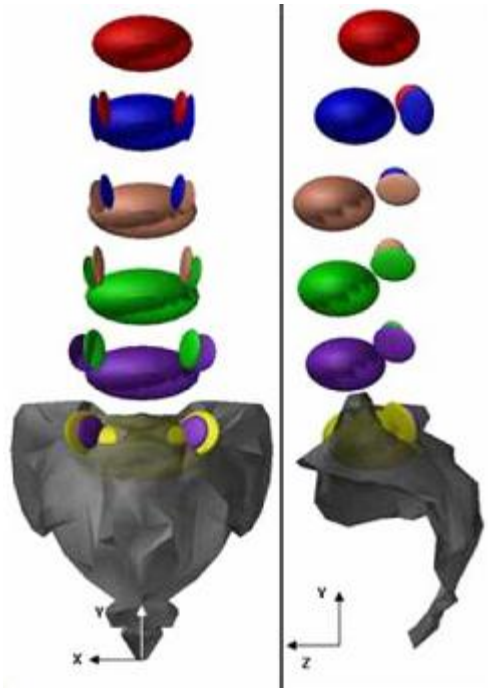

Figure 1.9 – Lumbar spine model (L1-sacrum) obtained with MSC.ADAMS® software {Adapted from (Abouhossein *et al.*, 2011)}.

1.3. Objectives of this Work

The main objective of this work is to develop a computer model of the lumbar spine, using the multibody system methodologies. For this purpose, specific formulations for the three main elements present on the spine multibody are proposed namely the ligaments, the intervertebral discs and the potential contacts between adjacent vertebrae.

The obtained model can be useful to simulate the biomechanics of the lumbar spine in non-pathologic situations, as well as during alterations verified throughout pathological conditions.

1.4. Structure of the Thesis

This thesis contains six main chapters organized as follows.

In the first Chapter, the motivation and scope of the present work are presented and a literature review of the state-of-the-art of this field of investigation is provided. The objectives and contributions of this work are also offered.

Chapter Two focuses on the characterization of the spine, starting from a brief description of that structure anatomy (regarding mainly the vertebrae, intervertebral discs and ligaments) and reporting previous studies and pathologies in this anatomical region, and emphasizing the characteristics of the most relevant for this work.

In the third chapter, the multibody system formulation is presented in a review manner. Therefore, the concept, the explanation of the cartesian coordinates, the kinematic constraints, equations of motion and the numerical integration are presented.

Chapter Four fully describes the developed spine model, namely the geometric description of the rigid bodies, the connection between bodies with bushing elements, the introduction of the forces applied by the ligaments and, finally, the constitutive laws applied when contact between bodies takes place.

The results obtained from computational simulation are analyzed and discussed in Chapter Five.

Chapter Six summarizes the main concluding remarks of this work and provides some future perspectives for future research.

Finally, this thesis ends with a full list of references.

1.5. Contribution of this Work

The contributions of this thesis can be listed in the following manner:

- A complete literature review on the existing spine multibody models is offered;
- A full characterization of the human spine is presented;
- The available solutions for degenerative disc disease are analyzed;
- The geometric, inertial, and material properties of the human spine are presented;
- A biomechanical spine multibody model for dynamic analysis is proposed.

Chapter 2

Characterization of the Spine

2.1. Anatomy

The vertebral column, or spine, is a complex structure that has three main functions: (i) transferring weights and the resulting bending moments of the head, trunk, and any weights lifted to the pelvis, (ii) allowing physiologic motion between the aforementioned body parts and (iii) protecting the spinal cord from damaging forces or motions produced by physiologic movements and/or trauma. The spine is composed typically by 33 bony elements (the vertebrae) divided in five regions, from head to pelvis, as described in Table 2.1.

Table 2.1 – Spinal regions and vertebrae numbering and main functions.

Spinal region	Vertebrae numbering	Main functions
Cervical	C1 – C7	Axial skeleton of the spine; Support the head and allow motion.
Thoracic	T1 – T12	Suspend the ribs; Support the respiratory cavity.
Lumbar	L1 – L5	Allow mobility between the thoracic portion of the trunk and the pelvis.
Sacral	S1 – S5	Connect the vertebral column to the bones of the lower limb girdle.
Coccygeal	-	Support the pelvis floor.

Besides vertebrae, the spine includes other fundamental elements: from C2 to S1, between each pair of vertebrae, lies an intervertebral disc (IVD) that allows relative motion between bony parts. Articulations, ligaments, tendons and muscles are also present along the whole vertebral column, allowing or restraining some movements.

The unique arrangement of the different regions provides stability, resistance and elasticity to the spine, as well as the absorption of vibrations and/or impacts. There are four physiologic curvatures of the vertebral column in the sagittal plane, as illustrated in Figure 2.1.

Two of these curvatures are anteriorly convex in the cervical and lumbar regions (lordotic) and the other two are posteriorly convex in the thoracic and sacral regions (kyphotic). These curvatures and arrangements allow the spine to perform three different basic kinds of movements: the flexion/extension (forward/backward, respectively), lateral bending and axial rotation.

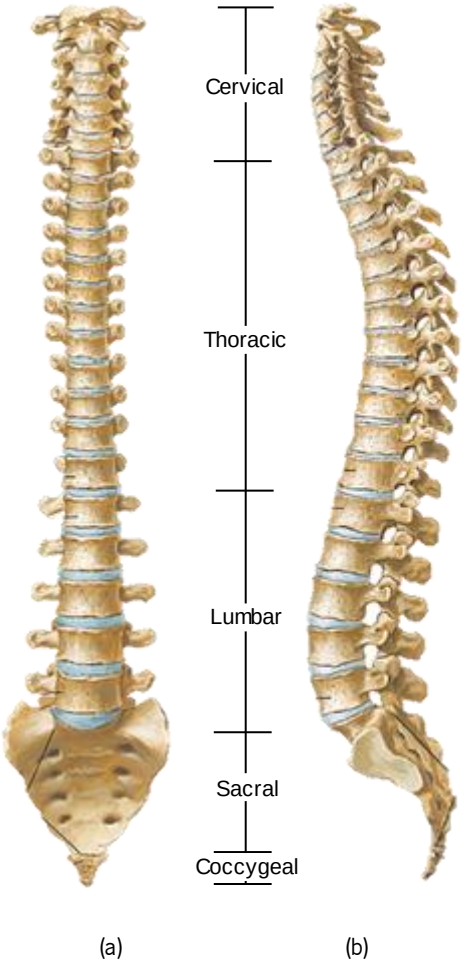

Figure 2.1 - Views of the vertebral column, showing the different regions: (a) frontal view; (b) lateral view {Adapted from (Gray, 1918)}.

The possible movements of the spine, as well as the range of motion for each one, regarding the vertebral column as a whole are illustrated in Figure 2.2

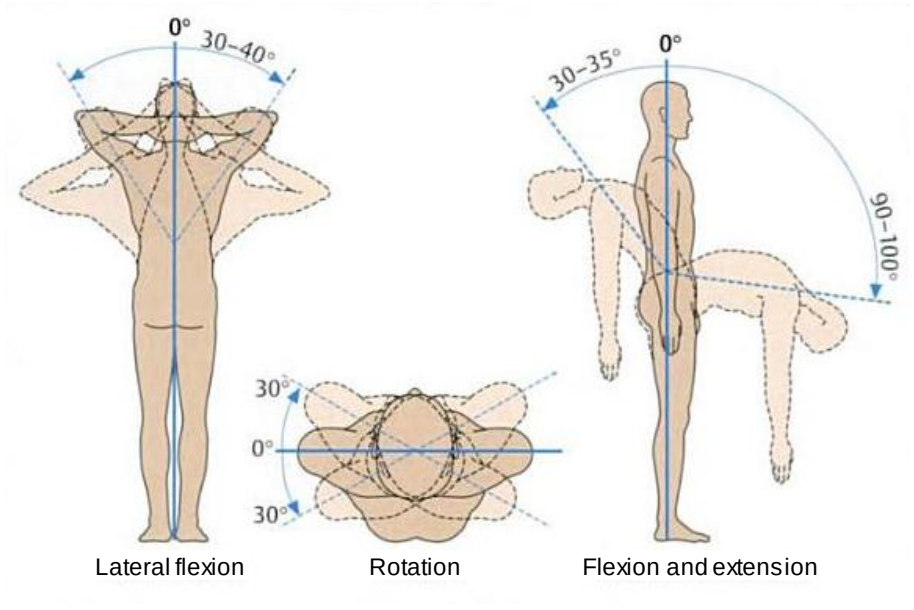

Figure 2.2 – Mobility of the vertebral column: the extent of mobility from zero position (0°) is given in degrees {Adapted from (Faller *et al.*, 2004)}.

Even though the cervical spine is the region with the wider range of motion, the thoracic segment allows primarily axial rotation and the lumbar region is the main responsible for flexion and extension movements. It is verified an increase of the flexion and extension range of motion from the first lumbar vertebra (L1) to the fifth (L5), and the lumbosacral joint (L5-S1) permits a wider motion in the sagittal plane than the other lumbar joints. Hence it is speculated that the high incidence of disc disease at the L4-L5 and L5-S1 levels is related to mechanical problems, as these two areas tolerate the highest loads and amount of motion in the sagittal plane (White and Panjabi, 1990). For this reason, the analysis performed in this work focuses on the lumbar spine, and Table 2.2 shows the limits and representative values of the ranges of rotation in this spinal region.

Table 2.2 – Limits and representative values of ranges of rotation of the lumbar spine {Adapted from (White and Panjabi, 1990)}.

Interspace	**Combined flexion-extension**		**One side lateral bending**		**One side axial rotation**	
	Range of rotation [deg]	**Representative angle [deg]**	**Range of rotation [deg]**	**Representative angle [deg]**	**Range of rotation [deg]**	**Representative angle [deg]**
L1-L2	5 - 16	12	3 - 8	6	1 - 3	2
L2-L3	8 - 18	14	3 - 10	6	1 - 3	2
L3-L4	6 - 17	15	4 - 12	8	1 - 3	2
L4-L5	9 - 21	16	3 - 9	6	1 - 3	2
L5-S1	10 - 24	17	2 - 6	3	0 - 2	1

2.1.1. The Vertebrae

Although the vertebrae of each spinal region have different characteristics, some features are common to all of them. The vertebra is composed by two main parts: a vertebral body and the posterior elements. Between these two parts exists a space called the vertebral foramen, through where the neural elements (*e.g.* the spinal cord) pass.

The vertebral body is the disc-shaped bony part in the anterior area of the spine and it is essential to withstand the compressive forces of the vertebral column. Two pedicles, bony parts between the superior and inferior surfaces of the vertebral body, project one from each side of it. Projecting backwards from each pedicle is a sheet of bone called lamina, and both laminae meet at a midline is the posterior part of the vertebrae. The assembly of the two pedicles and the two laminae forms an element called neural arch, as it surrounds the neural elements of the spine (as the spinal cord) and envelops the vertebral foramen, as visible in Figure 2.3(a).

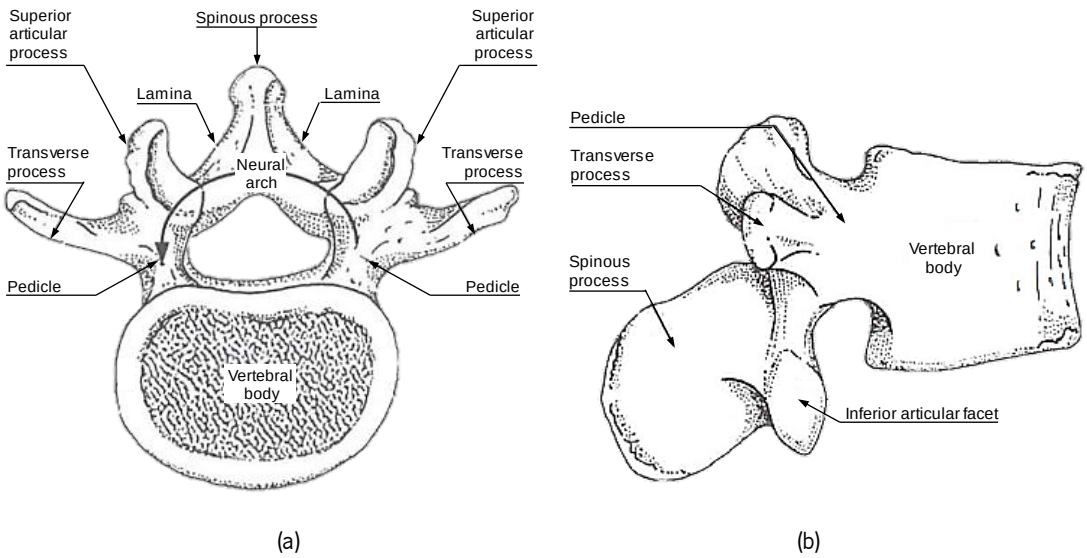

Figure 2.3 – Parts of a typical lumbar vertebra: (a) top view; (b) lateral view {Adapted from (Bogduk, 2005)}.

Other bony elements extend from the junction between lamina and pedicle: when directed upwards, this extension is called superior articular process; the downwards extension is called inferior articular process. Therefore, each vertebra has four articular processes: two on the right and other two on the left side. The medial surface of each superior articular process and the lateral surface for each inferior articular process are covered by articular cartilage and thus those regions are called the articular facets of the articular processes.

Each junction lamina-pedicle has another flat, rectangular process that extends laterally from it, called the transverse process, due to its orientation. Once again, each vertebra has a pair of these processes, which are used as attachment sites for ligaments and muscles.

Located on the most posterior part of the vertebral, after the midline junction of the two laminae, there is spinous process which is the element easily perceived through its protuberance under the skin of the back. As visible in Figure 2.3(b), this process merges imperceptibly with the laminae and it is an attachment point for muscles and ligaments.

All the vertebral components have an outer shell of hard, strong cortical bone whereas the inside is composed of soft, spongy cancellous bone.

Even though all the aforementioned elements are common to vertebrae from all the spinal regions, the lumbar vertebrae have some characteristics that are unique to this region, such as the mammillary and accessory processes, useful for muscle attachment.

After the lumbar vertebrae is the sacrum, an aggregate of five vertebrae fused with each other. It is the foundation for the pelvic girdle and the anterior and posterior sides of the sacrum contain four pairs of sacral foramina, through which nerves and blood vessels pass. The coccyx is composed by the fusion of the four coccygeal vertebrae. The top of the coccyx articulates with the sacrum.

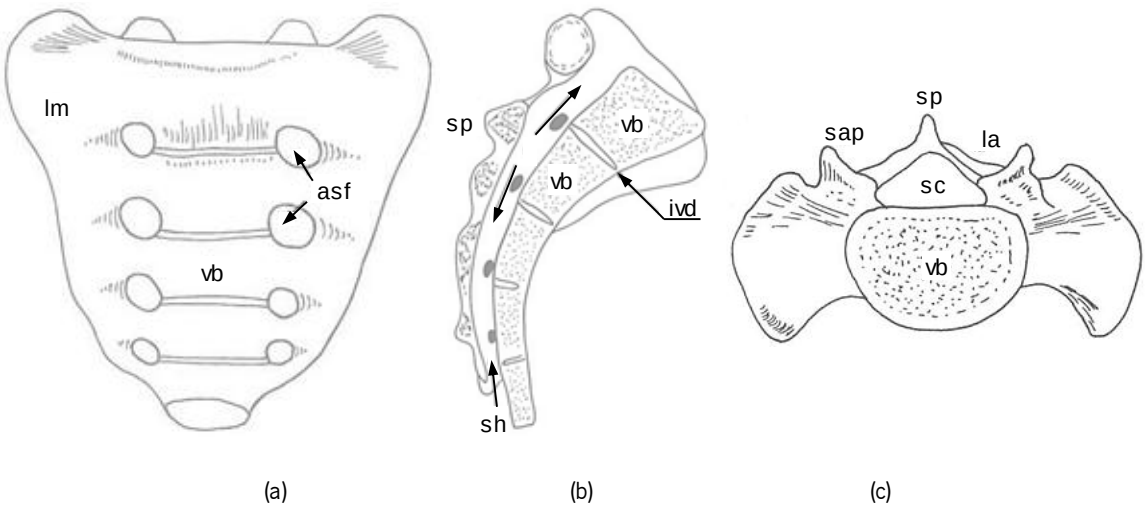

Figure 2.4 – The sacrum: (a) frontal, (b) sagittal and (c) transverse view. Anterior sacral foramina (asf), remnants of the intervertebral disc (ivd), lamina (la), lateral mass (lm), superior articular process (sap), sacral canal (sc), sacral hiatus (sh), spinous process of S1 (sp) and vertebral bodies (vb) {Adapted from (Bogduk, 2005)}.

2.1.2. The Intervertebral Disc

There are 23 intervertebral discs (IVD) in the vertebral column, between each pair of vertebrae from C2 to S1. Their deformable characteristics allow a small amount of movement in

each spine level, but a large range of motion (from -30° to 90°, in the sagittal plane) when functioning simultaneously (Faller *et al.*, 2004). Altogether, they represent 20-33% of the entire height of the spine and each one can be divided in three different parts (White and Panjabi, 1990): (i) the nucleus pulposus (NP), (ii) the annulus fibrosus and (iii) the cartilaginous vertebral endplates, as visible in Figure 2.5.

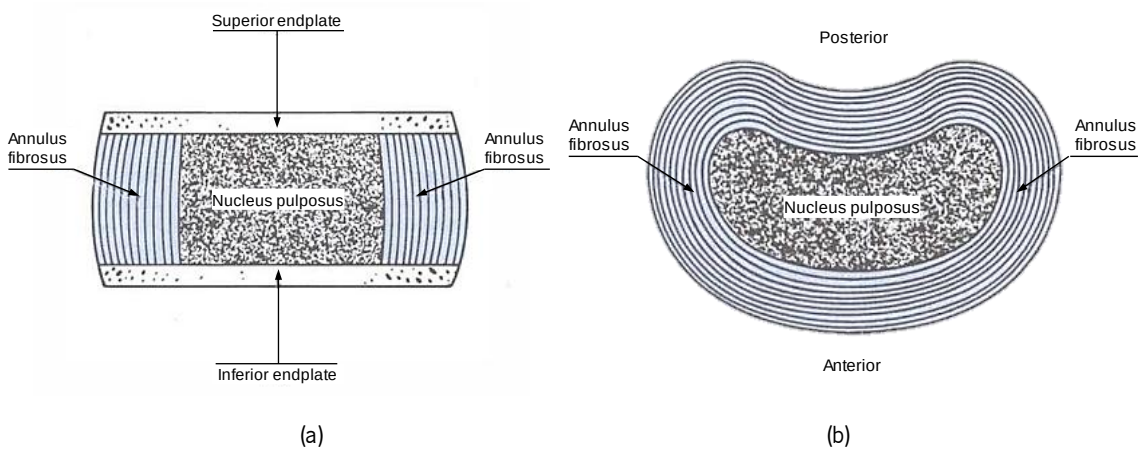

Figure 2.5 - The intervertebral disc: (a) sagittal section and (b) transverse section {Adapted from (Bogduk, 2005)}.

The NP is the central area of the IVD and it is composed mostly by water in a matrix of collagen, proteoglycans and other matrix proteins. This water content is higher at birth (approximately 90%) and decreases to 80% at the age of 20 and to 70% at 60 years old. The NP has up to 65% of the dry weight in proteoglycans (proteins), several types of glycosaminoglycans (polysaccharides) and circa 15% of various types of collagen. There are still some cartilage cells in the NP, although in a concentration inferior to the AF and the endplates (Séguin *et al.*, 2004).

The AF is a fibrocartilaginous element that encapsulates the NP and consists of 10-20 concentric lamellae of collagen fibers, in which those fibers are arranged parallel to each other. However, in each adjacent lamella the collagen fibers have different orientations: -30° with the vertical in a lamella and 30° in the adjacent lamella.

The cartilaginous endplates (present above and below each NP and AF) are hyaline cartilages that separate the NP and AF from the bony vertebrae.

2.1.3. The Lumbar Ligaments

The ligaments are elements with a complex architectural hierarchy that connect two or more bones. They are bands of fibrous connective tissue, composed mainly by water (55-65%). The remaining dry matter (35-45% of the total weight) is divided in 70-80% of collagen (type I), 10-15%

of elastin and 1-3% of proteoglycans. Figure 2.6 depicts the hierarchical organization of the ligament, showing the names and diameters of the different subelements.

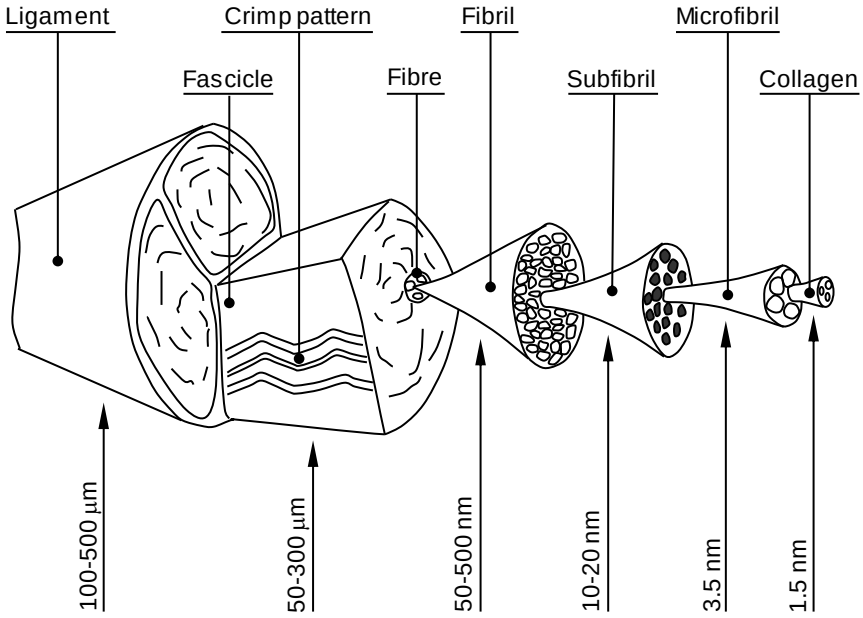

Figure 2.6 – Hierarchical organization of the ligaments: names and diameters of the subelements {Adapted from (Herman, 2007)}.

Furthermore, the ligaments can be divided in two main categories: intrasegmental and intersegmental. The first group comprises ligaments that connect two bones and the second contains ligaments that join more than two bones (Boos and Aebi, 2008). Figure 2.7 shows a scheme that distributes the ligaments present in the lumbar spine for each of the abovementioned groups.

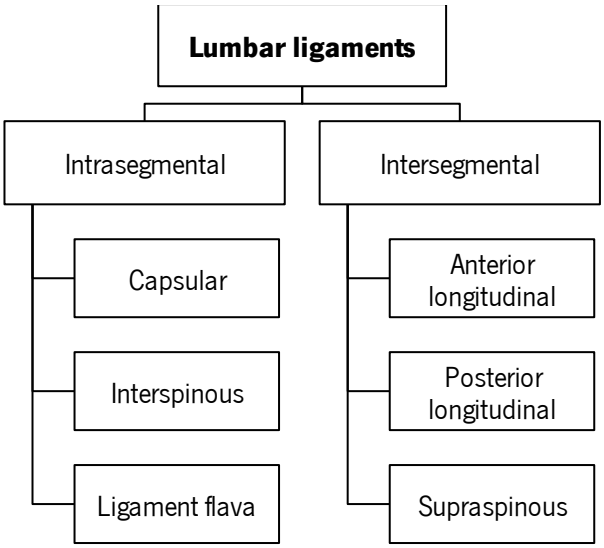

Figure 2.7 – Ligaments in the lumbar spine: division in intra- and intersegmental.

As visible in Figure 2.7, from all of the spinal ligaments it is possible to highlight six types in the lumbar region: in the intrasegmental group, the capsular ligaments (CL), ligament flava (LF) and the interspinous ligament (ISL), and in the intersegmental group, the anterior and posterior longitudinal ligaments (ALL and PLL) and the supraspinous ligament (SSL). Figure 2.8 shows two adjacent lumbar vertebrae and the ligaments present between them.

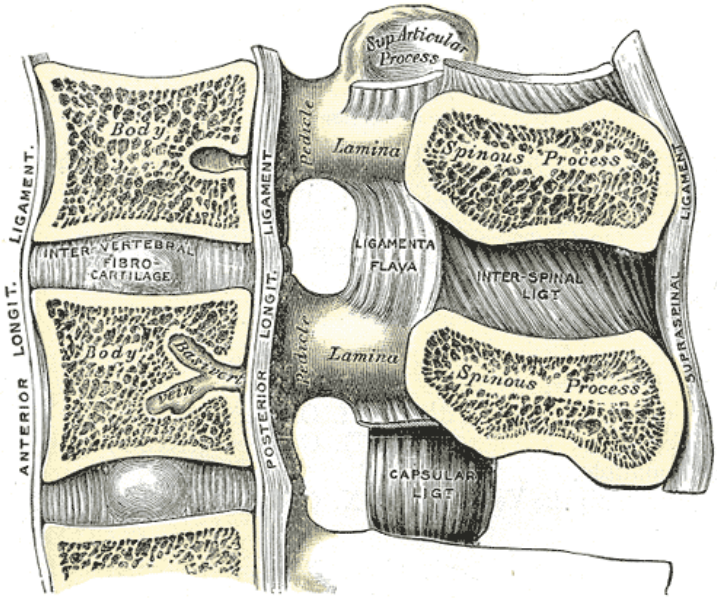

Figure 2.8 - Medial sagittal section of two lumbar vertebrae and their ligaments {Adapted from (Gray, 1918)}.

It is possible to observe that the ligamentum flavum, an intersegmental ligament, only connects two adjacent vertebrae and, in the other hand, the posterior longitudinal ligament, an intrasegmental one, runs along the posterior surface of several vertebral bodies.

In order to simplify the understanding of the properties of each ligament, Table 2.3 summarizes the lumbar ligaments names, acronyms, anatomical areas connected and main functions (Behrsin and Briggs, 1988; Rogers and Jacob, 1992).

Table 2.3 – Lumbar ligaments: acronyms, anatomical areas connected and functions.

	Ligament name	**Acronym**	**Connects**	**Functions**
Intersegmental	Capsular	CL	Envelopes surrounding the facet joints.	Resist axial rotation of the spine
	Interspinous	ISL	Roots of spinous processes of adjacent vertebrae	Little resistance to forward bending spinal movements
	Ligamentum Flavum	LF	Front surface of the laminae of adjacent vertebrae	Resist excess separation of laminae

Table 2.3 – Lumbar ligaments: acronyms, anatomical areas connected and functions (*continued*).

	Ligament name	Acronym	Connects	Functions
Intrasegmental	Anterior Longitudinal	ALL	Anterior aspects of the vertebral bodies and IVD	Resists extension of the spine
	Posterior Longitudinal	PLL	Posterior aspects of the vertebral bodies and IVD	Resists separation of the posterior ends of the vertebral bodies
	Supraspinous	SLL	Posterior edges of the spinous processes	Little resistance to separation of the spinous processes

2.2. Spinal Disorders

Spinal disorders are a broad variety of diseases that affect the spinal components: the vertebrae, intervertebral discs, facet joints, ligaments and tendons, muscles, spinal cord and nerve roots of the spine. It is possible to classify these disorders in two groups, as noticeable in Figure 2.9: (i) the specific and (ii) the non-specific spinal disorders. The first group comprises 10-15% of all the reported disorders, and includes all those which are directly relatable to their source, such as congenital, developmental, traumatic, infectious, tumorous, metabolic and degenerative (the latter depends on the type of disorder). The non-specific spinal pain (cervical, thoracic or lumbar) belongs to the second group, involving 85-90% of the cases (Boos and Aebi, 2008).

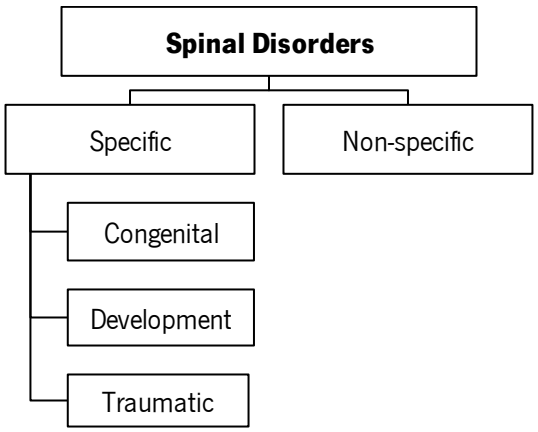

Figure 2.9 – Spinal disorders: a division in specific and nonspecific disorders.

Various diseases that affect the vertebral column are usually painful and influence the patient's everyday life.

- Disc herniation is a leakage of the nucleus pulposus through a tear in the wall of the annulus fibrosus. This leakage presses on the local nerve root causing the pain. Tears in the wall usually occur due to aging and/or trauma.

- Spinal stenosis is the narrowing of the spinal canal and can be caused by different conditions such as disc herniation, osteoporosis, or a tumor. Sometimes, and especially when the reason is a disc herniation, stenosis occurs at the same level of the disc.
- Degenerative disc disease is the gradual deterioration of the disc causing loss of its functions. This disease usually develops with aging or from continuous activities that press on the disc space. It starts with a small injury in the annulus fibrosus causing damage to the nucleus pulposus and loss of its water contents. Further damage causes malfunctioning of the disc and thus collapsing the upper and lower vertebrae. As time passes, the vertebrae facet joints twist creating bone spurs that grow into the spinal canal and pinching the nerve root (stenosis).
- Disc desiccation is the drying of the water contents in the inner pulposus. Usually, it is caused by aging and sudden weight loss.
- Spinal infection occurs when a bacterial infection travels via the bloodstream into an intervertebral disc. This weakens the annulus fibrous, decays it, and might cause collapsing of the disc and thus pressure on the nerve root. Further infection might cause fusion of the enclosing vertebrae.

Degenerative Disc Disease

The degenerative disc disease (DDD) arises as a series of symptoms rather than a pathology by itself. However, the morphologic changes of the intervertebral disc throughout the degenerative process are evident macroscopically. Thompson *et al.* (1990) established a grading system in order to categorize the degeneration stage of the IVD. This classification comprises five stages, from grade I to grade V: (i) normal juvenile disc, (ii) normal adult disc, (iii) early stage, (iv) advanced stage, and (v) end stage. Figure 2.10 illustrates the different degenerative grades.

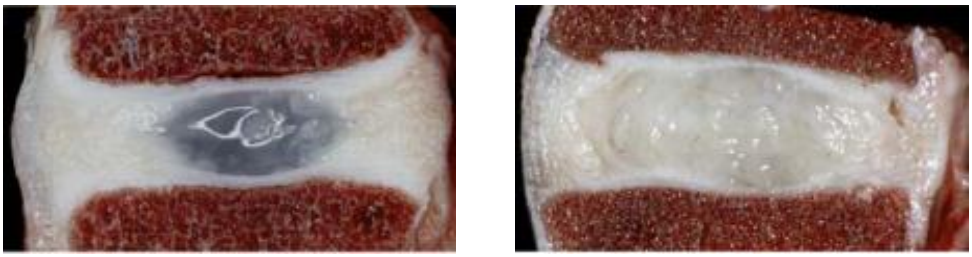

(a) (b)

Figure 2.10 – Macroscopic disc changes due to DDD, according to Thompson's classification: (a) grade I; (b) grade II; (c) grade III; (d) grade IV; (e) grade V {Adapted from (Boos and Aebi, 2008)}.

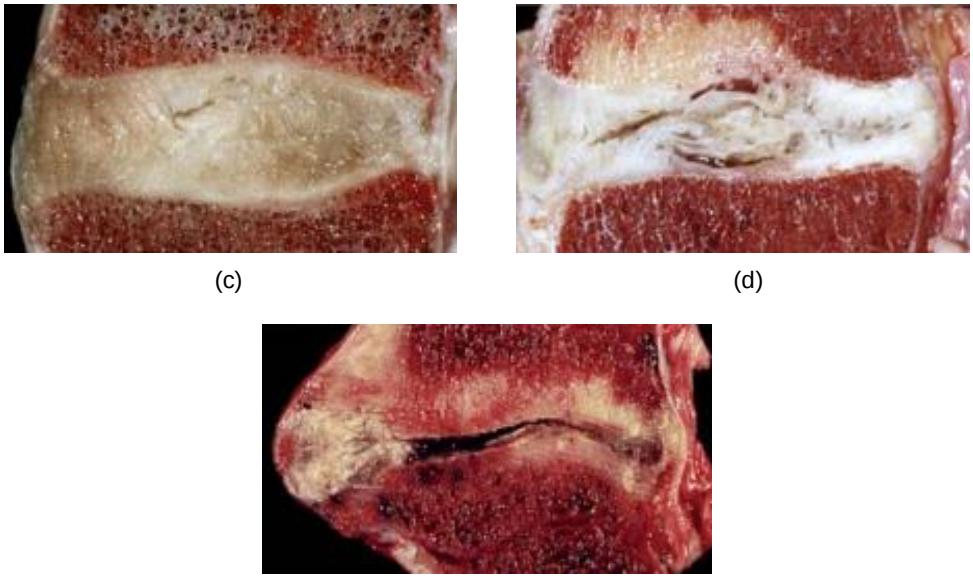

(c) (d)

(e)

Figure 2.10 – Macroscopic disc changes due to DDD, according to Thompson's classification: (a) grade I; (b) grade II; (c) grade III; (d) grade IV; (e) grade V {Adapted from (Boos and Aebi, 2008)} (*continued*).

Regarding Thompson's classification, a segmental flexibility study was performed by Fujiwara *et al.* (2000) and Tanaka *et al.* (2001). Human functional spinal units (FSU) with different grades of disc degeneration were mechanically tested through the application of moments in flexion/extension, axial rotation and lateral bending. The resultant three rotation angles of the superior vertebra relatively to the inferior fixed one were plotted. It was possible to conclude that the axial rotational motion was the most affected by degeneration, and that the segmental flexibility increased with the increase of the severity of disc degeneration until grade IV, but decreased from grade IV to grade V. Moreover, it was verified that segmental flexibility depends also on cartilage degeneration and gender.

Adams and Dolan (2005) analyzed the current trends in spine research and outlined the desirable areas for investigation. According to these authors, there should be a focus on understanding the interactions between IVDs and the adjacent vertebrae, as well as in the development of prosthetic and tissue-engineered discs, and in the quantification of the spinal function during rehabilitation. Within this perspective review, a study by Pollintine *et al.* (2004) was referred in which the degeneration of the IVD was associated with "stress shielding" of the anterior vertebral body, and possibly with one of the causes of osteoporotic vertebral fracture. Figure 2.11 shows the load sharing in the lumbar spine in erect posture. With a normal disc (Figure 2.11(a)), the neural arch resists only 8% of the applied compressive force and the rest is shared by the anterior and posterior areas of the vertebral body. However, in a situation of severe intervertebral

disc degeneration (Figure 2.11(b)), the neural arch bears 40% of the load, leaving only 19% of the load in the anterior part of the vertebral body.

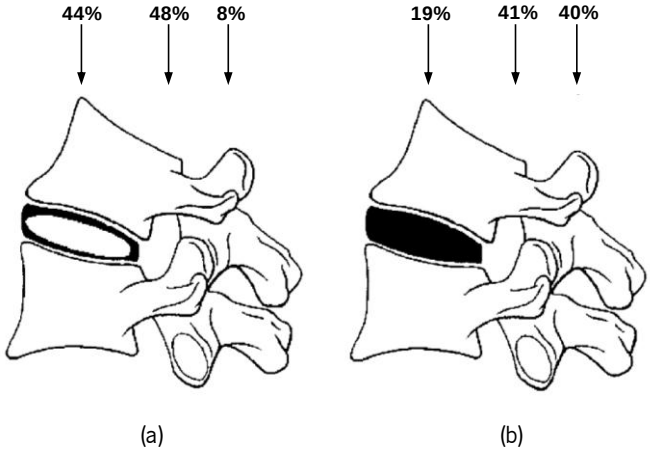

Figure 2.11 – Load sharing and intervertebral disc degeneration: (a) normal disc; (b) degenerated disc {Adapted from (Pollintine *et al.*, 2004)}.

Trauma in the Lumbar Spine

In 1983, Denis created a classification for thoracolumbar fractures that has been used since then by several authors. For this arrangement it was assumed that the vertebral column can be divided in three areas in the sagittal plane, as visible in Figure 2.12: the anterior (a), the middle (b) and the posterior (c) column.

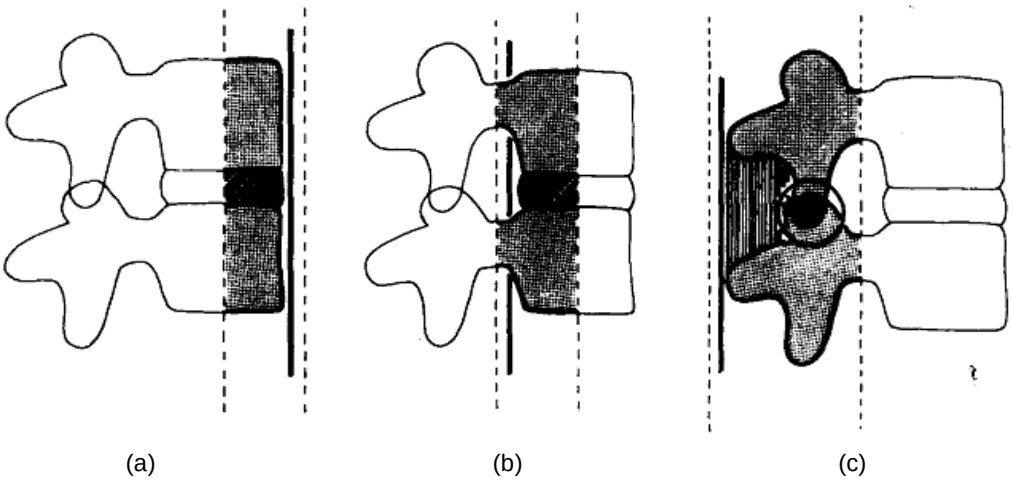

Figure 2.12 – The three column spine: (a) anterior, (b) middle, and (c) posterior column {Adapted from (Denis, 1983)}.

The anterior column comprehends the anterior longitudinal ligament (ALL), the anterior annulus fibrosus (AF) and the anterior part of the vertebral body. The middle column includes the posterior longitudinal ligament (PLL), the posterior AF and the posterior wall of the vertebral body.

Finally, the posterior column is formed the neural arch and remaining ligaments (ligamentum flavum (LF) and capsular (CL), interspinous (ISL) and supraspinous (SSL) ligaments).

Regarding the nomenclature above defined, the types of fractures can be easily explained. As clarified in Figure 2.13, the major spinal injuries (the ones that cause acute spinal instability) are divided in four types: (i) compression fractures, (ii) burst fractures, (iii) fracture dislocations, and (iv) seat-belt type injuries.

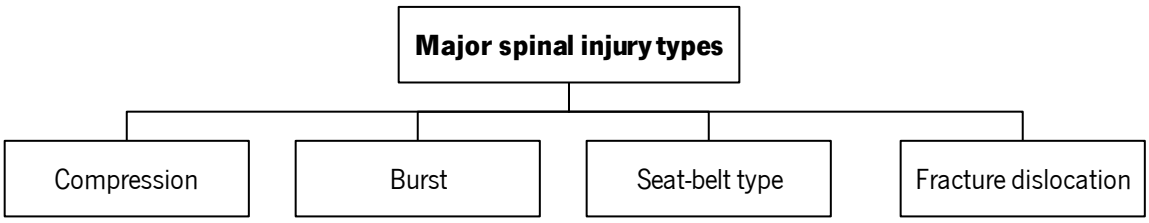

Figure 2.13 – Major spinal injury types {Adapted from (Denis, 1983)}.

The biomechanics of the different injury types are as follows:

- Compression fracture:
  - Failure under compression of the anterior column;
  - Middle column remains intact.
- Burst fracture:
  - Failure of the vertebral body under axial load, which results in failure of the anterior and middle columns both under compression;
  - Are further divided in fracture of both or only the superior or inferior endplates, burst rotation and burst lateral flexion.
- Seat-belt type injuries:
  - Failure of both posterior and middle columns under tension forces generated by flexion;
  - Includes the one-level, through bone Change fractures.
- Fracture dislocations:
  - Failure of all columns under compression, tension, rotation or shear.

From all the types, the compression fractures have the largest number of records, representing almost half of the cases. Understanding and quantifying the biomechanical changes inherent to these injuries is of great importance in the medical area, both from the solutions development point-of-view and the rehabilitation procedure.

2.3. Solutions for Degenerative Disc Disease

In this section, some of the fundamental and common solutions to overcome degenerative disc disease (DDD) of the lumbar spine are presented. Most of the people who suffer from low back pain (LBP) have their problem solved with nonoperative treatments, such as the administration of anti-inflammatory medication, exercise, and physical therapy. However, when these solutions are not effective, an operative solution must be applied. Nowadays, there are three main techniques to treat DDD of the lumbar spine, as visible in Figure 2.14: (i) fusion, (ii) intradiscal electrothermal therapy (IDET), and (iii) disc replacement (An *et al.*, 2003).

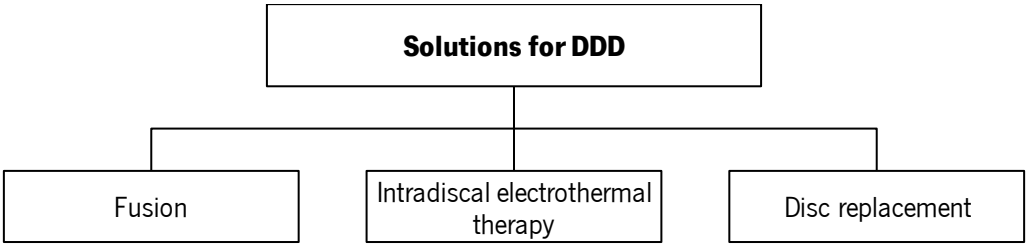

Figure 2.14 – Operative techniques for the treatment of lumbar DDD.

The fusion technique is used to join two or more vertebrae in order to reestablish structural integrity, to maintain correction after straightening of the spine or to prevent progression of an existing deformity, or even to diminish pain the constraining by the movement between various spine segments (White and Panjabi, 1990). There are several techniques used to perform fusion such as the so called posterolateral fusion with/without pedicle screw instrumentation, anterior/posterior lumbar interbody fusion, combined anterior and posterior fusion, cage devices, and minimally invasive techniques. Besides the wide range of choice among fusion techniques, there is no consensus in which is the best fusion procedure to follow. Furthermore, anomalies can happen with the lumbar spine fusion procedure. It can be seen increased/decreased motion, degenerative changes in the discs or facets, spinal stenosis, degenerative spondylolisthesis or even fracture dislocation.

The intradiscal electrothermal therapy (IDET) is indicated to treat pain originated from discs affected by radial fissures (Bogduk *et al.*, 2005). The technique requires the introduction of a flexible electrode circumferentially around the interface between the annulus fibrosus (AF) and the nucleus pulposus (NP), with the goal of closing the radial fissure at its base through the delivery of heat that denervates the painful nociceptors (sensory receptor involved in the perception of pain) and contracts collagen fibers in the AF (An *et al.*, 2003).

Compared to spinal fusion, the disc replacement approach maintains the motion between vertebrae but, as every prosthesis, the clinical results of the introduction of these devices are almost unknown, as well as their stability in a long-term application or the resistance of the components. There are some contraindications of the use of disc prosthesis, such as facet joint osteoarthritis (An *et al.*, 2003). Nevertheless, the offer of disc replacement prosthesis is very broad, including various designs, material and customized characteristics developed in order to improve its function in the vertebral column. The subsequent paragraphs describe some of the lumbar disc replacement prosthesis available on the market.

Prosthetic Solutions

There are innumerous prosthetic solutions for spinal problems available in the market. In this overview, the focus is given to lumbar disc replacement prosthesis. There are four main companies that distribute this type of product, namely Spine Art, Synthes, FH Orthopedics and B|Braun. Figure 2.15 shows four lumbar disc replacement prosthesis produced by each one of the mentioned companies.

The Swiss company Spine Art developed Baguera © L, a titanium prosthesis for the replacement of the IVD, coated with a DIAMOLITH® carbon layer. It comprises a polyethylene nucleus that allows the surgeon to choose the mobility desired for the disc (SpineArt, 2011).

Prodisc-L ® is a product by Synthes Holding AG, headquartered both in Switzerland and USA. This implant has three parts: two cobalt-chrome-molybdenum (CoCrMo) alloy endplates with a plasma-sprayed titanium coating, and an ultra-high molecular weight polyethylene (UHWMPE) inlay. A 7-to-11 year follow up study has been conducted by the company showing good efficiency of the product in the treatment of degenerative disc disease (DDD) symptoms (SYNTHES, 2011).

A collaborative work of the FH Orthopedics with the Pitié Salpétrière Hospital in Paris, the French Atomic Energy Commission, the University of Paris 6 and OSEO Innovation resulted in the creation of LP-ESP ®. This prosthesis comprises two titanium alloy plates, separated by a deformable part (FHOrthopedics, 2011).

B|Braun Melsungen AG, a german medical and pharmaceutical company, developed activ® L, an implant whose main goals are to minimize the biomechanical stress at the facet joints and to avoid facet joint arthrosis in a medium- and long-term prospect (B|Braun, 2011). The plates are composed of a chromium-cobalt alloy and the inlay of viscoelastic ultra-high molecular weight polyethylene (UHMWPE) (Kyriacou and Yeh, 2009).

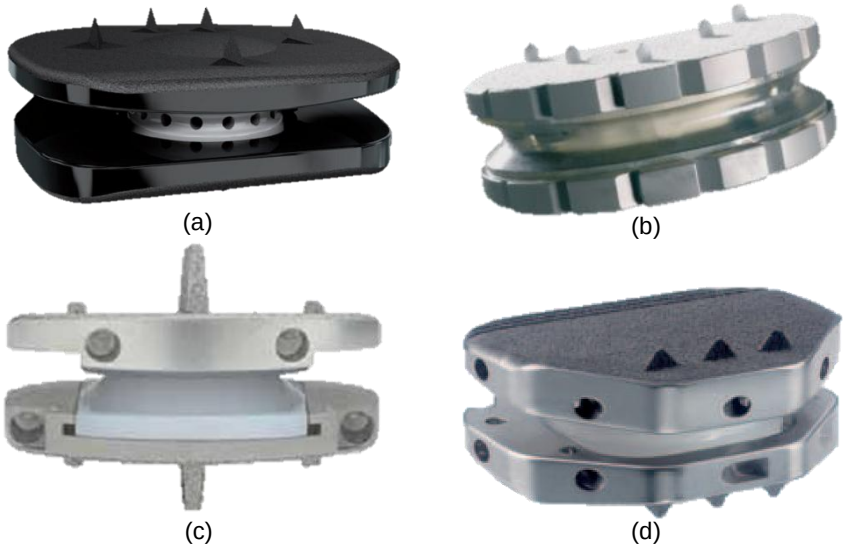

Figure 2.15 – Lumbar disc replacement prosthesis: (a) Baguera ® L, from Spine Art; (b) LP-ESP ®, from FH Orthopedics; (c) Prodisc-L ®, from Synthes; (d) activ® L, from B|Braun.

All the presented solutions aim to treat the DDD, reducing the discogenic pain and improving the patients function through the preservation of the motion in the affected vertebral level. However, the prosthetic solutions involve the removal of the diseased disc, converting this approach into a substitution rather than a treatment.

2.4. Summary and Discussion

In this Chapter, a description of the general anatomy of the spine was presented, focusing on the spinal regions and their functions, as well as the existent range of motion. Furthermore, a depiction of the spinal disorders was accomplished, centered on the set of pathologies which is in focus on this work, the degenerative disc diseases. Finally, some of the current solutions available on the market to solve this kind of problems were also depicted in this Chapter, showing that the answers to them can still evolve towards a biomimetic solution, rather than a substitution scenario.

Chapter 3

Multibody Systems Formulation

3.1. Multibody System Concept

A multibody system is a set of rigid and/or flexible bodies connected by kinematic joints that constrain their large relative translational and rotational motion, and actuated by external forces (Nikravesh, 1988). The kinematic joints that can be present in multibody systems constrain the relative motion between the bodies connected by them, while the force elements represent the forces that are produced in the system, and between system and the surrounding environment.

Figure 3.1 illustrates a generic multibody system with its most significant components, namely bodies, joints and force elements.

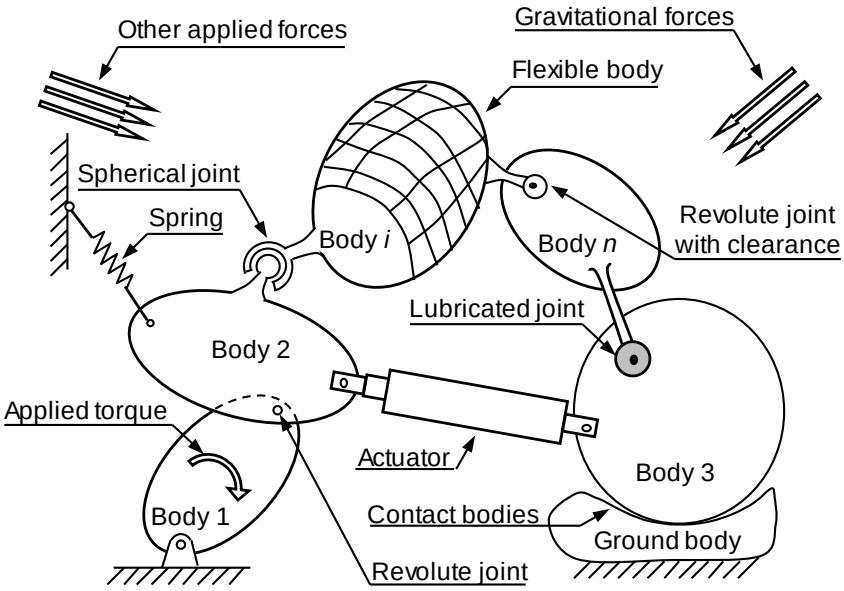

Figure 3.1 – Generic representation of a multibody system.

The multibody systems formulation is a powerful tool in what concerns the study of the motion of a given system. As Figure 3.2 shows, it can either be used a kinematic or a dynamic approach for the analysis of a system.

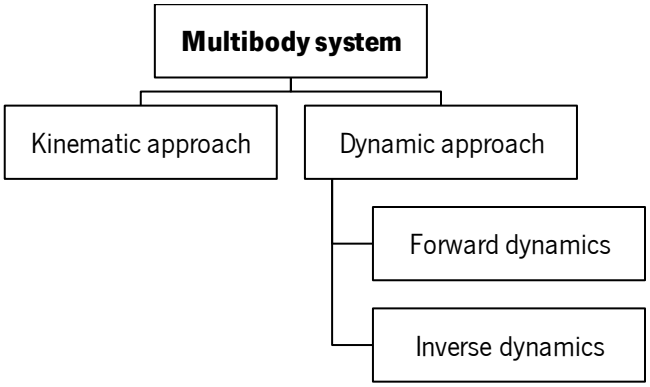

Figure 3.2 – Multibody systems and the possible analyses of biomechanical systems.

Through a kinematic approach it is possible to analyze the positions, velocities and accelerations of a given system without concerning about the causes involved. In turn, a dynamic approach considers the force produced motion, and can be further divided in (i) a forward dynamics analysis, in which the motion is determined as a result of the application of an external load, or (ii) an inverse dynamics analysis, through which a particular movement of the system is used to calculate the internal forces developed in each body and the corresponding reactions.

3.2. Cartesian Coordinates

Prior to establish the equations of motion of the constrained bodies, it is necessary to select the adequate coordinate system in order to univocally describe the positioning of the different structures involved in the process. In first place, to define a system using cartesian coordinates, the coordinate system xy in Figure 3.3 is defined as the global reference frame. Then it is necessary to attribute a local reference frame to the body i, which is denominated $\xi_i\eta_i$. Body i can be located in the plane by defining the global coordinates $\mathbf{r}_i = [x \quad y]_i^T$ of the origin of the body-fixed coordinate system and the angle ϕ_i of rotation of this $\xi_i\eta_i$ system relative to the global coordinate xy system. The angle is considered positive when measured counterclockwise. Regarding this information, a vector of coordinates $\mathbf{q}_i$ that describes the body i in the a planar context has the following format,

$$\mathbf{q}_i = \{x \quad y \quad \phi\}_i^T \tag{3.1}$$

Having this vector, any point located on the body can be expressed in global coordinates as a function of $\mathbf{q}_i$. Let P be a point on body i, and $\mathbf{s}_i^P$ the position vector that represents the location of point P relative to the reference frame $\xi_i\eta_i$. In further references $\mathbf{s}_i^P$ symbolizes the vector in global coordinates and $\mathbf{s}'^P_i$ represents the same vector in the coordinate system fixed in body i.

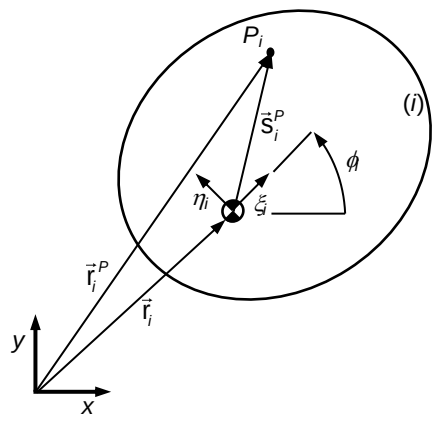

Figure 3.3 – Locating point P relative to the body-fixed and global coordinate systems {Adapted from (Nikravesh, 1988)}.

The local and global coordinates of point P_i are related by Equation (3.2),

$$\mathbf{r}_i^P = \mathbf{r}_i + \mathbf{s}_i^P = \mathbf{r}_i + \mathbf{A}_i \mathbf{s}'^P_i \tag{3.2}$$

where $\mathbf{A}_i$ is the transformation matrix given by Equation (3.3).

$$\mathbf{A}_i = \begin{bmatrix} \cos\phi_i & -\sin\phi_i \\ \sin\phi_i & \cos\phi_i \end{bmatrix} \tag{3.3}$$

The position of the point P_i can be described in global coordinates in the simplified form shown in Equation (3.4).

$$\begin{bmatrix} x_i^P \\ y_i^P \end{bmatrix} = \begin{bmatrix} x_i \\ y_i \end{bmatrix} + \begin{bmatrix} \cos\phi_i & -\sin\phi_i \\ \sin\phi_i & \cos\phi_i \end{bmatrix} \begin{bmatrix} \xi_i^P \\ \eta_i^P \end{bmatrix} \tag{3.4}$$

Despite the use of cartesian coordinates in this work, this is not the only type of coordinates available to describe the configuration of the system at a given instant. In a general perspective, the coordinate systems can be divided in independent and dependent coordinates. In the first group, the variables used are associated with the degrees of freedom of the system; the dependent coordinates are further split into three types: absolute, relative and natural coordinates. The absolute (or cartesian) were already explained. The relative define the position and orientation relative to a preceding body in the multibody system, and the natural (or fully cartesian) coordinates involve the employment of only two cartesian coordinates, not including the orientation (Flores and Seabra, 2010).

3.3. Equations of Motion for Constrained Systems

The configuration of the multibody system (MBS) is described by *n* cartesian coordinates, and therefore $\mathbf{\Phi}$, a set of *m* algebraic kinematic independent holonomic constraints[1], can be written in the compact form shown in Equation (3.5), as defined by (Nikravesh, 1988),

$$\mathbf{\Phi}(\mathbf{q}, t) = 0 \tag{3.5}$$

in which $\mathbf{q}$ is the vector of generalized coordinates as it was defined in Equation (3.1) and t is the time variable.

The velocities and accelerations of the system elements are evaluated using the velocity and acceleration constraint equations, defined respectively by Equations (3.6) and (3.7),

$$\mathbf{\Phi_q}\dot{\mathbf{q}} = \boldsymbol{\upsilon} \tag{3.6}$$

$$\mathbf{\Phi_q}\ddot{\mathbf{q}} = \boldsymbol{\gamma} \tag{3.7}$$

where $\mathbf{\Phi_q} = \partial\mathbf{\Phi}/\partial\mathbf{q}$ is the Jacobian matrix of the constraint equations, $\dot{\mathbf{q}}$ is the vector of generalized velocities, $\boldsymbol{\upsilon} = \partial\mathbf{\Phi}/\partial t$ is the right hand side of velocity equations, $\ddot{\mathbf{q}}$ is acceleration vector and $\boldsymbol{\gamma}$ is the right hand side of acceleration equations, *i.e.*, the vector of quadratic velocity terms, which contains the terms that are exclusively function of velocity, position and time.

The equations of motion used for a constrained multibody system of rigid bodies are described according to Nikravesh's formulation (Nikravesh, 1988),

$$\mathbf{M}\ddot{\mathbf{q}} = \mathbf{g} + \mathbf{g}^{(c)} \tag{3.8}$$

in which $\mathbf{M}$ is the system mass matrix, $\ddot{\mathbf{q}}$ is the vector that contains the systems accelerations, $\mathbf{g}$ is the generalized force vector, which contains all external forces and moments, and $\mathbf{g}^{(c)}$ is the vector of constraint reaction equations. The joint reaction forces can be expressed in terms of the Jacobian matrix of the constrained equations and the vector of Lagrange multipliers as in Nikravesh's publication (Nikravesh, 1988),

$$\mathbf{g}^{(c)} = -\mathbf{\Phi}_\mathbf{q}^T\boldsymbol{\lambda} \tag{3.9}$$

where $\boldsymbol{\lambda}$ is the vector that contains *m* unknown Lagrange multipliers associated with *m* holonomic constraints. The Lagrange multipliers are physically related to the reaction forces and moments generated between the bodies interconnected by kinematic joints. Thus,

$$\mathbf{M}\ddot{\mathbf{q}} + \mathbf{\Phi}_\mathbf{q}^T\boldsymbol{\lambda} = \mathbf{g} \tag{3.10}$$

[1] Holonomic constraints are nonlinear algebraic equations that involve generalized coordinates and, possibly, the time variable.

In a dynamic analysis, a unique solution is obtained when the constraint equations are considered simultaneously with the differential equations of motion, for a proper set of initial conditions. Thus, mathematically the simulation of constrained multibody system requires the solution of a set of *n* differential equations coupled with a set of *m* algebraic equations. This system of equations is solved for $\ddot{\mathbf{q}}$ and $\boldsymbol{\lambda}$, and is written as,

$$\begin{bmatrix} \mathbf{M} & \boldsymbol{\Phi}_{\mathbf{q}}^{T} \\ \boldsymbol{\Phi}_{\mathbf{q}} & \mathbf{0} \end{bmatrix} \begin{Bmatrix} \ddot{\mathbf{q}} \\ \boldsymbol{\lambda} \end{Bmatrix} = \begin{Bmatrix} \mathbf{g} \\ \boldsymbol{\gamma} \end{Bmatrix} \tag{3.11}$$

Then, in each integration time step, the accelerations vector, $\ddot{\mathbf{q}}$, together with the velocities vector, $\dot{\mathbf{q}}$, are integrated in order to obtain the system velocities and positions for the next time step. This procedure is repeated up to the final time analysis is reached (Flores *et al.*, 2008).

3.4. Solution of the Equations of Motion

In order to advance the analysis in time, the equations of motion need to be solved and the state variables integrated. Considering the high level of complexity of these equations, analytical solutions are impractical to obtain and, consequently, numerical integration algorithms must be applied.

The standard integration of the equations of motion, here called Direct Integration Method (DIM), converts the *n* second-order differential equations of motion into *2n* first-order differential equations. Then, a numerical scheme, such as the fourth-order Runge-Kutta method, is employed to solve the initial-value problem.

The commonly used numerical integration algorithms are useful in solving first-order differential equations that take the form,

$$\dot{\mathbf{y}} = f(\mathbf{y}, t) \tag{3.12}$$

Thus, the *n* second-order differential equations need to be transformed into *2n* first-order equations by defining the $\mathbf{y}$ and $\dot{\mathbf{y}}$ vectors, which contain, respectively, the system positions and velocities and the system velocities and accelerations, as follows,

$$\mathbf{y} = \begin{Bmatrix} \mathbf{q} \\ \dot{\mathbf{q}} \end{Bmatrix} \quad \text{and} \quad \dot{\mathbf{y}} = \begin{Bmatrix} \dot{\mathbf{q}} \\ \ddot{\mathbf{q}} \end{Bmatrix} \tag{3.13}$$

The reason for introducing the new vectors and is that most numerical integration algorithms deal with first-order differential equations. Diagram (3.14) can interpret the process of numerical integration at instant of time *t*,

$$\dot{\mathbf{y}}(t) \xrightarrow{integration} \mathbf{y}(t + \Delta t) \tag{3.14}$$

velocities and accelerations at instant t, after integration process, yield positions and velocities at next time step, $t = t + \Delta t$.

Figure 3.4 presents a flowchart that shows the algorithm of Direct Integration Method of the equations of motion. At $t = t^0$, the initial conditions on $\mathbf{q}^0$ and $\dot{\mathbf{q}}^0$ are required to start the integration process. These values cannot be specified arbitrarily, but must satisfy the constraint equations defined by Equations (3.5) and (3.6).

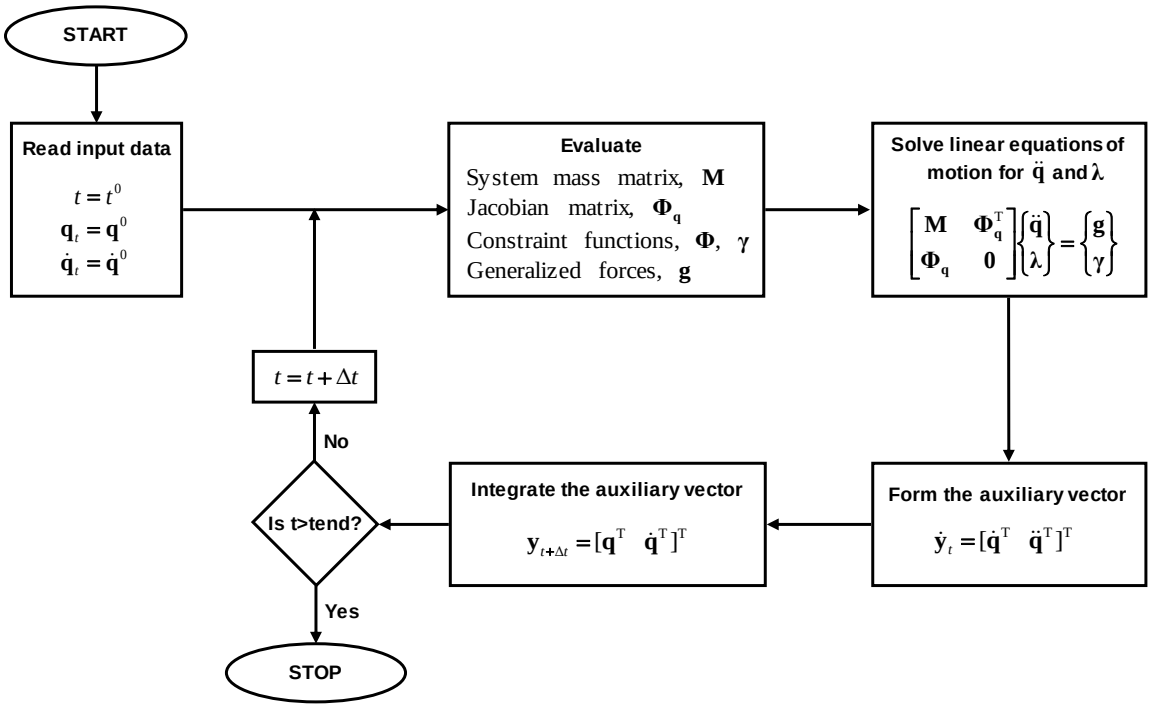

Figure 3.4 – Flowchart of computational procedure for dynamic analysis of multibody systems – Direct Integration Method {Adapted from (Flores and Seabra, 2010).

The direct integration algorithm presented in Figure 3.4 can be summarized by the following steps:

i) Start at instant of time t^0 with given initial conditions for positions and velocities.

ii) Assemble the global mass matrix $\mathbf{M}$, evaluate the Jacobian matrix $\mathbf{\Phi}_\mathbf{q}$, construct the constraint equations $\mathbf{\Phi}$, determine the right hand side of the accelerations $\boldsymbol{\gamma}$, and calculate the force vector $\mathbf{g}$.

iii) Solve the linear set of the equations of motion for a constrained multibody system in order to obtain the accelerations $\ddot{\mathbf{q}}$ at time t and the Lagrange multipliers $\boldsymbol{\lambda}$.

iv) Assemble the vector $\dot{\mathbf{y}}$, containing the generalized velocities $\dot{\mathbf{q}}$ and accelerations $\ddot{\mathbf{q}}$ for instant of time t.

v) Integrate numerically the $\dot{\mathbf{q}}$ and $\ddot{\mathbf{q}}$ for time step $t + \Delta t$ and obtain the new positions and velocities.

vi) Update the time variable and got to step ii) and process with the process for the new time step. Perform these steps until the final time of analysis is reached.

3.4.1. Simulation Software

A few computation simulation programs are available to perform a dynamic analysis of the musculoskeletal system. This type of software is of major importance in what concerns the validation of biomechanical models. From the range of available software, various have specific tools for lumbar spine simulation. Some of the programs of that selection are briefly described in the following paragraphs.

AnyBody™ Technologies (Aalborg, Denmark) developed the AnyBody Modeling System™, a software system to solve problems within the human movement and ergonomics using inverse dynamics and cartesian coordinates. It is possible to simulate muscle and joint forces for the whole body under complex movements. A musculoskeletal model of the lumbar spine is available, containing 194 muscles fascicles as well as the five lumbar vertebrae, sacrum and pelvis, and the joint between lumbar and thoracic parts. The models are customizable in the opening scripting language AnyScript™ (AnyBody, 2011).

LifeModeler® (San Clemente, California, USA) offers a solution named LifeMOD™. This is a complete, state-of-the-art virtual human modeling and simulation software tool, comprising an intuitive graphical interface and advanced capabilities. It is capable of performing forward and inverse dynamics analysis of three-dimensional models, and producing plots of force, displacement, velocities, accelerations, torques, and angles. In turn, LifeMOD™ has various modules, such as the plug-in module LumbarSIM, a detailed lumbar spine model that can be separated into individual vertebral segments (L1-L5) and disc force. The tool claims to be useful for orthopedic surgeons and researchers involved in spinal surgery, spinal cord stimulation implants and artificial disc replacement, as well as for aeronautical and automotive ride comfort and injury analysis (LumbarSIM, 2011).

The company MSC Software® (Santa Ana, California, USA) provides the multibody dynamics simulation Adams™, a widely used multibody dynamics and motion analysis software that allows

the study of the dynamics of moving parts, the force distribution throughout mechanical systems, and improvement and optimization of products (ADAMS, 2011).

OpenSim is a freely available, user extensible software system developed at Simbios, the National Institute of Health (NIH) Center for Biomedical Computation at Stanford University (California, USA). The software lets users develop models of musculoskeletal structures and create dynamic simulations of movement, with the underlying software written in ANSI C++, and graphical user interface in Java™. The OpenSim technology allows the development of customized controllers, analyses, contact models, and muscle models (among other possibilities). OpenSim provides a three-dimensional model of the lumbar spine using relative coordinates and Euler angles, including a variable amount of muscles (OpenSim, 2011).

SIMPACK AG (Gilching, Germany) created the general multibody simulation software SIMPACK™, used for the dynamic analysis of mechanical systems, enabling the generation and solving of three-dimensional models in order to predict and visualize motion, forces and stresses. The biomechanical branch of SIMPACK includes detailed human models, allows forward dynamic motion, is extendable by user defined elements, provides a realistic man-machine interaction and is compatible with other motion tracking software and model generators (SIMPACK, 2011).

The current work uses the multibody dynamics code MUBODYNA (acronym of Dynamic Analysis of Multibody Systems), a FORTRAN program for dynamic analysis of planar multibody systems developed at University of Minho by Flores (2010), and based on the DAP (acronym of Dynamic Analysis Program) code developed by Nikravesh (1988). The use of MUBODYNA over other programs is justified by the possibility of controlling all the variables involved in the simulation (*e.g.* contact force model), which is not possible with other software.

3.5. Summary and Discussion

In this chapter the main fundaments associated with the dynamics of multibody system were reviewed and discussed. In the process, the concepts of multibody system, the cartesian coordinates, and the formulation of the dynamic equations of motion for constrained multibody systems were analyzed. In the sequel of this process, the main numerical issues associated with the solution of the equations of motion were revisited. The computational strategy to perform dynamic analysis was discussed.

Chapter 4

Biomechanical Multibody Spine Model

4.1. Description of the Model

The model of the spine considered in this work comprises the six vertebrae (five lumbar vertebrae and the sacrum), five intervertebral discs (between each considered vertebra), as well as thirty ligaments of six different types exerting forces in the lumbar spine, and five potential contacts between spinous processes. The vertebrae are modeled as rigid bodies, the IVDs as linear 3 DOF bushing elements, the ligaments as nonlinear viscoelastic elements and the contact follows the Flores *et al.* model for contact (2011). All these geometric and mechanic description of these elements can be found in the following subsections.

4.1.1. The Vertebrae

It is considered that the S1 vertebra is stationary and that the model is symmetric relatively to the sagittal plane. Table 4.1 summarizes the global cartesian coordinates of the centers of mass of the vertebral bodies and the orientation of each local frame relatively to the global coordinate system, as well as the mass and the moment of inertia of each vertebra (Monteiro, 2009).

Table 4.1 – Initial coordinates of the center of mass, local frame orientation, mass and moment of inertia of the rigid bodies considered in the presented model {Adapted from (Monteiro, 2009)}.

Body	x [m]	y [m]	ϕ [rad]	Mass [kg]	Moment of inertia [kg.m^2]
L1	-0.00155	0.17413	0.2217	1.486	0.0242690
L2	0.00745	0.14173	0.2618	1.572	0.0154390
L3	0.01825	0.10843	0.2374	1.632	0.0085155
L4	0.02505	0.07263	0.1222	1.664	0.0047212
L5	0.02305	0.03953	-0.1257	1.406	0.0038544
S1	0.00000	0.00000	-0.3700	4.918	0.0490150

Some other geometrical information is essential for the accurate description of each vertebral body. The posterior vertebral body height (VBHp), and the upper (EPDu) and lower (EPDl)

endplate depths of each vertebral body were retrieved from (Panjabi *et al.*, 1992). Table 4.2 summarizes the aforementioned lengths and Figure 4.1 depicts them in a particular vertebra.

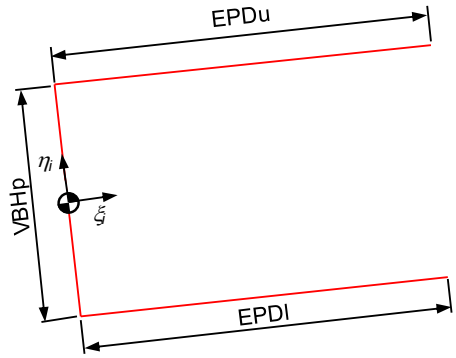

Figure 4.1 - Posterior vertebral body height (VBHp), and upper (EPDu) and lower (EPDl) endplate depth in a vertebra.

Table 4.2 – Posterior vertebral body height (VBHp), and upper (EPDu) and lower (EPDl) endplate depth of each considered vertebral body {Adapted from (Panjabi *et al.*, 1992)}.

Body	VBHp [m]	EPDu [m]	EPDl [m]
L1	0.02380	0.03410	0.03530
L2	0.02430	0.03460	0.03490
L3	0.02380	0.03520	0.03480
L4	0.02410	0.03550	0.03390
L5	0.02290	0.03470	0.03320
S1	-	-	-

Each upper and lower endplate has its own inclination relative to the local reference frame. These inclinations are of vital importance for the exact location of the elements used to simulate the intervertebral disc (IVD), as well as the longitudinal ligaments, since these are attached to the upper and lower extremities of the vertebral body. In this line of sight, Figure 4.2 displays the upper (ψ_U) and lower (ψ_L) endplate inclination of a vertebral body and Table 4.3 includes this information for each vertebral body considered in the model.

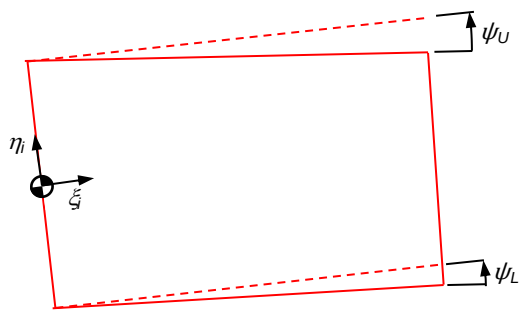

Figure 4.2 – Upper (ψ_U) and lower (ψ_L) endplate inclination for a vertebral body considered in the model.

Table 4.3 – Upper (ψ_U) and lower (ψ_L) endplate inclination for each vertebral body considered in the model (Adapted from (Panjabi *et al.*, 1992)).

Body	ψ_U **[rad]**	ψ_L **[rad]**
L1	-0.047124	-0.069813
L2	-0.061087	-0.036652
L3	-0.029671	-0.047124
L4	-0.082030	-0.047124
L5	-0.038397	-0.031416
S1	0.000000	-

It should be noted that additional points are important in the geometric description of the vertebrae, such as the origin and attachment points of the elements used to simulate the IVD, ligaments and spinal contacts. Throughout the next subsections, and according to the needs, those points will be described in detail.

4.1.2. The Intervertebral Discs

The intervertebral discs (IVD) are modeled as 3 degree-of-freedom linear viscoelastic bushing elements (BE). Those elements are used because a vertebra can move and rotate in any direction relatively to the adjacent one and, in a two-dimensional approach, 3 DOF represent the possible horizontal and vertical translation, and rotation movements.

As a crucial element for the definition of the spinal motion, the correct input of the location of these elements in the model is a factor of major importance. In this matter, for each BE it is important to define a master body (correspondent to the vertebra located below the IVD) and a slave body (located above the IVD). The BE is defined between two points: (i) the origin, located in the geometric center of the upper endplate of the master body; and (ii) the insertion point, located in the geometric center of the upper endplate of the slave body. Table 4.4 presents the local ξ and η coordinates of the aforementioned geometric centers for each BE (referring the slave and master body for each pair), as well as the translational (Δxx^0 and Δyy^0) and angular ($\Delta\theta^0$) offset between them at the initial instant of the simulation.

Table 4.4 – Local coordinates of the points defining the bushing element (BE) and initial translational and angular offset between those points: S - slave body; M - master body {Adapted from (Monteiro, 2009)}.

BE (S-M)	**Vertebra**	**Reference Coordinates [m]**		**Initial Offset**		
		ξ	η	Δxx^0 **[m]**	Δyy^0 **[m]**	$\Delta\theta^0$ **[rad]**
L1-L2	L2	0.01730	0.01110	-0.000499	0.008698	0.040
	L1	0.01770	-0.01310			

Table 4.4 – Local coordinates of the points defining the bushing element (BE) and initial translational and angular offset between those points: S - slave body; M - master body {Adapted from (Monteiro, 2009)} (*continued*).

BE (S-M)	Vertebra	Reference Coordinates [m]		Initial Offset		
		ξ	η	Δxx^0 [m]	Δyy^0 [m]	$\Delta\theta^0$ [rad]
L2-L3	L3	0.01630	0.01110	-0.001160	0.011456	-0.024
	L2	0.01750	-0.01280			
L3-L4	L4	0.01780	0.01140	-0.001390	0.014306	-0.115
	L3	0.01750	-0.01270			
L4-L5	L5	0.01740	0.01060	0.000070	0.014200	-0.248
	L4	0.01700	-0.01290			
L5-S1	S1	0.02650	0.02610	-0.000252	0.011492	-0.244
	L5	0.01660	-0.01200			

The translational offsets are measured relatively to a new frame located on the geometric center of the upper endplate of each master body, which inclination was chosen so that the abscissae axis was tangent to the referred endplate (and therefore, the ordinates axis is perpendicular to the endplate), as visible in Figure 4.3. This orientation is useful for the determination of the developed forces, as explained ahead.

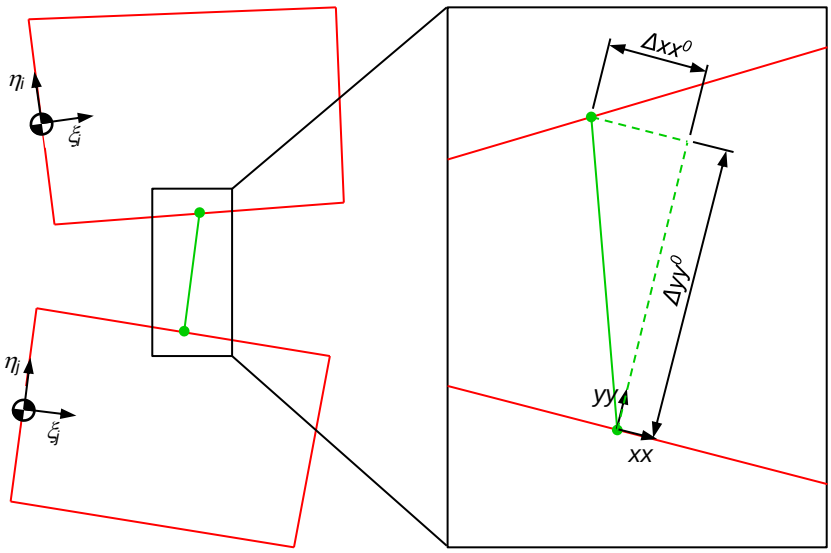

Figure 4.3 - Geometric definition of the bushing element and representation of the initial translational offset.

The angular offset $\Delta\theta^0$ is found by calculating the inclination of the lower endplate of the slave body relative to the upper endplate of the master body, for each BE. That is,

$$\Delta\theta^0 = (\phi_S^0 - \phi_M^0) + (\psi_S^L - \psi_M^U) \tag{4.1}$$

The translational and angular initial offsets are necessary to compute the forces and moments developed at the bushing elements. The difference between the offsets at each instant and the initial offsets becomes the displacement used for the computations.

Each BE applies restrictions in the motion (as opposing forces and moments) in the form of two different components: springs and dampers. Therefore, the BE behavior can be divided in:

(i) The spring component, in which the force/moment exerted is given by

$$F_K = K_{\pm xx,yy} d \tag{4.2}$$

or

$$M_K = K_{\pm\theta} \theta_d \tag{4.3}$$

(ii) The damper component, ruled by

$$F_D = D_{\pm xx,yy} \dot{d} \tag{4.4}$$

or

$$M_D = D_{\pm\theta} \dot{\theta}_d \tag{4.5}$$

where $K_{\pm xx,yy,\theta}$ and $D_{\pm xx,yy,\theta}$ are the stiffness and damping coefficients for each direction. The displacement d and the displacement velocity $\dot{d}$ have horizontal and vertical components, associated with different positive and negative translational stiffness and damping coefficients, and angular displacement θ_d and angular displacement velocity $\dot{\theta}_d$ follow the same tendency.

This dual behavior needs to be depicted in the form of input data to the model. Stiffness and damping coefficients for the different load directions are specified in Table 4.5.

Table 4.5 - Material properties of the bushing elements (BE) for several load directions {Adapted from (Monteiro, 2009)}.

Load direction	**Stiffness [N/m]**	**Damping [N.s/m]**
F_{xx}: Anterior Shear	260000	1000
F_{-xx}: Posterior Shear	260000	1000
F_{yy}: Tension	213200	1000
F_{-yy}: Compression	1825000	1000
Load direction	**Stiffness [N.m/rad]**	**Damping [N.m.s/rad]**
M_z: Flexion	3.88	1.5
M_{-z}: Extension	5.88	1.5

4.1.3. The Ligaments

Following the descriptions by Wismans (1980), it is possible to conclude that ligaments have a nonlinear behavior, as visible in Figure 4.4. A first region, called toe-in region where the load response to strain is approximately a quadratic function, between zero and a transition strain ε_T; an intermediate section, the linear region, in which the ligament behaves according to a linear

relation – for strains between ε_T and the limit strain ε_{LIM} ; and finally the failure region of the ligament, where collagen fibers suffer disruption.

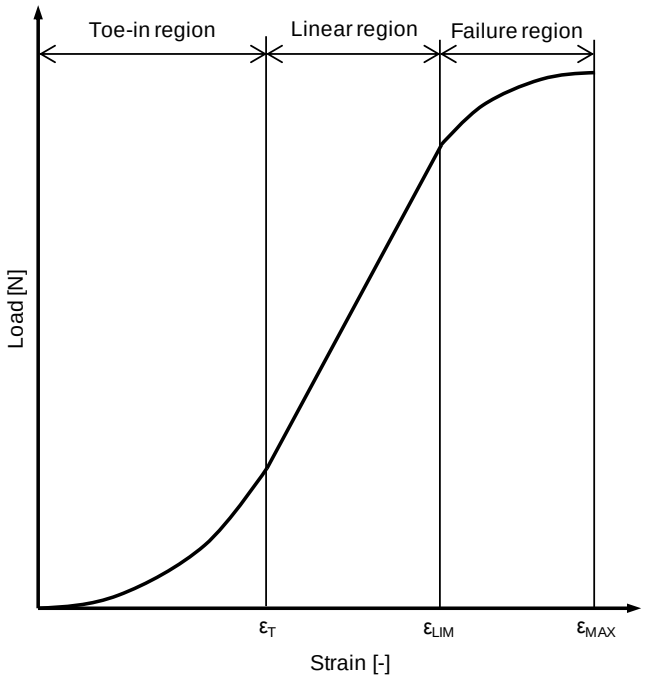

Figure 4.4 – Mechanical behavior of the ligament: load-strain curve Adapted from (Wismans, 1980).

As depicted in Equation (4.6), the elastic force module, F_E, has two components: F_E^{TI} represents the toe-in region, until the ligament reaches the transition strain ε_T; and F_E^L represents the linear region, for strains above ε_T.

$$F_E = \begin{cases} F_E^{TI} & , \quad 0 < \varepsilon < \varepsilon_T \\ F_E^L & , \quad \varepsilon_T \leq \varepsilon < \varepsilon_{LIM} \end{cases} \tag{4.6}$$

The toe-in region behavior can be approximated by a quadratic strain dependent relation, as explained in Equation (4.7),

$$F_E^{TI} = \frac{K l_0 \varepsilon^2}{2\varepsilon_T} \tag{4.7}$$

where K is the ligament stiffness, l_0 is the undeformed length of the ligament and ε is the ligaments strain at a given instant, and can be calculated through Equation (4.8), in which l is the ligament's length at the instant of analysis.

$$\varepsilon = \frac{l - l_0}{l_0} \tag{4.8}$$

The linear region force, as the name explains, can be approximated by a linear strain relation, as represented in Equation (4.9).

$$F_E^L = Kl_0\left(\varepsilon - \frac{\varepsilon_T}{2}\right) \tag{4.9}$$

Besides this analysis, the ligament is considered to follow a viscous behavior, namely through the inclusion of the hysteresis effect. Figure 4.5 shows the different ligament responses on loading and unloading phases as well as the energy loss (shaded area) due to hysteresis.

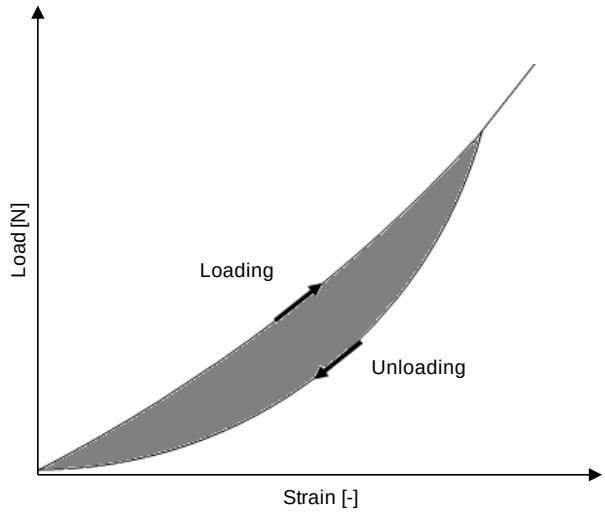

Figure 4.5 – Ligament hysteresis: loading and unloading. The shaded area represents the energy loss due to the hysteretic behavior (Yahia *et al.*, 1991).

This means that the behavior of the ligament depends on being under a loading (positive strain rate $\dot{\varepsilon}$) or unloading situation (negative strain rate $\dot{\varepsilon}$), and a strain rate dependent component force is introduced when the ligament is in loading phase, as visible in Equation (4.10),

$$F^T = \begin{cases} F_E & , \quad \varepsilon > 0 \quad \wedge \quad \dot{\varepsilon} \leq 0 \\ F_E(1 + C\dot{\varepsilon}) & , \quad \varepsilon > 0 \quad \wedge \quad \dot{\varepsilon} > 0 \\ 0 & , \quad \varepsilon \leq 0 \end{cases} \tag{4.10}$$

in which the parameter C is associated with the energy dissipation. A higher value of C is representative of a larger energy loss in the load-deformation cycle. In turn, the strain rate $\dot{\varepsilon}$ is obtained by the ratio between the ligament velocity $\dot{l}$ and the undeformed ligament length l_0, as Equation (4.11) shows.

$$\dot{\varepsilon} = \frac{\dot{l}}{l_0} \tag{4.11}$$

For this matter, it is also important to mention the stiffness coefficient and transition strains (ε_T) for each type of ligament, as well as the limit strains (ε_{LIM}). The coefficient C is assumed to be 0.4 for all cases, according to the work of van der Horst (2002). In this analysis the ligament's failure behavior is not studied, being assumed that after the maximum strain is exceeded, the ligament continues to apply the same force.

Table 4.6 – Properties of the lumbar ligaments: stiffness coefficient, and transition and maximum strains {Adapted from (Pintar *et al.*, 1992)}.

Ligament	K **[N/m]**	ε_T	ε_{LIM}
CL	33900	0.261	0.655
ISL	11500	0.227	0.779
LF	27200	0.226	0.708
ALL	33000	0.081	0.384
PLL	20400	0.043	0.145
SSL	23700	0.271	0.933

Furthermore, it is important to clearly define the local coordinates of the origin and insertion points of each ligament for each spinal level, as well as their undeformed length l_0. The following tables provide that information.

Table 4.7 shows the local coordinates used to define the CL, and the respective length of the ligament in the undeformed state.

Table 4.7 – Local coordinates used in the definition of the capsular ligaments (CL) in the lumbar spine {Adapted from (Monteiro, 2009)}.

Spine Level	**Vertebra**	**Coordinates [m]**		**Length [m]**
		ξ	η	
L1-L2	L2	-0.01402	0.01215	0.02115
	L1	-0.02659	-0.02025	
L2-L3	L3	-0.01740	0.01190	0.02445
	L2	-0.02797	-0.02055	
L3-L4	L4	-0.01374	0.01205	0.02003
	L3	-0.03033	-0.02010	
L4-L5	L5	-0.01360	0.01145	0.01967
	L4	-0.02852	-0.01635	
L5-S1	S1	0.00000	0.02610	0.02396
	L5	-0.02623	-0.01480	

Table 4.8 shows the local coordinates used to define the ISL, and the respective length of the ligament in the undeformed state.

Table 4.8 – Local coordinates used in the definition of the interspinous ligaments (ISL) in the lumbar spine {Adapted from (Monteiro, 2009)}.

Spine Level	**Vertebra**	**Coordinates [m]**		**Length [m]**
		ξ	η	
L1-L2	L2	-0.03410	-0.00403	0.04194
	L1	-0.02584	-0.01271	

Table 4.8 – Local coordinates used in the definition of the interspinous ligaments (ISL) in the lumbar spine {Adapted from (Monteiro, 2009)} (*continued*).

Spine Level	Vertebra	Coordinates [m]		Length [m]
		ξ	η	
L2-L3	L3	-0.03403	-0.00290	0.04151
	L2	-0.02750	-0.01258	
L3-L4	L4	-0.03342	-0.00219	0.04218
	L3	-0.02781	-0.01073	
L4-L5	L5	-0.03147	-0.00054	0.03909
	L4	-0.02653	-0.00992	
L5-S1	S1	-0.01281	0.00392	0.03726
	L5	-0.02378	-0.00726	

Table 4.9 shows the local coordinates used to define the LF, and the respective length of the ligament in the undeformed state.

Table 4.9 – Local coordinates used in the definition of the ligamentum flavum (LF) in the lumbar spine {Adapted from (Monteiro, 2009)}.

Spine Level	Vertebra	Coordinates [m]		Length [m]
		ξ	η	
L1-L2	L2	-0.01820	0.00488	0.03201
	L1	-0.01987	0.00358	
L2-L3	L3	-0.01750	0.00398	0.03337
	L2	-0.01913	0.00270	
L3-L4	L4	-0.01860	0.00380	0.03576
	L3	-0.01934	0.00171	
L4-L5	L5	-0.01970	0.00275	0.03385
	L4	-0.01966	0.00176	
L5-S1	S1	-0.00985	0.00783	0.03720
	L5	-0.02050	0.00109	

Table 4.10 shows the local coordinates used to define the ALL, and the respective length of the ligament in the undeformed state.

Table 4.10 – Local coordinates used in the definition of the anterior longitudinal ligaments (ALL) in the lumbar spine {Adapted from (Monteiro, 2009)}.

Spine Level	Vertebra	Coordinates [m]		Length [m]
		ξ	η	
L1-L2	L2	0.03460	0.01003	0.03358
	L1	0.03530	-0.01437	
L2-L3	L3	L3	0.03250	0.03618
	L2	L2	0.03490	

Table 4.10 – Local coordinates used in the definition of the anterior longitudinal ligaments (ALL) in the lumbar spine {Adapted from (Monteiro, 2009)} (*continued*).

Spine Level	Vertebra	Coordinates [m]		Length [m]
		ξ	η	
L3-L4	L4	0.03550	0.00913	0.03566
	L3	0.03480	-0.01354	
L4-L5	L5	0.03470	0.01012	0.03449
	L4	0.03390	-0.01365	
L5-S1	S1	0.04305	0.02610	0.05170
	L5	0.03320	-0.01249	

Table 4.11 shows the local coordinates used to define the PLL, and the respective length of the ligament in the undeformed state.

Table 4.11 – Local coordinates used in the definition of the posterior longitudinal ligaments (PLL) in the lumbar spine {Adapted from (Monteiro, 2009)}.

Spine Level	Vertebra	Coordinates [m]		Length [m]
		ξ	η	
L1-L2	L2	0.00000	0.01215	0.03364
	L1	0.00000	-0.01190	
L2-L3	L3	0.00000	0.01190	0.03502
	L2	0.00000	-0.01215	
L3-L4	L4	0.00000	0.01205	0.03645
	L3	0.00000	-0.01190	
L4-L5	L5	0.00000	0.01145	0.03318
	L4	0.00000	-0.01205	
L5-S1	S1	0.00985	0.02610	0.04577
	L5	0.00000	-0.01145	

Table 4.12 shows the local coordinates used to define the SSL, and the respective length of the ligament in the undeformed state.

Table 4.12 – Local coordinates used in the definition of the supraspinous ligaments (SSL) in the lumbar spine {Adapted from (Monteiro, 2009)}.

Spine Level	Vertebra	Coordinates [m]		Length [m]
		ξ	η	
L1-L2	L2	-0.04999	-0.01294	0.03676
	L1	-0.04698	-0.01338	
L2-L3	L3	-0.05056	-0.00978	0.03553
	L2	-0.04999	-0.01294	
L3-L4	L4	-0.04824	-0.00817	0.03457
	L3	-0.05056	-0.00978	

Table 4.12 – Local coordinates used in the definition of the supraspinous ligaments (SSL) in the lumbar spine {Adapted from (Monteiro, 2009)} (*continued*).

Spine Level	Vertebra	Coordinates [m]		Length [m]
		ξ	η	
L4-L5	L5	-0.04323	-0.00383	0.03111
	L4	-0.04824	-0.00817	
L5-S1	S1	-0.01576	0.00000	0.02596
	L5	-0.04323	-0.00383	

Figure 4.6 represents an example of the location of a ligament (in this case the supraspinous ligament) between two vertebrae, connecting the most posterior point of the spinous processes.

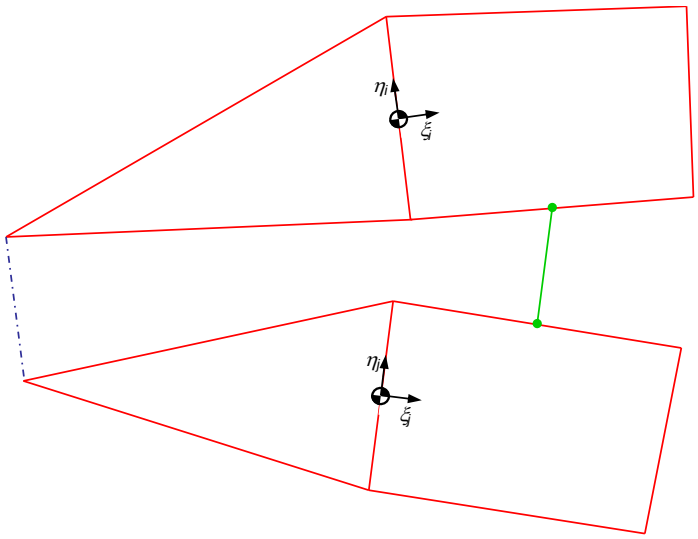

Figure 4.6 – Location of the supraspinous (SSL) ligament.

4.2. Kinematics of the Contact

The problem of the contact between rigid bodies in the spine has been addressed by several authors throughout the last decades, since this represents a major importance issue on the accurate modeling and analysis of a multibody system.

A contact problem focuses typically in three tasks:

(i) Defining of geometric properties;

(ii) Developing of a methodology for detecting contact;

(iii) Applying appropriate constitutive laws for contact forces that develop in the normal and tangential directions.

In this work, due to the geometries of the bodies in the areas of potential contacts, it was considered a contact between a sphere and a plane, as Figure 4.7 shows.

The formulation used assumes that the possible contact events can be developed at two main regions: the spinous processes and the articular facets. Figure 4.7 shows a schematic representation of the contact and will help in the process of understanding how to compute the contact forces.

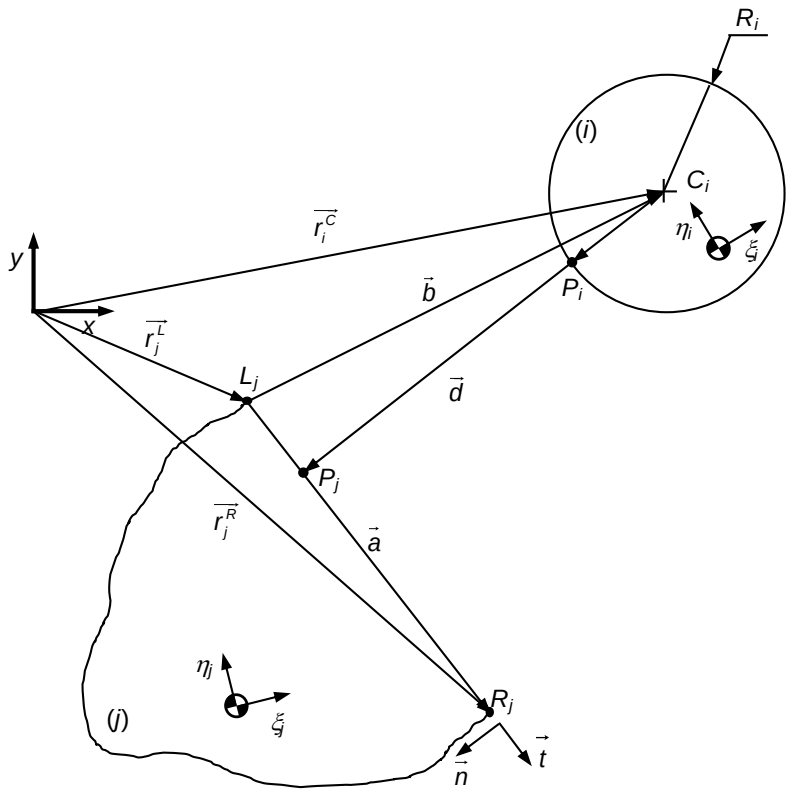

Figure 4.7 – Schematic representation of the contact between a sphere and a plane.

Let C_i be the center of the sphere located in the body i, with a radius R_i, and L_j and R_j be the most extreme left and right points of the contact plane, in body j.

First, a vector $\mathbf{a}$ connecting L_j and R_j is defined, setting the contact plane. For this calculation, the vector $\mathbf{r}_j^L$ (that defines the position of point L_j relative to the global frame) is subtracted to vector $\mathbf{r}_j^L$ (that defines the position of point L_j relative to the global frame), as explained by Equation (4.12).

$$\mathbf{a} = \mathbf{r}_j^R - \mathbf{r}_j^L = \mathbf{r}_j + \mathbf{A}_j \mathbf{s}_j'^R - \mathbf{r}_j^L - \mathbf{A}_j \mathbf{s}_j'^L \tag{4.12}$$

The length of this vector can be found by Equation (4.13).

$$a = \|\mathbf{a}\| = \sqrt{\mathbf{a}^T \mathbf{a}} \tag{4.13}$$

Once defined the plane, a tangent unitary vector $\mathbf{t}$ is readily found, as well as the normal unitary vector, as shown in Equations (4.14) and (4.15), respectively.

$$\mathbf{t} = \frac{\mathbf{a}}{a} \tag{4.14}$$

$$\mathbf{n} = [\mathbf{t}_y \quad -\mathbf{t}_x]^T \tag{4.15}$$

The goal of this formulation is to find a vector that quantifies the distance between the sphere and plane, in the normal direction relative to the plane, in order to use it later in the calculus of the normal contact force. That distance vector $\mathbf{d}$ is defined between a point P_i belonging to the sphere surface and a point P_j from the contact plane, always in the normal direction.

The definition of the distance vector can be achieved by transposing a vector $\mathbf{b}$, which connects points L_j and C_i, to the desired normal direction. Vector $\mathbf{b}$ is calculated following the described on Equation (4.16).

$$\mathbf{b} = \mathbf{r}_i^C - \mathbf{r}_j^L = \mathbf{r}_i + \mathbf{A}_i \mathbf{s}'^C_i - \mathbf{r}_j - \mathbf{A}_j \mathbf{s}'^L_j \tag{4.16}$$

Then, locating the point P_j relatively to point L_j, in the contact plane, is a matter of finding the plane tangential component of vector $\mathbf{b}$ (according to vector $\mathbf{t}$). Obtaining length $\overline{L_j P_j}$ is done through the calculus of the dot product between vectors $\mathbf{b}$ and $\mathbf{t}$, as shown in Equation (4.17).

$$\overline{L_j P_j} = \mathbf{b} \cdot \mathbf{t} = \mathbf{b}^T \mathbf{t} \tag{4.17}$$

Once this distance is defined, locating points P_i and P_j is attainable by the definition of vectors $\mathbf{r}_i^P$ and $\mathbf{r}_j^P$, from the origin of the global frame to each of the points, respectively, following Equations (4.18) and (4.19).

$$\mathbf{r}_i^P = \mathbf{r}_i^C + R\,\mathbf{n} = \mathbf{r}_i + \mathbf{A}_i \mathbf{s}'^C_i + R\,\mathbf{n} \tag{4.18}$$

$$\mathbf{r}_j^P = \mathbf{r}_j^L + (\mathbf{b}^T \mathbf{t})\mathbf{t} \tag{4.19}$$

The distance vector $\mathbf{d}$ is calculated by subtracting vector $\mathbf{r}_i^P$ to vector $\mathbf{r}_j^P$, as explained in Equation (4.20).

$$\mathbf{d} = \mathbf{r}_j^P - \mathbf{r}_i^P = \mathbf{r}_j^L + (\mathbf{b}^T \mathbf{t})\mathbf{t} - \mathbf{r}_i^C - R\,\mathbf{n} \tag{4.20}$$

The final stage of the process is the determination of the pseudo-penetration δ.

$$\delta = \mathbf{d}^T \mathbf{n} \tag{4.21}$$

Finally, the contact condition is defined according to Equation (4.22).

$$\begin{cases} \text{Contact} & if \quad \delta \leq 0 \\ \text{No contact} & if \quad \delta > 0 \end{cases} \tag{4.22}$$

If a contact event takes place, the pseudo-penetration is used on the computation of the normal contact force, according to one of the models described in Section 4.3.

Most of the contact force models include a damping component that depends on the pseudo-velocity $\dot{\delta}$. Figure 4.8 and the following paragraphs aim to clarify the process of computing that value.

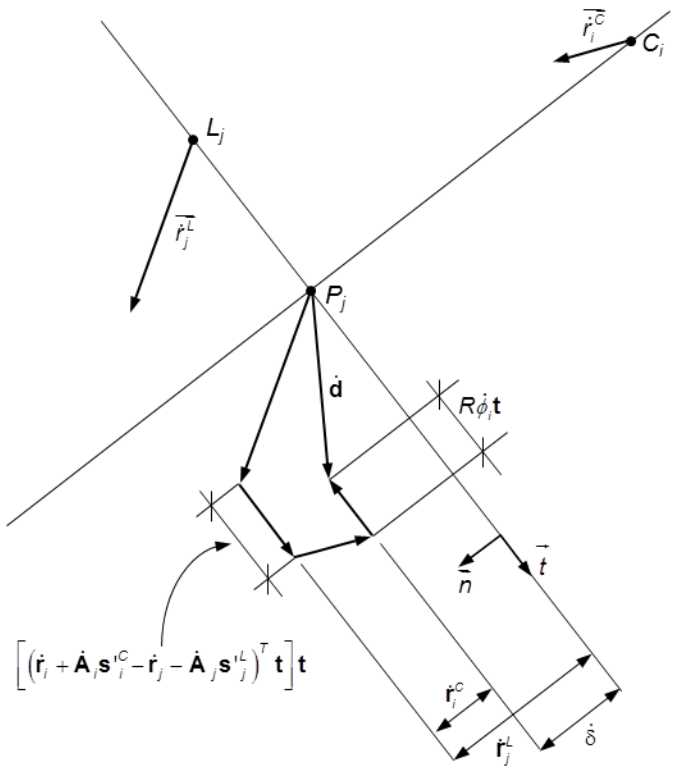

Figure 4.8 – Schematic representation of the relative contact velocity.

To find the pseudo-velocity (or normal contact velocity) it is necessary to derivate the distance vector $\mathbf{d}$, obtaining the distance velocity vector $\dot{\mathbf{d}}$ shown in Equation (4.23).

$$\dot{\mathbf{d}} = \dot{\mathbf{r}}_j^P - \dot{\mathbf{r}}_i^P \tag{4.23}$$

One must have in attention that the derivatives of the normal and tangential unit vector have to be calculated according to Equations (4.24) and (4.25).

$$\dot{\mathbf{n}} = \phi \ \mathbf{t} \tag{4.24}$$

$$\dot{\mathbf{t}} = -\dot{\phi}\,\mathbf{n} \tag{4.25}$$

The derivatives of $\mathbf{r}_i^P$ and $\mathbf{r}_j^P$ are calculated by Equations (4.26) and (4.27), respectively, after some mathematical manipulation.

$$\dot{\mathbf{r}}_i^P = \dot{\mathbf{r}}_i^C + R\,\dot{\mathbf{n}} = \dot{\mathbf{r}}_i^C + R\,\dot{\phi}_i\mathbf{t} \tag{4.26}$$

$$\dot{\mathbf{r}}_j^P = \dot{\mathbf{r}}_j^L + \left[\left(\dot{\mathbf{r}}_i + \dot{\mathbf{A}}_i\mathbf{s}_i'^C - \dot{\mathbf{r}}_j - \dot{\mathbf{A}}_j\mathbf{s}_j'^L\right)^T\mathbf{t}\right]\mathbf{t} \tag{4.27}$$

Finally, it is possible to compute the normal contact velocities, as stated in Equation (4.28):

$$\dot{\delta} = \dot{\mathbf{d}}^T\mathbf{n} = \left(\dot{\mathbf{r}}_j^L - \dot{\mathbf{r}}_i^C\right)^T\mathbf{n} \tag{4.28}$$

This normal contact velocity (or pseudo-velocity) is applied in contact models that include the use of a velocity-dependent component.

4.2.1. Articular Facets

The four articular facets of each vertebra are located symmetrically to the sagittal plane, one pair (superior and inferior) per side. As the analysis performed in this work is two-dimensional, a single sagittal contact was considered for the articular facets per FSU. It was assumed a sagittal projection of both sphere and plane components of the contact.

Table 4.13 shows the used geometric data for the implementation of the contacts between articular facets, giving information about the local coordinates of the left and right limits of the plane and the local coordinates of the center of the sphere and respective radius considered in the contact.

Table 4.13 – Geometrical properties of the sphere-plane contacts: plane and sphere reference point and its corresponding limits for the articular facets {Adapted from (Monteiro, 2009)}.

Body	**Plane**				**Body**	**Sphere**		
	Lj		**Rj**			**Ci**		**Radius**
	ξ [m]	**η [m]**	**ξ [m]**	**η [m]**		**ξ [m]**	**η [m]**	**Ri [m]**
L2	-0.015016	0.004918	-0.011590	0.019925	L1	-0.02659	-0.02025	0.00144
L3	-0.018716	0.004034	-0.016084	0.019766	L2	-0.02797	-0.02055	0.00159
L4	-0.015239	0.003836	-0.012241	0.020264	L3	-0.03033	-0.02010	0.00170
L5	-0.014376	0.002760	-0.012824	0.020140	L4	-0.02852	-0.01635	0.00180
S1	-0.002635	0.017573	0.002635	0.034627	L5	-0.02623	-0.01480	0.00198

4.2.2. Spinous Process

Table 4.14 includes the used geometric data for the implementation of the contacts between spinous processes, giving information about the local coordinates of the left and right limits of the plane and the local coordinates of the center of the sphere and respective radius considered in the contact.

Table 4.14 – Geometrical properties of the sphere-plane contacts: plane and sphere reference points and its corresponding limits for the spinous process contacts {Adapted from (Monteiro, 2009)}.

Body	Plane				Body	Sphere		
	Lj		Rj			Ci		Radius
	ξ [m]	η [m]	ξ [m]	η [m]		ξ [m]	η [m]	Ri [m]
L2	-0.066876	-0.022409	-0.033104	-0.003471	L1	-0.046980	-0.013380	0.004450
L3	-0.067867	-0.016980	-0.033253	-0.002580	L2	-0.049990	-0.012940	0.004280
L4	-0.063824	-0.014458	-0.032656	-0.001882	L3	-0.050560	-0.009780	0.003920
L5	-0.055534	-0.007267	-0.030926	-0.000393	L4	-0.048240	-0.008170	0.003870
S1	-0.018714	-0.003916	-0.012806	0.003916	L5	-0.043230	-0.003830	0.003360

4.3. Contact Force Model

Once the geometry of the contact and the methodology for detecting contact are defined, it is possible to apply the appropriate constitutive laws to calculate the contact forces.

Several studies have been developed regarding the contact between spinal surfaces. In the case of the spinous processes, this study started by computing the normal contact force (F_N) through the formulation developed by Hertz (1881), following the force law depicted in Equation (4.29),

$$F_N = K\delta^n \tag{4.29}$$

in which K is the generalized stiffness parameter, δ is the relative indentation and n is a nonlinearity parameter often considered to be equal to 1.5. The generalized stiffness parameter depends on the geometry of the surfaces in contact. In the sphere-plane contact, this parameter can be calculated through Equation (4.30),

$$K = \frac{4}{3\left(\frac{1-\nu_S^2}{E_S} + \frac{1-\nu_P^2}{E_P}\right)}\sqrt{R_S} \tag{4.30}$$

where R_S is the sphere radius, ν_S and ν_P are the sphere and plane Poisson's ratio, respectively, and E_S and E_P are the Young's moduli of each of the contacting surfaces.

The Hertz contact model represents a basic approach to the contact with elastic deformations and no damping effect. The Kelvin-Voigt approach (Timoshenko and Goodier, 1969) denotes an enhancement to the Hertz one, since it introduced the energy dissipation component, as explained in Equation (4.31).

$$F_N = K\delta + D\dot{\delta} \tag{4.31}$$

The introduced variables in this model are the hysteresis coefficient D, and the relative normal contact velocity $\dot{\delta}$. Within this model a linear spring working in parallel with a linear damper was considered, and one of its limitations is the possibility of developing a contact force when the pseudo-penetration is lower than zero (no contact situation).

Hunt and Crossley (1975) replaced the linear spring-damper Kelvin-Voigt model for a Hertz force-deformation law with a nonlinear viscoelastic element, as depicted in Equation (4.32),

$$F_N = K\delta^n + \chi\delta^n\dot{\delta} \tag{4.32}$$

where χ is the hysteresis damping factor. The contact force models presented further differ on this parameter, which is replaced directly in the equations in order to simplify the understanding of its influence. The contact force model with the hysteresis damping factor proposed by Hunt and Crossley has the form shown in Equation (4.33),

$$F_N = K\delta^n + \left(\frac{3K(1-c_r)}{2\dot{\delta}^{(-)}}\right)\delta^n\dot{\delta} \tag{4.33}$$

in which c_r is the coefficient of restitution and $\dot{\delta}^{(-)}$ is the initial contact velocity. Lankarani and Nikravesh (1990) upgraded the previous approach and equalized the kinetic energy loss to the work done by the contact force, resulting in the model of Equation (4.34).

$$F_N = K\delta^n + \left(\frac{3K(1-c_r^2)}{4\dot{\delta}^{(-)}}\right)\delta^n\dot{\delta} \tag{4.34}$$

Flores *et al.* (2011) enriched the classic force models by overpassing the disadvantages they presented when modeling low or medium restitution contacts. The force model of Equation (4.35) is suitable for soft and hard materials, as it depends on the geometrical, material, mechanical, and kinematical properties of the contacting bodies.

$$F_N = K\delta^n + \left(\frac{8K(1-c_r)}{5c_r\dot{\delta}^{(-)}}\right)\delta^n\dot{\delta} \tag{4.35}$$

4.4. Summary and Discussion

In this Chapter a full description of all data used to define the geometry of the spinal components (vertebral bodies, ligaments, intervertebral discs, and spinal contacts) and their mechanical behavior was presented.

Chapter 5

Results and Discussion

In this section, some results obtained from computational simulation are presented with the intent to validate the implementation purposed models. It was aimed to predict the mechanical behavior of the lumbar spine in different situation such as (i) forcing the system to its motion limits, (ii) introducing the physiologic alteration due to a pathology in the model (by changes in properties of its components) and (iii) testing the effect of the application of a load to the model. For this analysis, a functional spinal unit was considered rather than the full lumbar spine model already developed, in order to easily obtain results and therefore studying and improving the response of part of the model.

5.1. Validation of the Developed Methodologies

To validate the developed methodologies, a series of tests was done with simple systems, using properties that did not correspond in some cases to the ones of the lumbar spine model.

5.1.1. Ligaments

The subroutine developed and implemented for the computation of the ligament forces was validated using the system depicted in Figure 5.1. Bodies *i* and *j* have a mass of 1.0 kg each, and the ligament between them had an initial length equal to 1.0 m, with a stiffness coefficients of 50 N/m and a parameter C value of 0.1. Body *i* was fixed while body *j* was actuated by gravity.

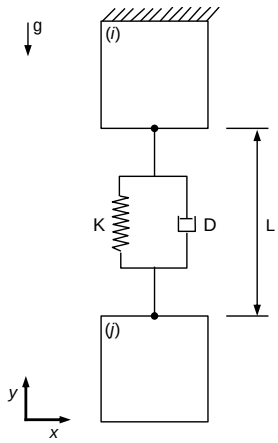

Figure 5.1 – Schematic representation of a ligament.

The configuration of the system allowed body j to describe a descending motion and different force laws given by Equation (4.6) were applied depending on the strain (ε) of the ligament. The transition (ε_T) and limit (ε_{LIM}) strains considered were 0.2 and 0.5, respectively.

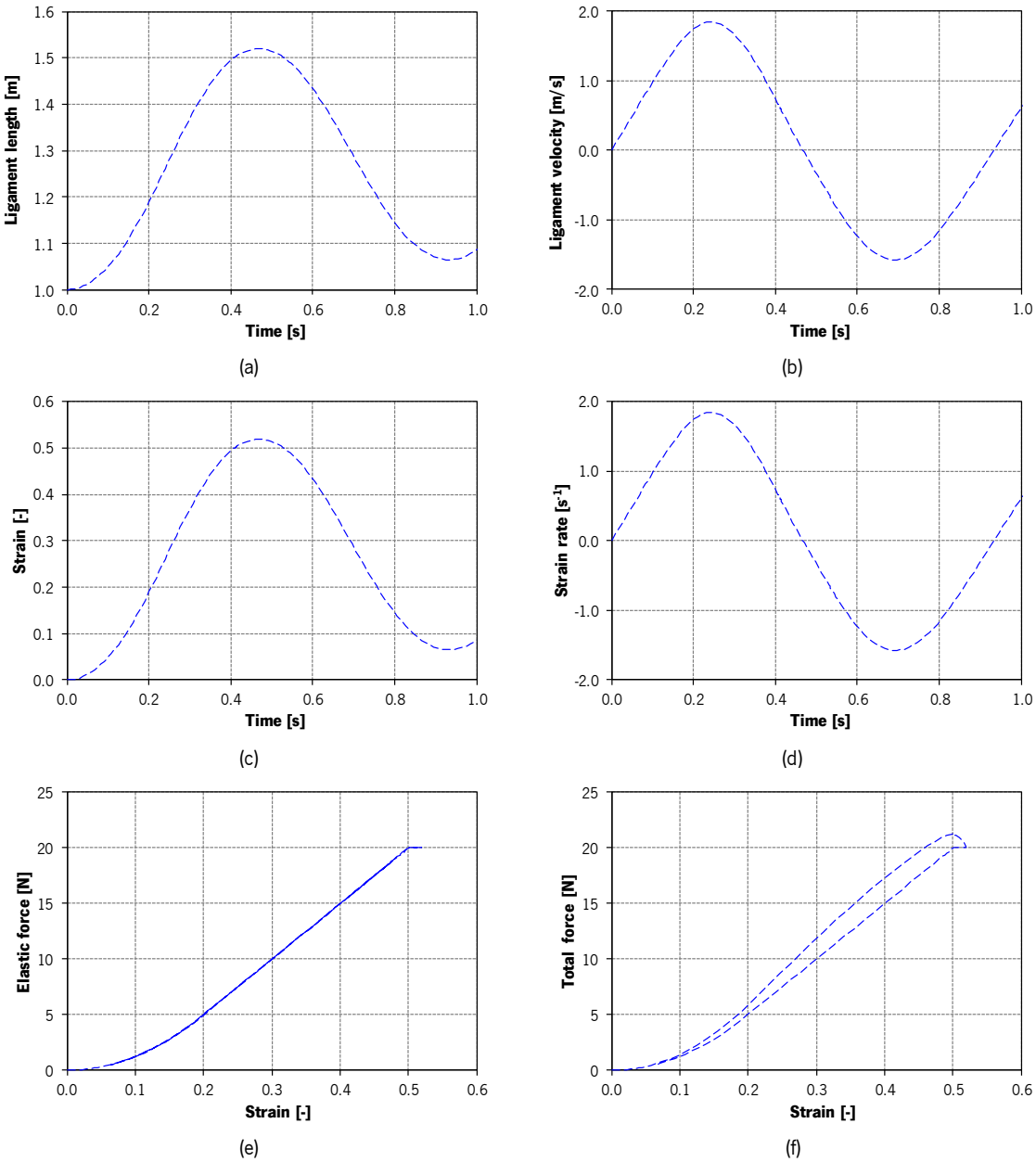

Figure 5.2 – Ligament behavior: (a) ligament length versus time; (b) ligament velocity versus time; (c) strain versus time; (d) strain rate versus time; (e) elastic force versus strain; (f) total force versus strain.

The dynamic response of the system is quantified by plotting the ligament length, ligament velocity, strain and strain rate against time, as well as the elastic force versus strain and the total force versus strain, as illustrated in Figure 5.2. It is possible to verify the similarity between the

ligament length and strain plots, as well as between ligament velocity and strain rate, since the latters are the derivatives of the first ones. In Figure 5.2(a) it is visible the difference between the mechanical behaviors of the ligament: for strains between 0.0 and 0.2, a quadratic response can be identified; for strains between 0.2 and 0.5, the plot shows a linear behavior, and above the limit strain 0.5, the elastic force is kept constant in the maximum value before failure.

The influence of the hysteretic behavior of the ligament is visible in Figure 5.2(f), where the loading and unloading phases can be identified. The upper curve represents a loading condition when both strain and strain rate are positive, and the lower line corresponds to the unloading situation, with a positive strain and negative strain rate. The area enclosed by the hysteresis loop denotes the energy loss due to the internal damping of the ligament.

5.1.2. Bushing Elements

In order to test the behavior of the bushing elements (BE), an analysis was performed with the simple system visible in Figure 5.3. The upper body *i* was actuated by gravity on the negative direction of the *y*-axis and by the BE in the opposite direction. Both bodies have a mass of 1.0 kg and initially are separated by a BE with an initial length of 1.0 m. The BE stiffness coefficient is equal to 1000 N/m and damping coefficient is equal to 30 N.s/m.

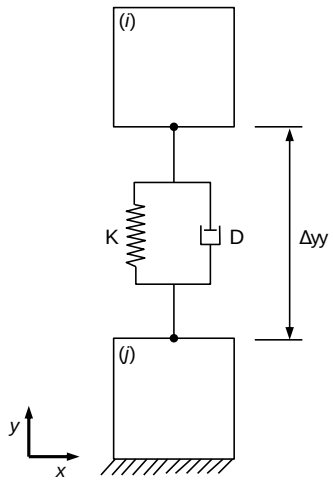

Figure 5.3 – Schematic representation of a bushing element actuating on the y-direction.

Figure 5.4 shows the outputs diagrams for the bushing length, bushing velocity, elastic force, damping force and total vertical force are plotted against time. The system is initialized with null velocity, and the simulation was performed during 0.5 seconds.

Figure 5.4(a) shows the fall of the body *i* until a length of approximately 9.88 mm, when it is actuated by the BE. In this instant, the force produced by the BE overcomes the gravitational force of body *i* and, therefore, the body is returned to a higher point (circa 9.90 mm). The corresponding bushing velocity represented in Figure 5.4(b) is the derivative of the bushing length showed in Figure 5.4(a).

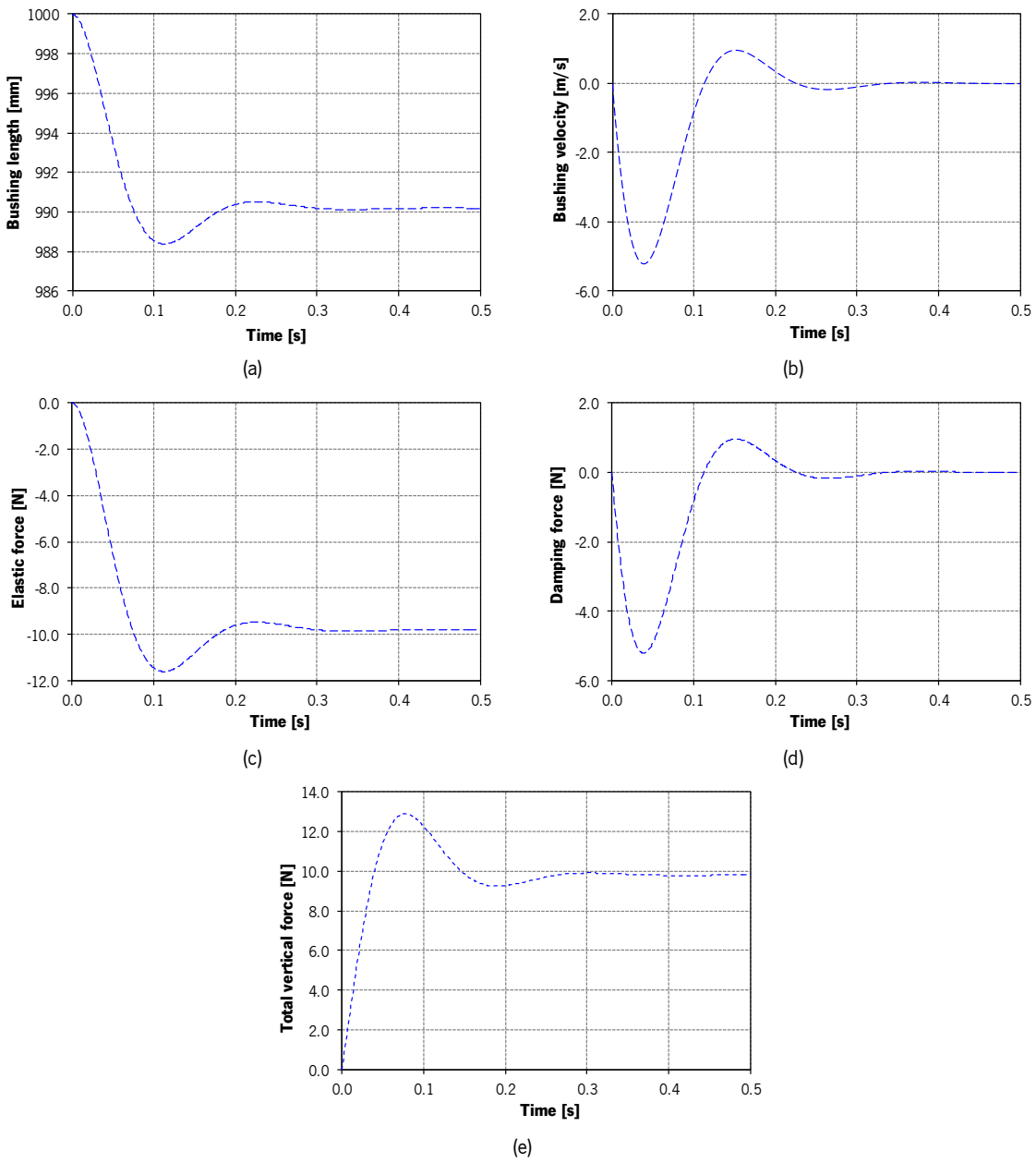

Figure 5.4 – Behavior of the bushing element (y-direction, v_i^0=0 m/s): (a) bushing length; (b) bushing velocity; (c) elastic force; (d) damping force; (e) total vertical force.

As it was expected, Figure 5.4(c) and Figure 5.4 (d) depict similar behaviors to Figure 5.4(a) and Figure 5.4(b). The magnitude of the total vertical force, illustrated in the diagram of

Figure 5.4(e), is the sum of the elastic and damping force components. Throughout this computational test, the bushing element presented only its behavior in compression.

After this analysis, an initial vertical velocity of 10 m/s was applied on the upper body *i* in order to observe the influence of the velocity on the produced forces, as well as the behavior of the BE in tension. Figure 5.5 shows the outputs obtained for the described simulation in which the bushing length, velocity, elastic force, damping force and total vertical force are plotted.

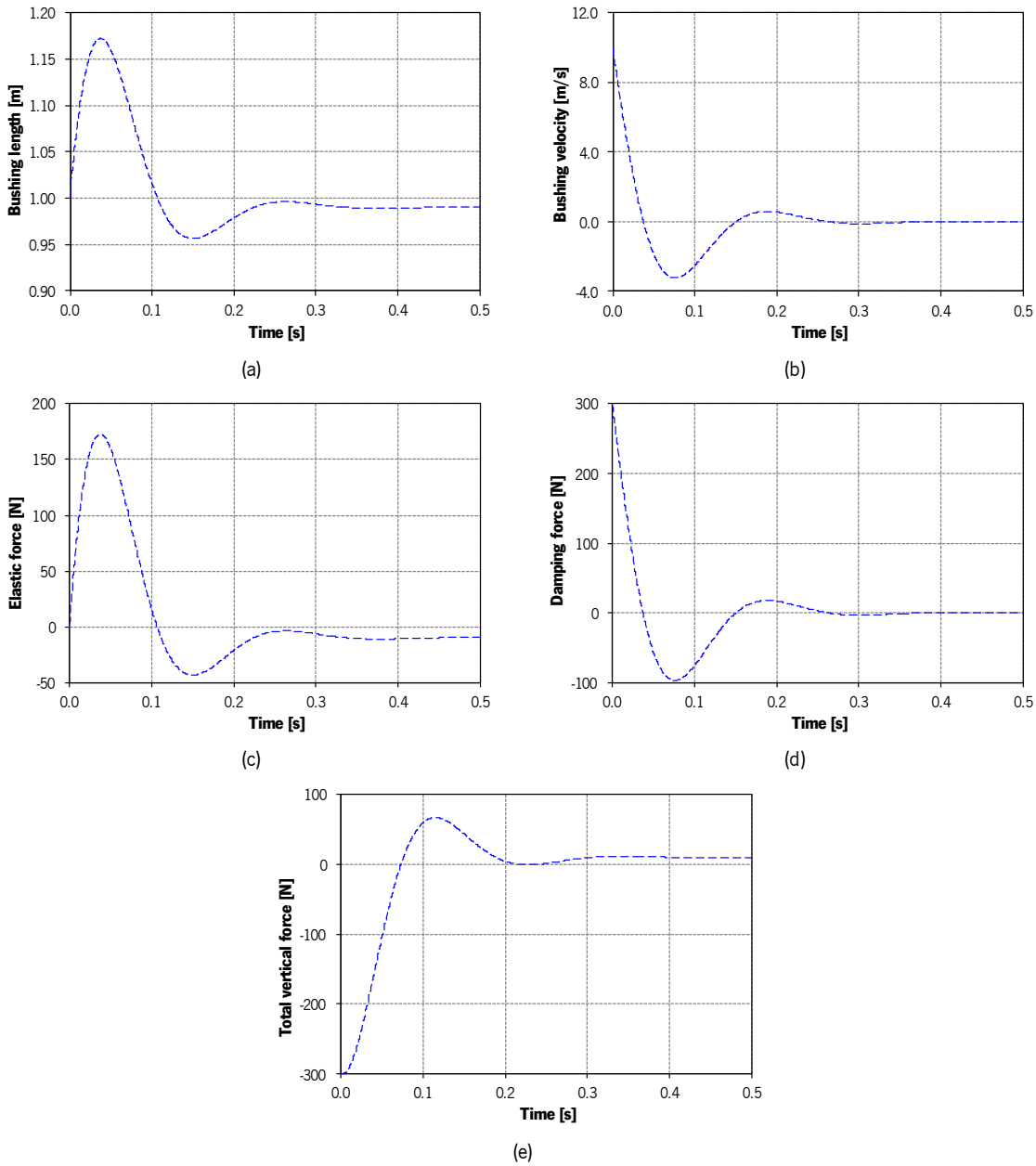

Figure 5.5 - Behavior of the bushing element (y-direction, v_i^0=10 m/s): (a) bushing length; (b) bushing velocity; (c) elastic force; (d) damping force; (e) total vertical force.

The response of the bushing element with an initial velocity exhibits some differences when compared to the outputs obtained with null initial velocity, as shown in Figure 5.4. For instance, in

the Figure 5.5(a) it can be observed that during the first 0.1 seconds of simulation, the length of the bushing is higher that the initial length. This is a result of the application of an initial vertical velocity of 10 m/s to the body *i*. The bushing velocity also reflects its expected dynamic response. The results obtained for the elastic and damping forces are directly related to the bushing length and velocity, respectively. The vertical force on body *i* is once more the sum of the elastic and damping forces in that body.

For the evaluation of the response of the bushing element (BE) in the horizontal direction, the locations of the body *i* and the bushing element were altered, so that the bushing could actuate only in the *x*-direction, as visible in Figure 5.6. The parameters applied were the same of the previous simulation.

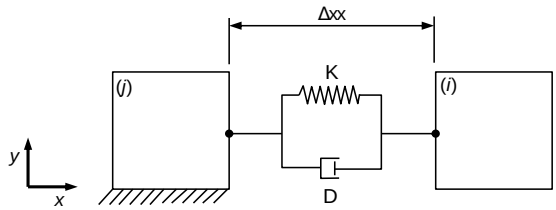

Figure 5.6 – Schematic representation of a bushing element acting on the *x*-direction.

The simulation was done without gravitational effect, being acted by a force to simulate gravity on the negative *x*-direction. The obtained results with that setup are shown in Figure 5.7.

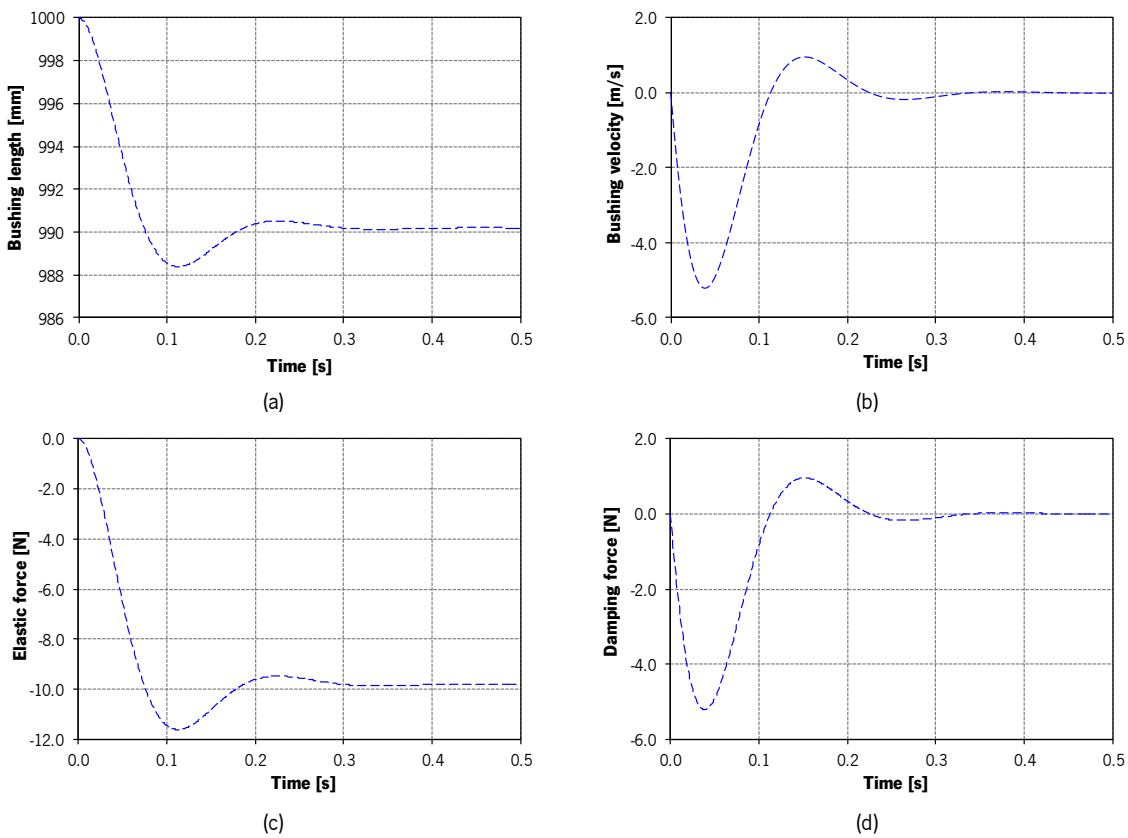

Figure 5.7 - Behavior of the bushing element (*x*-direction, v_i^0=0 m/s): (a) bushing length; (b) bushing velocity; (c) elastic force; (d) damping force; (e) total horizontal force.

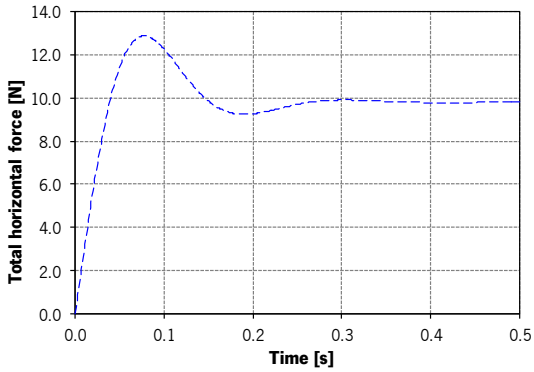

(e)

Figure 5.7 - Behavior of the bushing element (*x*-direction, v_i^0=0 m/s): (a) bushing length; (b) bushing velocity; (c) elastic force; (d) damping force; (e) total horizontal force (*continued*).

The outputs for the horizontal testing of the bushing element are similar to those for the vertical simulation presented before. This is obvious as both represent a similar simulation scenario.

Finally, the rotational behavior of the BE was assessed by a different approach, whose results are plotted in Figure 5.8. Two equal bodies with a mass of 1.0 kg and a moment of inertia of 0.1 kg.m^2 were placed in the same initial position, being the centers of mass of the bodies the points to which the rotational BE were linked. This procedure guaranteed that the initial horizontal and vertical bushing lengths were zero. The initial orientation of body *i* was set as 1 rad whereas the body *j* had a zero inclination and was stationary. The initial angular offset was defined as 1 rad, with stiffness and damping coefficients of 3 N.m/rad and 0.5 N.m.s/rad, respectively. The effect of gravity was ignored and a moment of 1 N.m was applied to the center of mass of the body *i*.

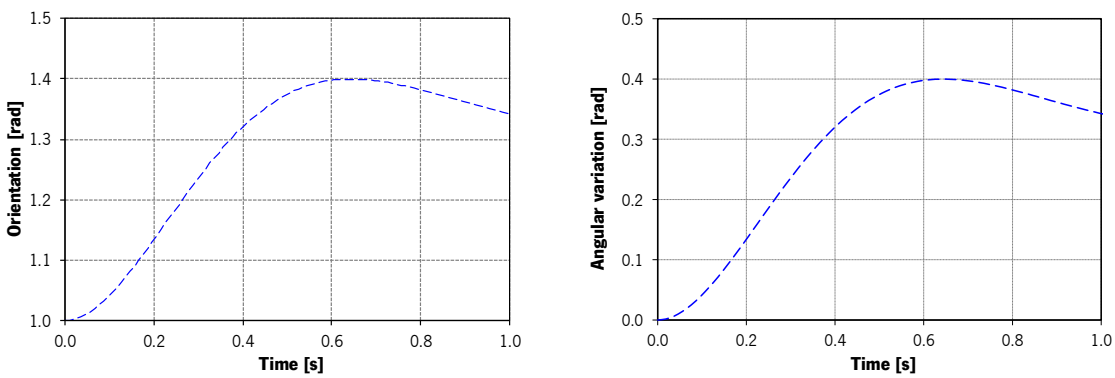

(a) (b)

Figure 5.8 – Behavior of the bushing element (ϕ-direction): (a) orientation of body *i*; (b) angular variation; (c) relative angular velocity; (d) elastic moment; (e) damping moment; (f) total bushing moment.

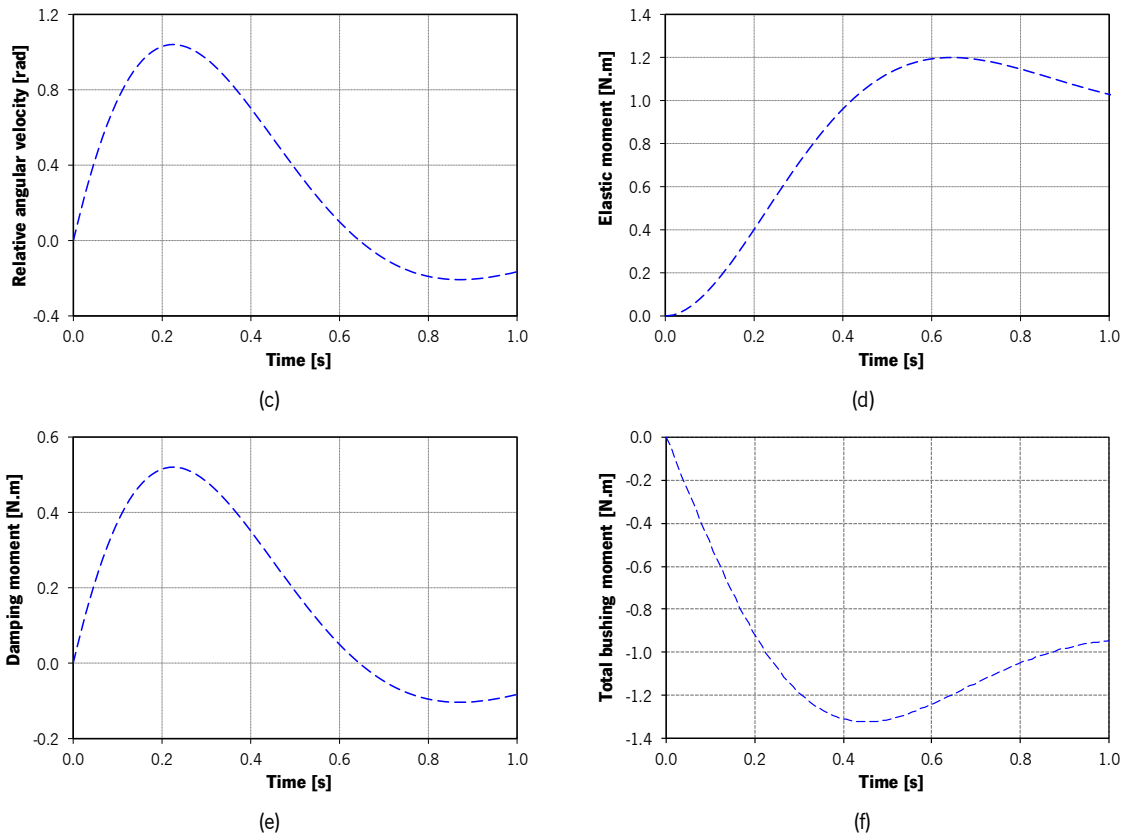

Figure 5.8 - Behavior of the bushing element (ϕ-direction): (a) orientation of body *i*; (b) angular variation; (c) relative angular velocity; (d) elastic moment; (e) damping moment; (f) total bushing moment. (*continued*).

The orientation of body *i* and the angular variation of the bushing element (BE) show an agreement with each other. The relative angular velocity of the BE displays a zero value approximately around 0.6 seconds, the same instant of the maximal angular variation as it was expected. The elastic and damping moments show similar evolution to the angular variation and velocity, respectively. The total bushing moment represents the sum of elastic and damping moments.

5.1.3. Contact

The contact methodology was validated using a simple bouncing ball example illustrated in Figure 5.9. The ball is released from an initial height and actuated by gravity. The ball will collide with the plane and bounce after the impact height, which position can be the same as the initial if the contact is purely elastic (following the hertzian law) or lower than the first (the height loss depends on the coefficient of restitution between contacting surfaces). In this study, a 1.0 kg ball with a radius of 0.1 m was dropped from a height of 1 m to a stationary ground plane. A

generalized stiffness parameter of 140×10^6 $N^{3/2}$ was applied, and the coefficient of restitution is equal to 0.9.

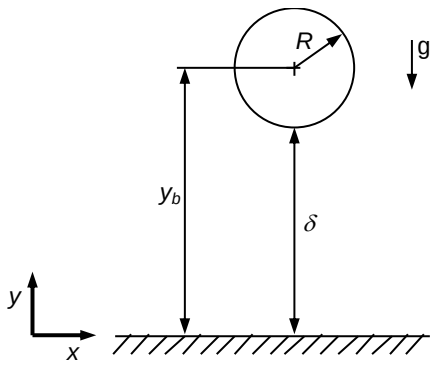

Figure 5.9 – Bouncing ball example.

Two different contact force models were applied in the present analysis, according to the description made in Section 4.3: (i) the Lankarani and Nikravesh model (L & N), and (ii) the Flores *et al.* model (F). These two formulations differ on the calculation of the hysteresis damping factor χ.

Figure 5.10 illustrates the ball behavior, showing the plot of its position and velocity for the first 10 seconds of simulation.

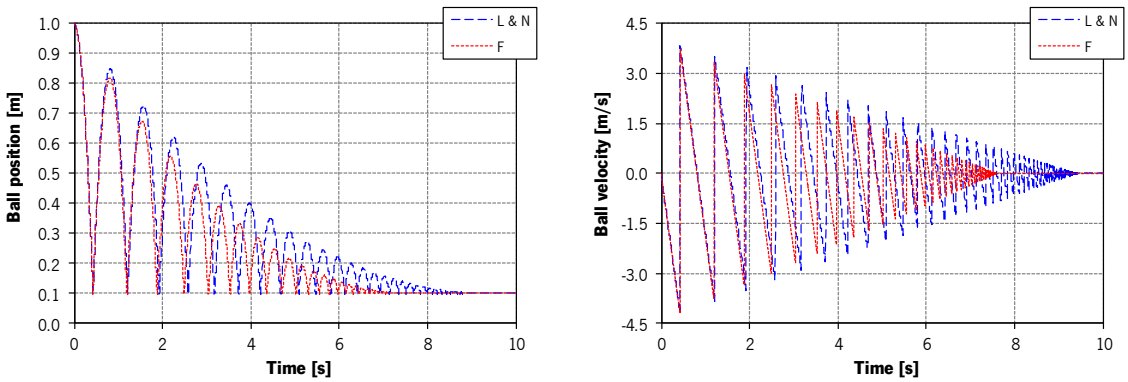

(a) (b)

Figure 5.10 – Kinematic simulation results of a ball falling on the ground: (a) ball position; (b) ball velocity.

A first simulation was performed with a coefficient of restitution of 0.9, in order to compare the response of both models in a high elastic situation. It is possible to verify a decrease in the maximal height of the ball and a reduction of the maximal ball velocity (in absolute value) from 0 to 10 seconds of simulation. Applying the contact force model of Lankarani and Nikravesh, the ball takes more time to stop than with the use of model of Flores *et al.*, which is indicative of a larger energy loss with the latter than with the first. This also denotes that a Flores *et al.* contact is longer

than a Lankarani and Nikravesh contact. This happens as a result of the focus of application of Lankarani and Nikravesh force model to the contact between hard materials (high coefficients of restitution), typically a metal-metal contact, whereas the Flores *et al.* model is suitable for both hard and soft materials, which is the case of biomechanical systems.

Figures 5.11(a-c) show the time plots of deformation, velocity of deformation and contact force developed during the first contact between the ball and the plane, and Figure 5.11(d) illustrates the contact force versus deformation.

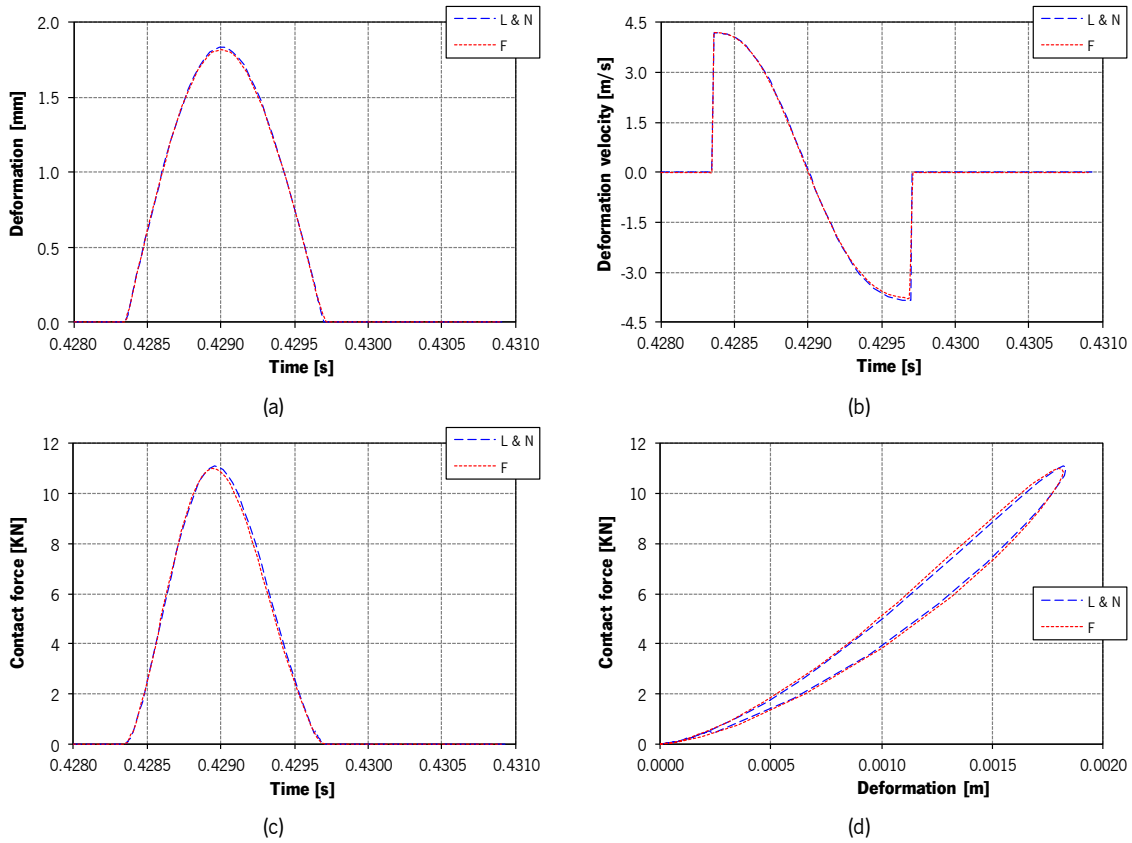

Figure 5.11 – Influence of the contact model on the bouncing ball behavior (c_r=0.9): (a) deformation; (b) velocity of deformation; (c) contact force; (d) contact force-deformation relation.

For the analysis of Figure 5.11, it can be observed that the models produce very similar outputs, not being clear the influence of the contact force model in the obtained results. However, as previously stated, the main difference between the two models arises with the application of low or moderate coefficients of restitution (below 0.8).

To assess the influence of the coefficient of restitution, another simulation was performed with a coefficient of restitution equal to 0.616, which is the value typically found in articular cartilage-on-bone case (Burgin and Aspden, 2008) and can be considered to be a soft and inelastic contact. Figures 5.12(a-c) show the time plots of deformation, velocity of deformation and contact

force developed during the first contact between the ball and the plane, and Figure 5.12(d) illustrates the contact force plotted versus deformation.

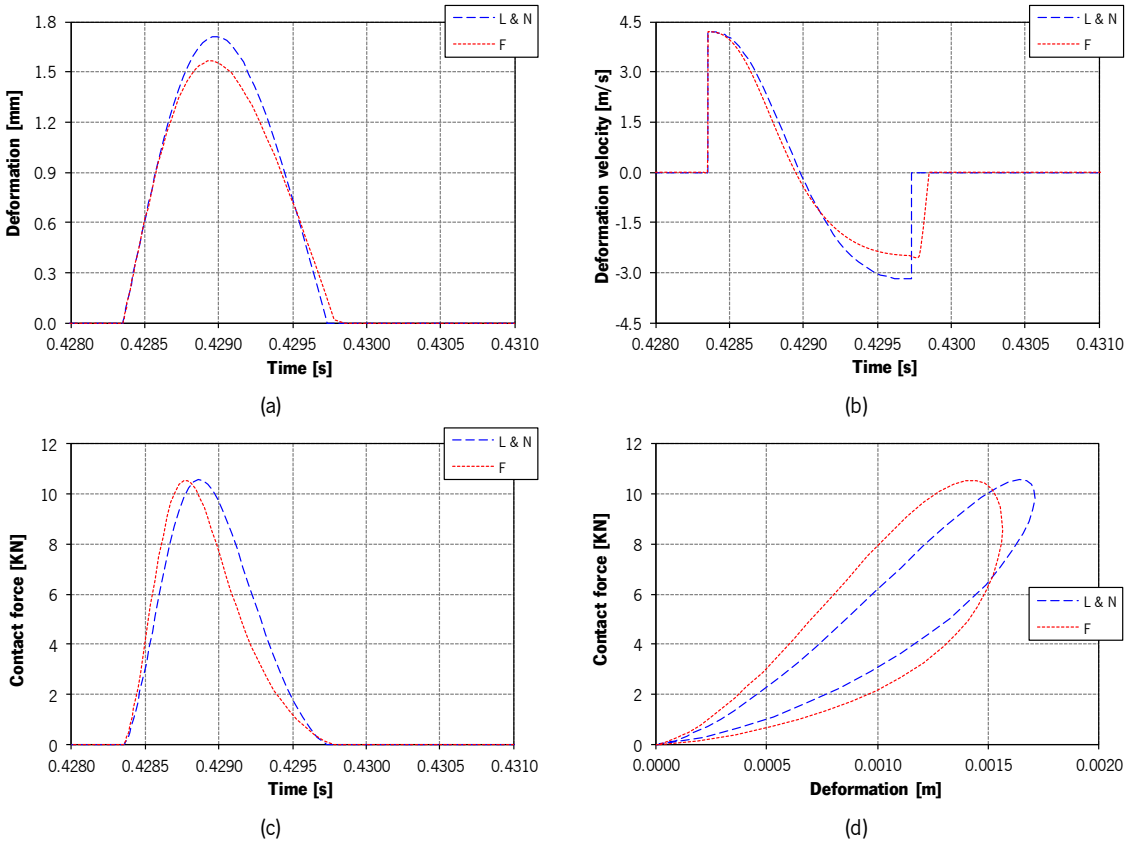

Figure 5.12 – Influence of the contact model on the bouncing ball behavior (c_r=0.616): (a) deformation versus time; (b) velocity of deformation versus time; (c) contact force versus time; (d) contact force-deformation relation.

The results allow to corroborate the previous statements about the differences between the contact force models. The deformation plot of Figure 5.12(a) shows, not only a larger maximal deformation, but also a shorter contact time, implying a lower loss of energy. The differences are even more evident in the deformation velocity chart in Figure 5.12(b), especially at the relative separation velocity. For both models this value is inferior to the relative approaching velocity, but the magnitude of the velocity obtained with Flores *et al.* model is lower than the obtained with Lankarani and Nikravesh model (in absolute values).

The force developed during the contact has a lower maximal value for Flores *et al.* model and has lower values throughout the phase of rebound, due to the dissipation of energy. Finally, the contact force-deformation relation allows a clear identification of a larger energy loss (area inside the loop) for Flores *et al.* model than for Lankarani and Nikravesh's approach.

All the methodologies developed under the objectives of this work were implemented and validated successfully with the series of simulation described in the previous pages. The

procedures for the computation of forces and moments of ligaments, bushing elements and potential contacts were corroborated by the validation results.

5.2. Application to a Functional Spinal Unit

After the validation of the proposed methodologies for ligaments, bushing elements and contact, they have to be applied to a functional spinal unit (FSU). This FSU is a set of two vertebrae, their surrounding ligaments and joining intervertebral disc. Figure 5.13 shows the FSU with the respective multibody system elements, for a better understanding of the problem.

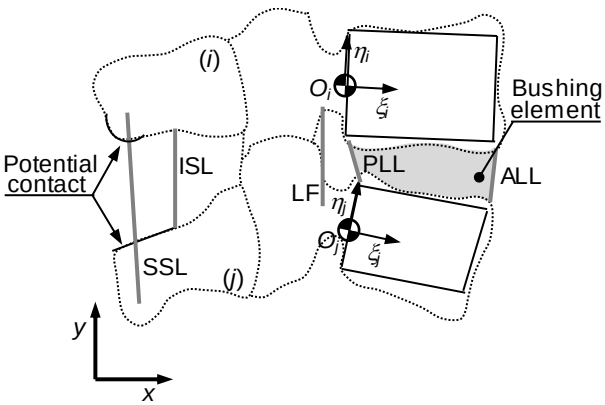

Figure 5.13 – Multibody model of two consecutive vertebrae and their fundamental elements (bodies, ligaments, bushing elements and potential contact areas) {Adapted from (Tribuzi *et al.*, 2012)}.

The model represents the vertebral bodies with a solid line quadrilateral, which contain the vertebra center of mass at the mid-height of left edge. The vertebrae are modeled as rigid bodies. The superior and inferior edges of each vertebral body play a key role in the model since they represent the cartilaginous endplates, and the geometric center of those is essential for simulating the viscoelastic behavior of the intervertebral discs (IVD).

The grey-shaded area represents the IVD that is modeled as a linear bushing element (BE) with three degrees-of-freedom. The origin point of the BE is the center a new frame *xxyy*, whose location is the key point for understanding how the BE simulates forces and moments between vertebrae, for instance, the different responses in uniaxial loading such as compression-tension.

Each FSU comprises a set of six different ligaments, as described in Chapter Four, namely ALL, CL, ISL, LF, PLL and SSL. The capsular ligament (CL) is not visible in Figure 5.13, but can be seen on Figure 2.8. Each of the ligaments has different properties despite following the same mechanical behavior, which is characterized as nonlinear spring with an associated damping coefficient in loading situation.

The potential contact occurs typically in two regions in each FSU. In Figure 5.13 is shown the spinous processes contact, in the most posterior area of the vertebrae. Due to the high amplitude of motion necessary to force those areas to interact, this is not a contact as common as the articular facet contact. For a visualization simplification, those facets are not drawn in Figure 5.13. However, the lateral view of a vertebra of Figure 2.3(b) shows the location of those elements.

For the development of the present two-dimensional multibody model it was assumed that, for the sake of simplicity, the articular facets could be projected from their natural sagittal symmetric location (two superior facets, one on the left and another on the right side, and two inferior ones, following the same arrangement) to the sagittal plane. However, it is important to point out that facet contact pair (per FSU) will support twice as much force, in order to better simulate that anatomical region.

Besides some minor geometrical changes and location differences, the behavior of the FSU can be replicable for the remaining lumbar spine. Hence, it is possible to build a full lumbar spine multibody model, from the first lumbar vertebra (L1) to the beginning of the sacrum (S1), as it is illustrated in Figure 5.14. The model comprises six rigid bodies, five bushing elements, thirty ligaments and ten contact pairs (five for the spinous processes and five for the articular facets).

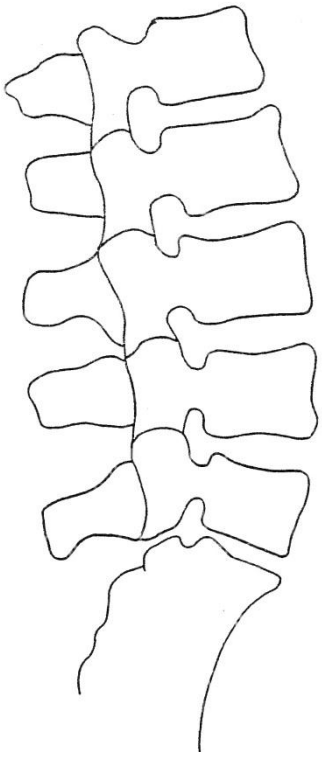

Figure 5.14 - Developed lumbar spine multibody model (from L1 to S1).

After the development of the model, the test scenarios need to be defined in order to validate it rather than the methodologies. Three different situations can be analyzed as a coherent set of trials in which a lumbar spine model is believed to produce useful outputs.

First, the physiologic range of motion should be tested in the sagittal plane. That is, the model should be subjected to a control motion in order to calibrate its elements response. As mentioned in Chapter Two, the range of motion and representative angle for the different spinal levels is known for a healthy situation. The first simulation should reflect that input, and not represent any type of damaging force for any of the lumbar components.

As a second situation, and regarding the motivation of this dissertation, the effect of the existence of spinal disorder should be introduced. In this case, the biomechanical changes (*e.g.* material properties) inherent to the degenerative disc disease (DDD) in the lumbar spine are documented by several authors, and that information can be taken into consideration in the input for the model, such as the stiffness and damping coefficients, the coefficient of restitution or even the range of motion of a given spinal segment.

Another interesting test could be performed in the simulation of traumatic events in the lumbar spine, and studying the behavior of the spinal elements under mechanical overload, such as an automotive accident, the handling of heavy objects by workers or even the exposure to cyclic loads or vibration.

Each of the suggested trials involves providing the model (and simulation program), a set of data that can be used to mimic these situations. In order to do this, one of two options can be followed: (i) guiding constraints or (ii) actuators. A guiding constraint is a series of linear and angular positions aligned in time that compels one or more bodies to follow a predetermined path. Through the *BodyKinematics* analysis of the software OpenSim™, it is possible to extract some guiding constraints for each of the lumbar vertebrae. Another possibility is the use of actuators, such as directly applying a force or moment at a given point.

Chapter 6

Conclusions and Future Work

6.1. Conclusions

The present work comprised several components. First, a literature review over the main works already developed in the biomechanical simulation of the spine was performed, followed by an anatomical description of the elements needed in order to accurately describe the lumbar spine region. The focus on this anatomical area was due to the high incidence of medical disorders in this region, particularly the ones concerning the mechanical overload of the vertebral elements.

Moreover, the description of the effects of degenerative disc disease was performed, aiming to adapt the response of the developed spine model to this kind of pathologies.

A review approach of the multibody systems was also done, regarding general aspects such as the different methodologies in what concerns kinematic or dynamic approaches, as well as the differences between forward and inverse dynamics. This brief depiction was followed by the description of the used type of coordinates, the introduction to the equations that describe constraints in the model, as well as the equations of motion and their solving, passing through the computational/mathematical methods used for its solving.

This introduction to the multibody systems dynamics led to the description of the developed model, taking into account the geometry of the rigid bodies, the mechanical models used for the simulation of the different spinal elements, such as ligaments, intervertebral discs and possible contacts between rigid bodies. A depiction of the contact detection and different existent contact force models was done.

An individual analysis of each of their issues was performed in order to validate their implementation in the context of multibody dynamics. Simple models were used for the validation and the obtained outputs were analyzed and discussed regarding the application of the methodologies to a biological system.

Finally, it was described a set of test scenarios in which the developed model can be applied.

6.2. Future Work

The following items aim to contribute for the improvement of the formulation:

- Extend the proposed methodologies from a functional spinal unit to the whole lumbar spine, since the model is already developed;
- Test the model for different simulation scenarios, such as the minimal and maximal motion limits for a healthy intervertebral disc, the motion limitations imposed by the pathologies on the focus of this work, the effect of loads or even an impact scenario;
- Obtain the geometrical and inertial properties experimentally, representing an up-to-date state of the human anatomy.
- Study the hypothesis of extending this analysis of the lumbar spine to a three-dimensional approach, representing, therefore, a more accurate description of the real phenomenon of lumbar motion.
- Refine the applied constitutive laws for the contact forces, in order to a more accurate simulation of the real behavior of these events.

References

ABOUHOSSEIN, A., WEISSE, B. and FERGUSON, S. J., 2011, A multibody modelling approach to determine load sharing between passive elements of the lumbar spine, *Computer Methods in Biomechanics and Biomedical Engineering*, 14, pp. 527-537.

ADAMS, 2011, MSC Software - Adams, http://www.mscsoftware.com/Products/CAE-Tools/Adams.aspx, accessed on 23rd September 2011.

ADAMS, M. A. and DOLAN, P., 2005, Spine biomechanics, *Journal of Biomechanics*, 38, pp. 1972-1983.

AN, H., BODEN, S. D., KANG, J., SANDHU, H. S., ABDU, W. and WEINSTEIN, J., 2003, Summary statement: emerging techniques for treatment of degenerative lumbar disc disease, *Spine*, 28, pp. S24-25.

ANYBODY, 2011, AnyBody Modeling System™, http://www.anybodytech.com/, accessed on 16th September 2011.

B|BRAUN, 2011, activ ® L, http://www.bbraun.com/cps/rde/xchg/bbraun-com/hs.xsl/products.html?prid=PRID00004594, accessed on 17th October 2011.

BAUER, S. and GRUBER, K., 2009, MBS Model of the Human Lumbar Spine - Development and Applications, *SIMPACK News*, University of Koblenz-Landau, Campus Koblenz, 18-19.

BEHRSIN, J. and BRIGGS, C., 1988, Ligaments of the lumbar spine: a review, *Surgical and Radiologic Anatomy*, 10, pp. 211-219.

BOGDUK, N., 2005, *Clinical anatomy of the lumbar spine and sacrum*, Elsevier/Churchill Livingstone, Philadelphia.

BOGDUK, N., LAU, P., GOVIND, J. and KARASEK, M., 2005, Intradiscal electrothermal therapy, *Techniques in Regional Anesthesia and Pain Management*, 9, pp. 25-34.

BOOS, N. and AEBI, M., 2008, *Spinal disorders: fundamentals of diagnosis and treatment*, Springer, Berlin.

BURGIN, L. and ASPDEN, R., 2008, Impact testing to determine the mechanical properties of articular cartilage in isolation and on bone, *Journal of Materials Science: Materials in Medicine*, 19, pp. 703-711.

CHRISTOPHY, M., 2010, *A Detailed Open-Source Musculoskeletal Model of the Human Lumbar Spine*, MSc Thesis, University of California, California, USA.

DE JAGER, M., 2000, *Mathematical Head-Neck Models for Acceleration Impacts*, PhD Thesis, Eindhoven University of Technology, Eindhoven, Netherlands.

DENIS, F., 1983, The three column spine and its significance in the classification of acute thoracolumbar spinal injuries, *Spine*, 8, pp. 817-831.

ESAT, V., 2006, *Biomechanical modelling of the whole human spine for dynamic analysis*, PhD Thesis, Loughborough University, Leicestershire, UK.

FAIRMAN, M., GHASEMPOOR, A. and ABDOLI-E, M., 2009, Development of a multibody computational model of the lumbar spine with simulink, *Proceedings of Science and Technology for Humanity (TIC-STH), 2009 IEEE Toronto International Conference*, 26-27 Sept. 2009, pp. 130-133.

FALLER, A., SCHÜNKE, M., SCHÜNKE, G. and TAUB, E., 2004, *The human body: an introduction to structure and function*, Thieme, Stuttgart.

FERREIRA, A., 2008, *Multibody Model of the Cervical Spine and Head for the Simulation of Traumatic and Degenerative Disorders*, MSc Thesis, Technical University of Lisbon, Lisbon, Portugal.

FHORTHOPEDICS, 2011, LP-ESP ®, http://www.fhorthopedics.com/lombar-disc-lp-esp.html, accessed on 17th October 2011.

FLORES, P., 2010, *MUBODYNA - A FORTRAN Program for Dynamic Analysis of Planar Multibody Systems - User's Manual Version 1.0*, University of Minho, Guimarães.

FLORES, P., AMBRÓSIO, J. and CLARO, J. C. P., 2008, *Kinematics and dynamics of multibody systems with imperfect joints: models and case studies*, Springer, Berlin.

FLORES, P., MACHADO, M., SILVA, M. T. and MARTINS, J. M., 2011, On the continuous contact force models for soft materials in multibody dynamics, *Multibody System Dynamics*, 25, pp. 357-375.

FLORES, P. and SEABRA, E., 2010, *Dynamics of Planar Multibody Systems*, VDM Verlag Dr. Mueller e.K., Saarbrücken.

FUJIWARA, A., LIM, T. H., AN, H. S., TANAKA, N., JEON, C. H., ANDERSSON, G. B. and HAUGHTON, V. M., 2000, The effect of disc degeneration and facet joint osteoarthritis on the segmental flexibility of the lumbar spine, *Spine (Phila Pa 1976)*, 25, pp. 3036-3044.

GRAY, H., 1918, Anatomy of the Human Body, Philadelphia, Bartleby.com, 2000,

HERMAN, I. P., 2007, *Physics of the human body*, Springer, Berlin.

HERTZ, H., 1881, Über die Berührung fester elasticher Körper, *Journal für die reine und angewandte Mathematik*, pp. 156-171.

HUNT, K. H. and CROSSLEY, F. R. E., 1975, Coefficient of Restitution Interpreted as Damping in Vibroimpact, *Journal of Applied Mechanics*, 42, pp. 440-445.

JUCHEM, S., 2009, *Entwicklung eines Computermodells der lumbalen Wirbelsäule zur Bestimmung mechanischer Belastungen*, PhD Thesis, Universität Koblenz-Landau, Koblenz, Germany.

JUCHEM, S. and GRUBER, K., 2009, MBS Model for the Estimation of Forces and Torques in the Human Lumbar Spine, *Proceedings of World Congress on Medical Physics and Biomedical Engineering*, Munich, Germany, September 7 - 12, 2009, pp. 2234-2237.

KRAEMER, J., 2008, *Intervertebral Disk Diseases: Causes, Diagnosis, Treatment and Prophylaxis*, Thieme, Stuttgart.

KYRIACOU, P. A. P., M.P. and YEH, J., 2009, Investigation of the *in-vitro* loading on a artificial spinal disk prosthesis, *Journal of Physics: Conference Series*, 178, pp. 1-6.

LANKARANI, H. M. and NIKRAVESH, P. E., 1990, A Contact Force Model With Hysteresis Damping for Impact Analysis of Multibody Systems, *Journal of Mechanical Design*, 112, pp. 369-376.

LUMBARSIM, 2011, LumbarSIM - a plug-in module for LifeMOD™, by LifeModeler, http://www.lifemodeler.com/products/lumbarsim, accessed on 21st September 2011.

MENON, R., 1995, *Multibody and Finite Element Approaches in the Development of a Model for the HUman Head-Neck-Torso System*, PhD Thesis, Wichita State University, Kansas, USA.

MINISTÉRIODASAÚDE, 2011, Doenças Reumáticas, http://www.min-saude.pt/portal/conteudos/enciclopedia+da+saude/doencas/doencas+reumaticas/default.htm, accessed on 13th October 2011.

MONTEIRO, N., 2009, *Analysis of the Intervertebral Discs Adjacent to Interbody Fusion using a Multibody and Finite Element Co-Simulation*, MSc Thesis, Technical University of Lisbon, Lisbon, Portugal.

NIKRAVESH, P. E., 1988, *Computer-aided analysis of mechanical systems*, Prentice-Hall, New Jersey.

OPENSIM, 2011, OpenSim - Lumbar spine applications, https://simtk.org/home/opensim, accessed on 19th September 2011.

PANJABI, M. M., GOEL, V., OXLAND, T., TAKATA, K., DURANCEAU, J., KRAG, M. and PRICE, M., 1992, Human lumbar vertebrae. Quantitative three-dimensional anatomy, *Spine*, 17, pp. 299-306.

PINTAR, F. A., YOGANANDAN, N., MYERS, T., ELHAGEDIAB, A. and SANCES JR, A., 1992, Biomechanical properties of human lumbar spine ligaments, *Journal of Biomechanics*, 25, pp. 1351-1356.

POLLINTINE, P., DOLAN, P., TOBIAS, J. H. and ADAMS, M. A., 2004, Intervertebral Disc Degeneration Can Lead to "Stress-Shielding" of the Anterior Vertebral Body: A Cause of Osteoporotic Vertebral Fracture?, *Spine*, 29, pp. 774-782.

ROGERS, A. W. and JACOB, S., 1992, *Textbook of anatomy*, Churchill Livingstone, Philadelphia.

SANAN, A. and RENGACHARY, S. S., 1996, The History of Spinal Biomechanics, *Neurosurgery*, 39, pp. 657-669.

SÉGUIN, C. A., GRYNPAS, M. D., PILLIAR, R. M., WALDMAN, S. D. and KANDEL, R. A., 2004, Tissue Engineered Nucleus Pulposus Tissue Formed on a Porous Calcium Polyphosphate Substrate, *Spine*, 29, pp. 1299-1306.

SIMPACK, 2011, SIMPACK - Multi-Body Simulation Software, http://www.simpack.com/, accessed on 4th September 2011.

SPINEART, 2011, Baguera ® L, http://www.spineart.ch/, accessed on 17th October 2011.

SYNTHES, 2011, Prodisc-L, http://www.synthesprodisc.com/html/Prodisc-L.33.0.html, accessed on 17th October 2011.

TANAKA, N., AN, H. S., LIM, T. H., FUJIWARA, A., JEON, C. H. and HAUGHTON, V. M., 2001, The relationship between disc degeneration and flexibility of the lumbar spine, *Spine*, 1, pp. 47-56.

THOMPSON, J. P., PEARCE, R. H., SCHECHTER, M. T., ADAMS, M. E., TSANG, I. K. and BISHOP, P. B., 1990, Preliminary evaluation of a scheme for grading the gross morphology of the human intervertebral disc, *Spine*, 15, pp. 411-415.

TIMOSHENKO, S. and GOODIER, J. N., 1969, *Theory of elasticity*, McGraw-Hill, New York.

TRIBUZI, S., FLORES, P. and CLARO, J. C. P., 2012, A Planar Multibody Lumbar Spine Model for Dynamic Analysis, *Proceedings of EUROMECH Colloquium 524 - Multibody system*

modelling, control and simulation for engineering design, Enschede, Netherlands, February 27 – 29, 2012, pp. 1-2 (accepted).

VAN DER HORST, M., 2002, *Human Head Neck Response in Frontal, Lateral and Rea End Impact Loading - modelling and validation*, PhD Thesis, Eindhoven University of Technology, Eindhoven, Netherlands.

WATERS, T., LI, F., HUSTON, R. and KITTUSAMY, N., 2003, Biomechanical Modeling of Spinal Loading Due to Jarring and Jolting for Heavy Equipment Operators, *Proceedings of XVth Triennial Congress of the International Ergonomics Association and 7th Joint Conference of Ergonomics Society of Korea/Japan Ergonomics Society*, Seoul, Korea, Aug. 24-29, 2003, pp. 4.

WHITE, A. A. and PANJABI, M. M., 1990, *Clinical biomechanics of the spine*, Lippincott, Philadelphia.

WISMANS, J., 1980, *A Three-dimensional Mathematical Model of the Human Knee Joint*, PhD Thesis, Eindhoven University of Technology, Eindhoven, Netherlands.

WORLDHEALTHORGANIZATION, 2011, Chronic rheumatic conditions, http://www.who.int/chp/topics/rheumatic/en/, accessed on 17th October 2011.

YAHIA, L. H., AUDET, J. and DROUIN, G., 1991, Rheological properties of the human lumbar spine ligaments, *Journal of Biomedical Engineering*, 13, pp. 399-406.

Appendix A – Input File for MUBODYNA

Throughout the development of this work, three routines were created for the MUBODYNA code, in order to upgrade the already existent code to the analysis of the spine. The new available routines are:

(i) Ligaments

(ii) Bushing Elements

(iii) Contact

Each of the abovementioned followed a similar construction process: it was added a subroutine for the input of the parameters needed for each analysis (INPUT_LIGAMENTS, INPUT_BUSHING_ELEMENT and INPUT_CONTACT) and a subroutine where the computation of the desired forces was done LIGAMENT_FORCES, BUSHING_ELEMENT_FORCES and CONTACT_FORCES).

On the first line of the program, in the same way of the existent data, it is necessary to input the following information:

NLIG	Number of ligaments
NBE	Number of bushing elements
NCONT	Number of contacts

LIGAMENTS

The data lines for ligaments are repeated NLIG times, and are as follows:

I J XI-P-I ETA-P-I XI-P-J ETA-P-J K C L0

where,

I	Index number of body *i*
J	Index number of body *j*
XI-P-I	ξ-coordinate of point *P* on body *i*
ETA-P-I	η-coordinate of point *P* on body *i*
XI-P-J	ξ-coordinate of point *P* on body *j*
ETA-P-J	η-coordinate of point *P* on body *j*
K	Ligament stiffness
C	Damping coefficient
L0	Undeformed length of the ligament
e_T	Transition strain between toe-in and linear regions
e_LIM	Limit strain between linear and failure regions

BUSHING ELEMENTS

The data lines for bushing elements are repeated NBE times, and are as follows:

I J XI-P-I ETA-P-I XI-P-J ETA-P-J DELTA-X-0 DELTA-Y-0 DELTA-THETA-0 K+X K-X K+Y K-Y K+THETA K-THETA D+X D-X D+Y D-Y D+THETA D-THETA

where,

I	Index number of body *i* (body *i* has to be the slave body)
J	Index number of body *j* (body *j* has to be the master body)
XI-P-I	ξ-coordinate of point *P* on body *i*
ETA-P-I	η-coordinate of point *P* on body *i*
XI-P-J	ξ-coordinate of point *P* on body *j*
ETA-P-J	η-coordinate of point *P* on body *j*
EPI-L-I	Lower endplate inclination of body *i*
EPI-U-J	Upper endplate inclination of body *j*
DELTA-X-0	Initial horizontal offset [m]
DELTA-Y-0	Initial vertical offset [m]
DELTA-THETA-0	Initial angular offset [rad]
K+X	Bushing stiffness for positive horizontal displacement
K-X	Bushing stiffness for negative horizontal displacement
K+Y	Bushing stiffness for positive vertical displacement
K-Y	Bushing stiffness for negative vertical displacement
K+THETA	Bushing stiffness for positive angular displacement
K-THETA	Bushing stiffness for negative angular displacement
D+X	Bushing damping coefficient for positive horizontal displacement
D-X	Bushing damping coefficient for negative horizontal displacement
D+Y	Bushing damping coefficient for positive vertical displacement
D-Y	Bushing damping coefficient for negative vertical displacement
D+THETA	Bushing damping coefficient for positive angular displacement
D-THETA	Bushing damping coefficient for negative angular displacement

CONTACT

The data lines for the contacts are repeated NCONT times, and are as follows:

I J TYPE MODEL XI-C-I ETA-C-I XI-L-J ETA-L-J XI-R-J ETA-R-J Ri NIUi NIUj Ei Ej RESTi RESTj FRICi FRICj

where,

I	Index number of body *i* (body *i* has to be the sphere)
J	Index number of body *j* (body *j* has to be the plane)
TYPE	A flag indicating what type of contact is present
MODEL	A flag indicating which contact force model is present
XI-C-I	ξ-coordinate of the center of the sphere *C* on body *i*
ETA-C-I	η-coordinate of the center of the sphere *C* on body *i*
XI-L-J	ξ-coordinate of point *L* on body *j*
ETA-L-J	η-coordinate of point *L* on body *j*
XI-R-J	ξ-coordinate of point *R* on body *j*

ETA-R-J	η-coordinate of point *R* on body *j*
Ri	Sphere radius
NIUi	Poisson coefficient of body *i* (sphere)
NIUj	Poisson coefficient of body *j* (plane)
Ei	Young modulus of body *i* (sphere)
Ej	Young modulus of body *j* (plane)
RESTi	Restitution coefficient of body *i*
RESTj	Restitution coefficient of body *j*
FRICi	Friction coefficient of body *i*
FRICj	Friction coefficient of body *j*